2016

School of Engineering
Howard College Campus
Durban

HIGHLY DISPERSED ZINC-BASED SORBENTS FOR DESULPHURISATION: SYNTHESIS AND APPLICATION

By:

Neelan Govender

BSc Chemical Engineering
2016

A dissertation submitted in the School of Engineering
University of Kwa-zulu Natal
Durban
In the fulfilment of the requirements of the degree of Master of Science in Engineering

DECLARATION

The work presented in this dissertation was undertaken at the School of Engineering, University of KwaZulu-Natal, Howard College Campus in Durban, South Africa, from February 2016 until December 2016.

All work presented is this dissertation is original unless otherwise stated. It has neither in whole nor part been submitted previously to any other University or Institute as part of a degree.

I, Neelan Govender , declare that

1. The research reported in this thesis, except where otherwise indicated, is my original research.
2. This thesis has not been submitted for any degree or examination at any other university.
3. This thesis does not contain other persons' data, pictures, graphs or other information, unless specifically acknowledged as being sourced from other persons.
4. This thesis does not contain other persons' writing, unless specifically acknowledged as being sourced from other researchers. Where other written sources have been quoted, then:
   a. Their words have been re-written but the general information attributed to them has been referenced
   b. Where their exact words have been used, then their writing has been placed in italics and inside quotation marks, and referenced.
5. This thesis does not contain text, graphics or tables copied and pasted from the Internet, unless specifically acknowledged, and the source being detailed in the thesis and in the References sections.

_____

Neelan Govender

As the candidate's supervisor hereby certify that I find this work to be suitable for submission for the degree of Master of Science in Chemical Engineering.

_____

Dr. David Lokhat

_____

Professor Milan Carsky

ACKNOWLEDGEMENTS

I would like to take this opportunity to acknowledge and show my deepest gratitude to the following who have all greatly contributed to the completion of this dissertation:

- Firstly and foremostly I would like to thank God and my parents for giving me the strength, motivation and support to pursue my masters as well as in all other endeavours in life.

- My supervisors, Doctor David Lokhat and Professor Milan Carsky, for imparting on me their vast knowledge, support and guidance. This includes the opportunity to broaden my horizons to the world of chemical engineering and international exposure via a conference visit to Taiwan.

- The lab technicians: Ms. Xoli Hadebe and Ms. Thobekile Mofokeng as well as the chemical engineering technical staff: Mr. Danny Singh, Mr. Sanjay Deeraj and Mr. Gerald Addieah .Thank you for your invaluable assistance throughout my work.

- The National Research Foundation for their greatly appreciated financial support and their dedication to helping scholars pursue their research with these much needed funds.

- The UKZN Westville Campus Microscopy Unit staff: Mr. Vishal Bharuth and Mr. Subashen Naidu, for their assistance in the Quantitative and Qualitative analysis of the sorbent samples.

- Final year chemical engineering students: Mr. Hassam Ghumran and Mr. Senthan Pillai, for their assistance in the modelling section as well as the many joyous hours spent in the lab during their laboratory work.

- Finally to my close friends and gym mates for their continued support and motivation throughout my life. It is thanks to all of you that I aspire to greatness and have the will to continue chasing my dreams.

ABSTRACT

The use of coal for electricity generation is prominent in South Africa. During gasification of coal, the sulphur present in the fuel is converted mainly to hydrogen sulphide. Hot gas desulphurisation (HGD) – which is an improvement on conventional desulphurisation- is an essential step for any gasification process because sulphur compounds are corrosive to process equipment and harmful to the environment. HGD is an efficient method which uses regenerable metal oxide sorbents to remove COS and H_2S from syngas at high pressure and high temperature (Yi et al., 2001). The removal of sulphur compounds from syngas is very important for the correct operation of the newer Integrated Gasification Combined Cycle (IGCC) for power generation.

This study focused on the enhancement of sulphur removal capacity and regeneration characteristics of solid zinc-based sorbents through ultrasound assisted dispersion of active components. The investigation attempted to determine if sonication during wet impregnation of the prepared precursor materials would yield a sorbent with highly dispersed metal oxide content. ZnO/SiO_2 sorbents using the wet impregnation technique and an ultrasonically assisted wet impregnation technique were prepared. The experiment was designed to be a 3^2 factorial design with two independent variables (wt. % ZnO loading and desulphurisation temperature) and three levels for each variable. The aim of the experimental design was to evaluate the effect of wt. % ZnO loading (10%, 20% and 30%) and temperature of the sorbent (350 °C, 450 °C and 550 °C) -both with and without sonication- on the breakthrough time achievable. The dispersion -of the zinc oxide on the surface of the silica support- of the different ZnO/SiO_2 sorbents was then characterized using scanning and transmission electron microscope measurements (SEM-EDX and TEM). A packed bed reactor using a shrinking core model was used to model a highly dispersed zinc-based sorbent for desulphurisation.

Sonicated and non-sonicated sorbent samples of 5g revealed longer desulphurisation breakthrough times at elevated temperatures and at higher wt. % ZnO loading. Sonicated sorbents had comparably better desulphurisation breakthrough times (on average 25.2 min as compared to 15 min) than non-sonicated sorbents. It was proved that the sorbents prepared via the Ultrasonic-assisted Impregnation (UAI) technique enhanced both breakthrough times and saturation capacities. The regeneration characteristics of the spent sorbent were determined from sulphur dioxide desorption measurements during high-temperature (550 °C) oxidative treatment of the material. The regeneration time of the higher desulphurisation temperature and lower wt. % ZnO loading spent sorbent samples were shorter. For higher wt. % ZnO loading (30%-20%) at equivalent desulphurisation temperature, sonicated sorbents had

a longer breakthrough time (on average 26.5 min as compared to 12.8 min) than non-sonicated sorbents. However, for lower wt. % ZnO loading (10%) at equivalent desulphurisation temperature, the converse was true (on average 5 min as compared to 8.3 min). Moreover, the sonicated spent sorbents at 350 °C desulphurisation temperature were not regenerable to the useable limit. Hence, the desulphurisation temperature range of regenerable zinc-based spent sorbents for this study laid in the range of 450°C to 550 °C. Since all of the spent sorbents were regenerable to a useable limit within ~60 min in this range, the 30 wt. % ZnO loading sonicated sorbent employed at 550 °C showed the best overall performance. With the aid of these results, technological improvement in the performance of solid zinc-based sorbents for hot gas desulphurisation is envisaged.

TABLE OF CONTENTS

LIST OF FIGURES

LIST OF TABLES

LIST OF PUBLICATIONS

- Gasification Modelling

  Puigjaner, L. (2011) *Syngas from Waste: Emerging Technologies*, 1st edition, London: Springer.

- Gas-Solid Reaction Modelling

  Ali, J.S. (2015) *High temperature production and desulphurisation of syngas*, Msc Dissertation edition, Durban: University of Kwa-zulu Natal.

  Levenspiel, O. (1999) *Chemical Reaction Engineering*, 3rd edition, New York: John Wiley & Sons.

NOMENCLATURE

Symbols	Definition	Units
a	Stoichiometric coefficient of reactant A in the gas phase	–
A	Reactant A in the gas phase (H_2S)	–
A_b	Packed bed area	cm^2
A_p	Peak Area	uV
b	Stoichiometric coefficient of reactant B in the solid phase	–
B	Reactant B in the solid phase (ZnO)	–
C_A	Molar concentration of reactant A in the gas phase	mol/cm^3
C_{Ag}	Bulk molar concentration of reactant A in the gas film	mol/cm^3
C_{A0}	Initial molar concentration of reactant A in the gas phase	mol/cm^3
C_B	Molar concentration of reactant B in the solid phase	mol/cm^3
C_{B0}	Initial molar concentration of reactant B in the solid phase	mol/cm^3
CI	Confidence interval	nm
D	Packed bed diameter	cm
D_e	Effective diffusivity	cm^2/min
D_p	Diameter of particle	cm
k	Intrinsic reaction rate constant	cm/min
k_g	Gas film coefficient for mass transfer	cm/min
K	Solubility of species	$g/ml.H_2O$
L	Packed bed length	cm
L_p	Length of particle	nm
$\overline{L_p}$	Mean length of particle	nm
m	Mass of species	g
MM	Molecular mass of species	g/mol
n	Number of moles of species	mol
N_A	Moles of reactant A in the gas phase (H_2S)	mol
N_B	Moles of reactant B in the solid phase (ZnO)	mol
Q_A	Molar flux of reactant A in the gas phase	$mol/cm^2.min$
r_A	Reaction rate	$mol\ A/cm^3.min$
r_c	Radius of unreacted core	cm
R	Radius of the particle	cm
SC	Saturation capacity	g S/g ZnO
t_b	Bubble flow meter time	s
t_B	Breakthrough time	min
$\widehat{t_B}$	Normalized breakthrough time	min
T	Desulphurisation temperature	K
u	Gas mixture velocity	cm/min
V	Peak volume	mL/mL injected
$\dot{V}$	Volumetric flow rate of gas mixture	cm^3/s
V_B	Packed bed volume	cm^3
$\acute{V}_B$	Packed bed volume from literature	cm^3

Symbols	Definition	Units
V_p	Volume of particle	cm^3
X	Fractional conversion	–
z	Axial position of packed bed reactor	cm
Greek		
α	Probability	–
ε	Packed bed porosity	–
μ	Viscosity of gas mixture	Pa.s
ρ	Density of gas mixture	kg/m^3
ρ_B	Molar density of reactant B	mol/cm^3
σ	Standard deviation of particle lengths	cm
σ^2	Variance of particle lengths	cm^2
τ	Gas hourly space velocity	hr^{-1}
$\acute{\tau}$	Gas hourly space velocity from literature	hr^{-1}

CHAPTER 1: INTRODUCTION

1.1. Problem identification

Most hydrocarbon fuels like petroleum, natural gas and coal contain other elements in small quantities which, after high-temperature processing, are transformed into various impurities. These impurities include compounds of sulphur. The use of coal for electricity generation is prominent in South Africa. During gasification of coal, the sulphur present in the fuel is converted mainly to hydrogen sulphide. The removal of sulphur compounds from coal gas is very important for the correct operation of the Molten/Gasifier Carbonate Fuel Cell processes and newer Integrated Gasification Combined Cycle (IGCC) for power generation. In both of these processes a commercial-level desulphurisation system is required. Conventional methods of desulphurisation involve absorption of the acid component using regenerative solvents moving counter currently with the coal derived gas in an absorption column. The corrosive and toxic nature of most of the commercially available solvents has prompted much research into the development of alternative desulphurisation technologies. Solid sorbents such as metal oxides may be used to accomplish coal gas desulphurisation. The effectiveness of metal oxides for desulphurisation of hot coal gas can be improved by dispersing the material over an inert support and by doping the prepared sorbent with transition metal promoters.

This research project aims to answer the following research questions:

1. Can the metal dispersion of ZnO/SiO_2 sorbents prepared by wet impregnation be improved by employing ultrasonic irradiation during preparation?

2. Does the improved dispersion of sonicated ZnO/SiO_2 sorbents result in enhanced sulphur removing capacity as well as increased breakthrough times for desulphurisation when compared to conventional ZnO/SiO_2 sorbents?

3. Does the improved dispersion of sonicated ZnO/SiO_2 sorbents result in a relatively shorter regeneration time when compared to conventional ZnO/SiO_2 sorbents?

1.2. Rationale and motivation

South Africa has abundant coal reserves and burning coal is still regarded as the most cost-effective way of generating electricity. An efficient way of producing electricity from coal is via a gasification process. The constituency of the derived coal gas is dependent on the feed system, gasifier, gasification temperature and the type of coal. Hydrogen and carbon monoxide (syngas) are the primary products, together with various impurities including hydrogen sulphide (Gasper-Galvin, Atimtay and Gupta, 1998). A coal-fired gasifier combined cycle process (a process using a combination of a steam turbine and a gas turbine) is a very efficient means of converting the energy in the combustion products into electricity. In a combined cycle process the sulphur compounds are removed from the gasifier gases before they enter the turbine combustor. Gas cleaning is not only necessary to protect the equipment against corrosion but also to prevent pollution of the environment (Bakker, Moulijn and Kapteijn, 2003). H_2S can be removed effectively by cooling the hot coal gas down to near ambient temperature and scrubbing it with an aqueous amine solution. However, for highest efficiency the process should proceed via hot gas desulphurisation. The economic viability of combined cycle processes is thus dependent on the development of a high temperature solid sorbent for desulphurisation.

Due to the chemical affinity of H_2S to surface metal sites and metal cations, removal of H_2S by metal oxide sorbents is a frequently employed technique for coal gas cleaning. Zinc oxide (ZnO) based sorbents are regarded as amongst the best materials for hot gas desulphurisation (Sofekun, 1996). The zinc absorbs the H_2S, forming zinc sulphide (ZnS), which is then regenerated with oxygen. One issue that has inhibited the commercialization of ZnO as a desulphurisation sorbent is the formation of $ZnSO_4$ during oxidative regeneration. The zinc sulphate tends to block the pores of the sorbent and can result in low sorbent utilization at H_2S breakthrough (Sofekun, 1996). The H_2S capacity of metal oxide sorbents can be improved by dispersing the active metal components over various porous inert supports. Supports such as alumina, silica, clay and zeolites have proven effective for this purpose (Wang and Yang, 2014). Montes et al. (2013) demonstrated the importance of small size of metal oxide particles and good dispersion for H_2S absorption capacity. They explained the effect in terms of the accessibility of the sulphur compounds to the metal oxide particles deep within the pores of the support. It has also been shown that the metal oxide dispersion and available surface area also play a key role in the regeneration characteristics of the prepared sorbent.

Yang and Tartarchuk (2010) showed that ZnO supported on silica could recover most of its original sulphur removing capacity at relatively low regeneration temperatures and that the overall performance of this sorbent was far superior to commercial ZnO. It was through the examination of hydrogenation reactions that ultrasound was used in the preparation of supported metal catalysts via wet impregnation (Bianchi et al., 1993). Studies show that ultrasound assists with the insertion of metal oxide particles into the pores of the support and hence improves dispersion. Through the formation of shockwaves and microjets, the metal ions are accelerated into the support material. Bianchi et al. (1993) showed that highly dispersed Ru/Al_2O_3 catalysts could be prepared using this technique.

Clean coal technology refers to a series of techniques that are being developed to mitigate the negative effects of coal-based power generation on the environment. One example of clean coal technology is the cleaning of coal gas used for energy generation. Most research in this regard has focused on the development of an appropriate high-temperature sorbent for removal of sulphur compounds from the coal gas. This project exploits the surface modifying property of ultrasonic irradiation and microwave heating to prepare highly-dispersed, silica supported, metal oxide based sorbent. The fabrication, characterization and use of these inorganic sorbents for desulphurisation of hot coal gas constitute a direct application of clean coal technology.

The Eskom TESP Clean coal technologies/high temperature processes centre at the University of KwaZulu-Natal has been involved in desulphurisation studies for a number of years. Work in this centre has focused on the fundamental understanding of the desulphurisation process over zinc-based sorbents. The present project will expand on this knowledge.

1.3. Objectives of the study

The objectives of this research project are:

Objective 1: To prepare a sorbent by an ultrasonically assisted wet impregnation technique and quantitatively determine the improvement in sulphur removing capacity as well as the dispersion of zinc oxide loaded onto the surface of a silica carrier.

Objective 2: To quantitatively evaluate the effect of wt. % ZnO loading and desulphurisation temperature on the breakthrough times of highly dispersed sonicated ZnO/SiO_2 sorbent for desulphurisation, when compared to conventional ZnO/SiO_2 sorbents.

Objective 3: To quantitatively evaluate the effect of wt. % ZnO loading and desulphurisation temperature on the regeneration characteristics of highly dispersed sonicated ZnO/SiO_2 spent sorbents, when compared to conventional ZnO/SiO_2 spent sorbents, both at the same regeneration temperature.

1.4. Scope of the study

The primary research method for this study is a quantitative scientific experiment involving the generation of statistically analysable data by systematic manipulation of independent variables. This type of research method allows one to make inferences about the relationship between independent and dependent variables. The system of scientific measurements will be interval based and the intervals will be uniform. The results of the quantitative experimental work will be used to test the hypotheses of the research. The primary research method will be supported by a literature review. The latter will guide the selection of the test limits of the experimental designs employed.

Preliminary results already available will also be used to govern the choice and form of the experimental designs.

In order to meet the three objectives associated with the fulfilment of the aims of the project, the following tasks need to be carried out:

1. The literature review will be conducted in two stages. The first stage will focus on the synthesis and characterization of solid sorbents for hot gas desulphurisation. It will cover both pure and supported metal oxides produced using precipitation and impregnation methods. All aspects of physical characterization will also be covered, including structure, surface morphology and crystallography. The second stage will focus on the laboratory techniques used to test the performance of sorbents for H_2S removal. A variety of different techniques described in the literature will be considered. The choice of H_2S breakthrough, sulphur removing capacity, recovery of capacity after multiple cycles and SO_2 desorption measurements for estimation of regeneration rates will be ratified based on literature evidence.

2. ZnO/SiO_2 sorbent samples will be prepared using a wet impregnation technique. An aqueous solution of $ZnCl_2$ will be used as the precursor and silica as the carrier. Modified sorbents will be prepared by sonicating the precursor solution during ageing of the carrier. The prepared sorbents will be characterized: SEM-EDX for dispersion and SEM/TEM for particle size and arrangement.

3. The efficacy of the prepared sorbents will be tested for hot gas desulphurisation using a high temperature flow-through apparatus. Breakthrough curves for H_2S absorption will be constructed from temporal measurements of the exit gas stream H_2S concentration, using a highly sensitive Flame Photometric Detector (FPD) equipped to a gas chromatograph.

4. The regenerative properties of the materials will be evaluated based on SO_2 desorption rates during high-temperature (550 °C) oxidative treatment. The SO_2 concentration in the exit gas will be monitored to determine the time required for complete regeneration of the sorbent.

1.5. Outline of the dissertation

This dissertation was divided into four phases:

- The theoretical background of this research topic: covered in chapter 2.
- The gas-solid reactor modelling for this process: covered in chapter 3.
- The experimental methodology for the process design and equipment: covered in chapter 4.
- A discussion of results as well as conclusion and recommendations: covered in chapters 5-7.

The main hypothesis is that a highly effective and easy to regenerate solid sorbent can be prepared from zinc precursors, using a wet impregnation technique modified by ultrasonic irradiation.

With the aid of the results presented in this dissertation, technological improvement in the performance of solid zinc-based sorbents for hot gas desulphurisation is envisaged.

CHAPTER 2: LITERATURE REVIEW

2.1. Gasification

2.1.1. Introduction

The process of gasification was discovered just before the turn of the century, in 1798, by the French and English independently. Early developments of gasification used coal as a source to produce 'Town gas'. By the early 1800's gasification technology had developed to a point where most of London could be supplied with thermal heating and lighting (Singer, 1958).

Gasification is a controlled partial oxidation process that coverts carbonaceous material into primarily carbon dioxide, hydrogen and carbon monoxide. It is a thermal conversion process much like combustion, though they are fundamentally different concepts. Table 2-1 contrasts gasification and combustion.

Table 2-1: Differences between Gasification and Combustion (Breault, 2010)

	Combustion	Gasification
Chemical process	full oxidation	partial oxidation
Chemical environment	excess oxygen (air)-oxidizing	oxygen-starved - reducing
Primary product	heat (e.g., steam)	syngas (CO & H_2)
"Downstream" products	electric power	electric power, pure H_2, liquid fuels, chemicals
Current application	dominates coal-fired power generation worldwide	mostly chemicals and fuels, power generation demonstrated
Efficiency	35–37% (HHV)	39–42% HHV
Emissions	~NSPS	~1/10 NSPS
Capital cost	$1,000–1,150 /kW	competitive
Maturity / risk	high experience, low risk	reliability needs improved

The gasification process follows several steps which include pyrolysis, gasification and combustion to produce a synthesis gas known as 'syngas'.

- Pyrolysis is the thermal degradation of a material in the absence of oxygen. The coal is vaporised of volatile components at about 300-600°C to form char (comprising of mainly ash and fixed carbons).

- In the gasification stage, the char is reacted with either hydrogen or steam at 700-1000°C to produce a mixture of gases. It is generally accepted that higher pressures favour H_2 and CO_2 production while higher temperatures favour H_2 and CO (Haryanto et al., 2009). Due to the rapid pyrolysis (devolatilization) stage, the char gasification stage is rate limiting in the gasification of coal. (Sadaka, 2008).
- A portion of the char is reacted with oxygen to form an exothermic combustion reaction which provides the heat energy required for the char gasification and pyrolysis reactions (EREN, 2002).

The Equations (2-1) to (2-6) are reactions to be considered in the gasification process:
(Krigmont, 1999)

Combustion with Oxygen

$$C + O_2 \rightarrow CO_2 \qquad (\Delta H = -393\ kJ/mol) \qquad (2\text{-}1)$$

Gasification with Carbon dioxide

$$C + CO_2 \rightarrow 2CO \qquad (\Delta H = +172\ kJ/mol) \qquad (2\text{-}2)$$

Gasification with Steam

$$C + H_20 \rightarrow CO + H_2 \qquad (\Delta H = +131\ kJ/mol) \qquad (2\text{-}3)$$

Gasification with Hydrogen

$$C + 2H_2 \rightarrow CH_4 \qquad (\Delta H = -74\ kJ/mol) \qquad (2\text{-}4)$$

Water-Gas Shift

$$CO + H_20 \rightarrow CO_2 + H_2 \qquad (\Delta H = -41\ kJ/mol) \qquad (2\text{-}5)$$

Methanation

$$CO + 3H_2 \rightarrow CH_4 + H_2O \qquad (\Delta H = -205\ kJ/mol) \qquad (2\text{-}6)$$

Current developments see the application of gasification in the power generation industry through the Integrated Gasification Combined Cycle (IGCC).

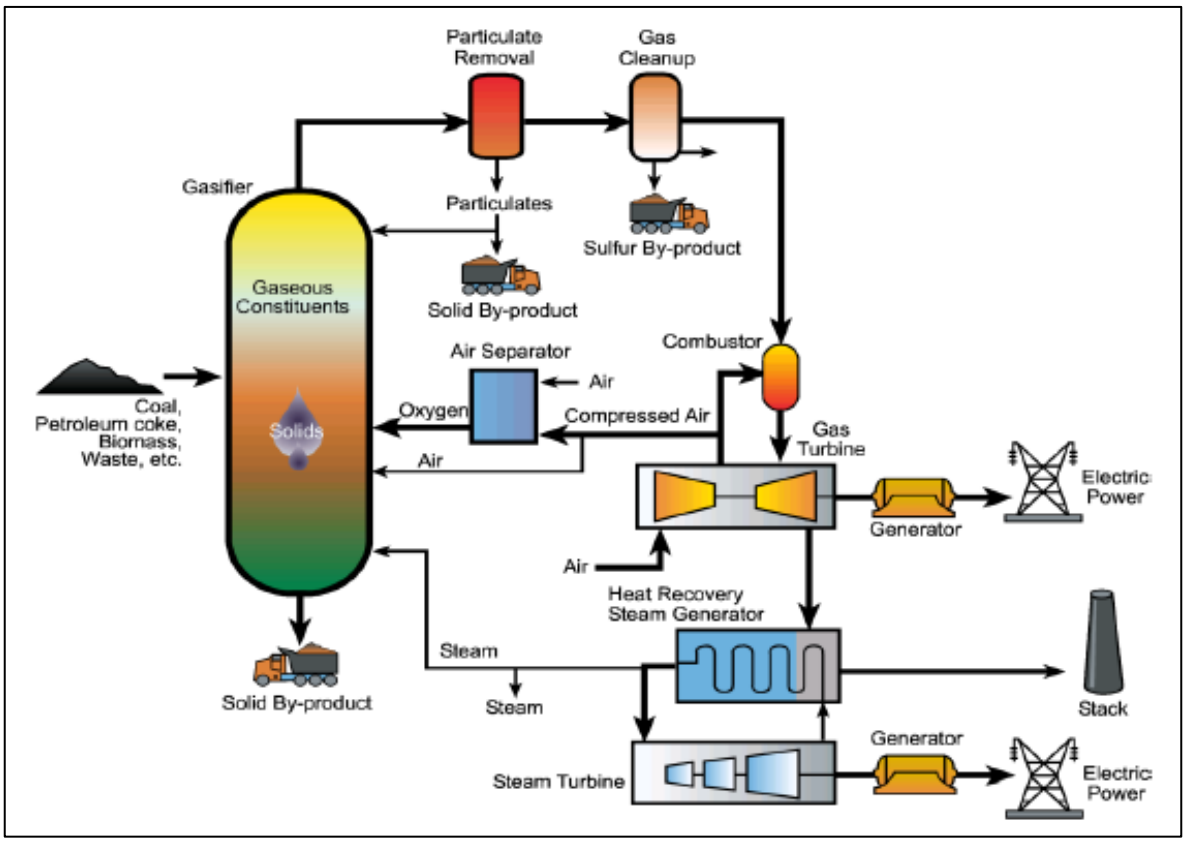

Figure 2-1: IGCC system (Van Nguyen, 2011)

Figure 2-1 shows the basic structure of an IGCC system. Raw syngas is produced by feeding the carbonaceous material along with steam and oxygen to a gasifier. After clean-up, the clean syngas is fed to a gas combustion turbine. The products are then fed to a steam turbine and heat recovery steam generator for power generation. A modification to the system can be made to remove the carbon from the syngas in the form of carbon dioxide. The syngas is passed through a Shift Reactor and reacted with water to form the products shown by equation (2-5). The carbon dioxide is then separated from the hydrogen resulting in the former going to sequestration.

2.1.2. Gasifier configurations

Gasifier configurations are classified according to the relative flow of the oxidant (oxygen or air) and biomass into the gasifier. Due to their configurations, commercial gasifiers can be divided into three different types: Fixed-bed, Fluidized-bed and Entrained-flow.

2.1.2.1. Fixed-bed gasifier

These are the most common type of gasifiers and are usually operated at moderate pressure (25-30 atm). The solid biomass is fed through the top of the gasifier and reacts with the oxidant on a grate which forms a fuel bed. The temperature of the syngas produces is primarily dependant on the moisture content of the solid biomass. The fixed-bed gasifier is partitioned into four different zones: Drying, Pyrolysis, Oxidation and Reduction. The biomass is heated and dried by radiation and forced convection currents in the drying zone. As previously discussed, the biomass is devolatilized in the pyrolysis zone due to the higher temperature gases. The reduction zone is responsible for the gasification of the devolatilized biomass by carbon dioxide (Equation 2-2) and water (Equation 2-3). The remaining char is reacted in the combustion zone with oxygen (Equation 2-1) to provide the driving process heat for the gasification process.

2.1.2.1(a) Updraft fixed-bed

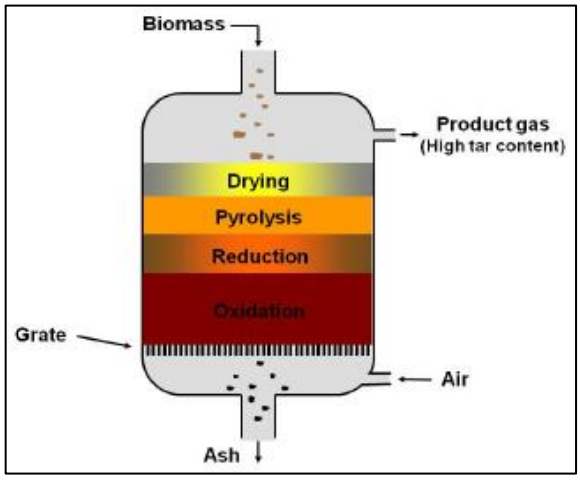

Figure 2-2: Updraft fixed-bed gasifier (Swedish Gas Centre, 2012)

Figure 2-2 shows that the biomass flows countercurrently to the oxidant in an Updraft fixed-bed gasifier. The biomass proceeds down the gasifier through the following sequence: Drying, Pyrolysis, Reduction and finally Oxidation. The biomass left after this gasification process exists as ash which falls on a grate and then exits at the bottom of the gasifier. The syngas exits near the top of the gasifier at approximately 400°C with a high tar content. This is a direct heating gasifier with its main application in a furnace or close-coupled boiler (Klein, 2002). An example of an Updraft fixed-bed gasifier is British Gas/Lurgi (BGL).

2.1.2.1(b) Downdraft fixed-bed

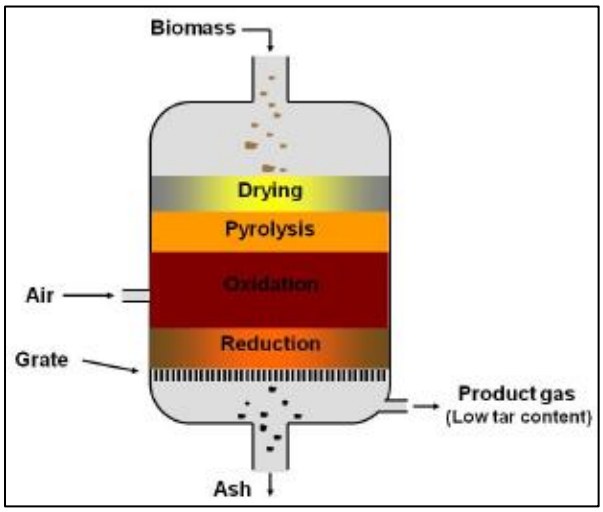

Figure 2-3: Downdraft fixed-bed gasifier (Swedish Gas Centre, 2012)

Figure 2-3 shows that the biomass flows co-currently to the oxidant in a Downdraft fixed-bed gasifier. The biomass proceeds down the gasifier through the following sequence: Drying, Pyrolysis, Oxidation and finally Reduction. The key differentiating factor between these two configurations is that the biomass products after pyrolysis are further decomposed in the oxidation zone. The resulting vapourised moisture then acts as a gasifying agent. The syngas exits near the bottom of the gasifier at approximately 700°C with a significantly lower tar content than an Updraft fixed-bed gasifier. Their main application is in the internal combustion engine due to a low tar content syngas production (Reed and Das, 1988).

There are many contributing factors that lead to the selection of one gasifier over another. Table 2-2 compares the advantages and disadvantages of Updraft fixed-bed gasifiers to Downdraft fixed-bed gasifiers.

Table 2-2: Advantages and disadvantage of different fixed-bed gasifier types (Rajvanshi, 1986)

Sr. No.	Gasifier Type	Advantage	Disadvantages
1.	Updraft	- Small pressure drop - good thermal efficiency - little tendency towards slag formation	- Great sensitivity to tar and moisture and moisture content of fuel - relatively long time required for start up of IC engine - poor reaction capability with heavy gas load
2.	Downdraft	- Flexible adaptation of gas production to load - low sensitivity to charcoal dust and tar content of fuel	- Design tends to be tall - not feasible for very small particle size of fuel

2.1.2.2. Fluidized-bed gasifier

The principle operation of a Fluidized-bed gasifier uses an oxidising agent (steam, air or oxygen) to fluidize a bed of inert material and the biomass. The flow of the oxidizing agent - which is the fluidizing medium - expands the bed, which acts like a boiling liquid, vertically (Klein, 2002). As compared to fixed-bed gasifiers, the fluidized-bed configuration is not divided into separate zones. Rather the Drying, Pyrolysis, Oxidation and Reduction reactions occur simultaneously (Sadaka, 2008). These gasifiers are characterised by high heat transfer and excellent mixing properties. The velocity of the oxidizing agent determines whether the fluidized bed is bubbling or circulating.

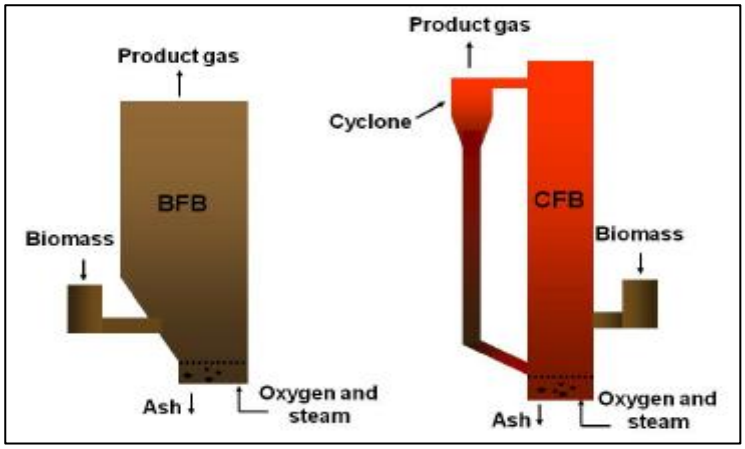

Figure 2-4: Bubbling fluidized-bed gasifier (left) and a Circulating fluidized-bed (right) (Swedish Gas Centre, 2012)

2.1.2.2(a) Bubbling fluidized-bed

The oxidising agent is passed through the bed of inert material at a sufficiently high velocity (usually 1-3 m/s) to expand the bed into bubbling like a liquid. The biomass enters through the side of the gasifier when the temperature of the heated bed is high enough (just below 900°C). The pyrolysis of the biomass liberates the product syngas at the top of the gasifier and the exothermic combustion reaction maintains the bed temperature while forming the ash (char) at the bottom. The bed temperature is maintained to ensure combustion without ash melting. An example of a commercially available Bubbling fluidized-bed gasifier is the U-GAS® Gasifier.

2.1.2.2(b) Circulating fluidized-bed

The oxidising agent gas flow velocity is increased (usually 5-10 m/s) to further expand the bed resulting in a greater fraction of the bed material being entrained in the upward flow. The biomass entering through the side of the gasifier is suspended with the bed material and reacts to form the syngas product. The mixture of the syngas and bed material leave through an external recirculation system which has a cyclone to separate them. The syngas leaves through the top of the cyclone while the bed material is conveyed to the gasifiers' base. The major difference between both configurations (see Figure 2.4) is that unlike the bubbling system, the circulating fluidized-bed gasifier does not differentiate between a dilute-solids zone and dense-solids zone (Klein, 2002).

Table 2-3 compares the advantages and disadvantages of Bubbling fluidized-bed gasifiers to Circulating fluidized-bed gasifiers.

Table 2-3: Advantages and disadvantages of different Fluidized-bed gasifier types (Sadaka, 2008)

Sr. No.	Gasifier Type	Advantages	Disadvantages
1.	Bubbling	- Better bed temperature control - High volume capacity - Improved bed storage heat capacity	- Non- uniform temperature distribution - Separation of inorganic material in feedstock unavailable
2.	Circulating	- larger processing capacity of feedstock over a range of moisture contents and composition - Greater turbulence - Improved gas-solid contact	- Height restrictions - Higher costs due to recirculation system requirements

2.1.2.2. Entrained-flow gasifier

Entrained-flow gasifiers have a high pressure and temperature operation. Figure 2-5 shows that the biomass enters the top of the gasifier co-currently with the steam and/or oxidant. The steam and oxidant then entrain the biomass particles as they move down the gasifier in a dense cloud of fine particles. In this turbulent flow the dense cloud of fine particles contact a flame (1200-1500°C) where the gasification reactions occur rapidly to produce syngas and ash. Entrained- flow gasifiers have two modes of operation: slagging or non-slagging. If the gasifier operating temperature is in excess to that of the biomass ash melting temperature then slagging occurs. The ash forms a molten slag which exits the gasifier at the bottom of the unit. Table 2-4 compares the advantages and disadvantages of an Entrained-flow gasifier.

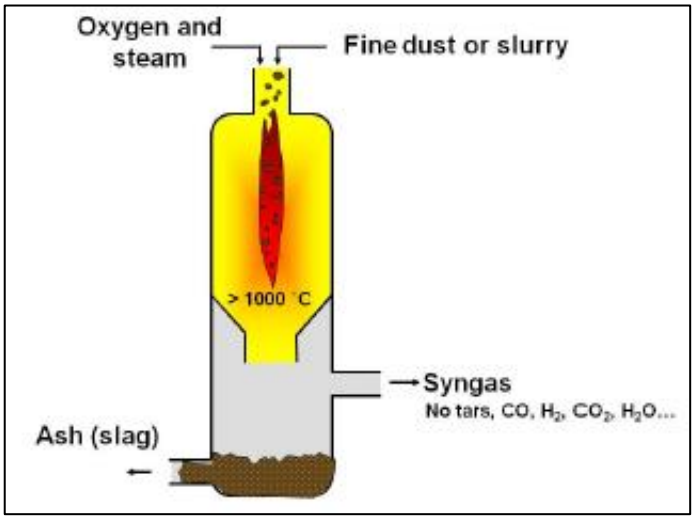

Figure 2-5: Entrained-flow gasifier (Swedish Gas Centre, 2012)

Table 2-4: Advantages and disadvantages of an Entrained-flow gasifier type (NETL, 2016)

Sr. No.	Gasifier Type	Advantages	Disadvantages
1.	Entrained-flow	- Short residence time in reactor - Higher conversion of carbon - High quality syngas production (trace amounts of contaminants)	- Efficiency of cold-gas lower - Costly heat recovery system is needed to improve efficiency - Larger requirement for oxidant supply

2.1.3. Gasification modelling studies

There are two types of models that are proposed. The equilibrium calculations are either restricted (i) by a set of chemical compounds or (ii) by a given set of equations (Puigjaner, 2011). The minimization of Gibbs's free energy is prevalent in both cases; however, in the first case all possible reactions are considered. Table 2-5 provides a brief review on the gasification modelling and is not a detailed study due to this not being the main focus of this thesis.

Table 2-5: Review of gasifier modelling (Puigjaner, 2011)

Source	Raw material	Gasifier type	P (bar), T[a] (°C)	Scale[b]	Time dependence	Approach
(Gautam, Adhikari and Bhavnani, 2010)	Biomass	Fixed	1, 800	Pilot-Small	Steady	Equilibrium chemical reactions
(Loeser and Redfern, 2009)	Biomass	Fixed	1, n.s.	Small	Steady	Equilibrium chemical compounds
(Melgar et al., 2007)	Biomass	Fixed	1, 700	Pilot-Small	Steady	Equilibrium chemical reactions
(Giltrap, McKibbin and Barnes, 2003)	Biomass	Fixed	1, 927	Small	Steady	Kinetic model
(Altafini, Wander and Barreto, 2003)	Biomass	Fixed	1, 800	Pilot-Small	Steady	Equilibrium chemical compounds
(Di Blasi, 2000)	Biomass	Fixed	1, 850	Small	Dynamic	Kinetic Model
(Wang and Kinoshita, 1993)	Biomass	Fixed	1, 800	Small	Dynamic-Steady	Kinetic Model
(Nikoo and Mahinpey, 2008)	Biomass	Fluidised	1, 800	Lab	Steady	Kinetic model for heterogeneous reactions; equilibruim chemical compounds for homogeneous reactions
(Jand and Foscolo, 2005)	Biomass	Fluidised	1, 675	Lab	Dynamic	Kinetic Model
(Ruggiero and Manfrida, 1999)	Biomass	Fluidised Entrained	1 and pressurised : n.s.[c]	Pilot-Large	Steady	Equilibrium chemical compounds
(Emun et al., 2009)	Coal slurry	Entrained	8, 1250	Large	Steady	Equilibrium chemical compounds
(Robinson and Luyben, 2008)	Coal slurry	Entrained	55.17, 1370	Large	Dynamic-Steady	Kinetic model
(Nathen, Kirkpatrick and Young, 2008)	Coal	Entrained	n.s.[c], 1500	Large	Steady	Equilibrium chemical compounds

Table 2-5 (Continued)

Source	Raw material	Gasifier type	P (bar), T[a] (°C)	Scale[b]	Time dependence	Approach
(Frey and Akunuri, 2001)	Coal slurry	Entrained	42, 1260	Large	Steady	Equilibrium chemical compounds
(Wen and Chaung, 1973)	Coal slurry and coal liquefaction residues	Entrained	22, 1800	Large (Pilot plant)	Dynamic-Steady	Kinetic model
(Govind and Shah, 1984)	Coal slurry and coal liquefaction residues	Entrained	22, 1800	Large (Pilot plant)	Dynamic-Steady	Kinetic model
(Ullmann, 2003)	General	General	General	General	Steady	Equilibrium chemical reactions with K_{eq}[d] values at a temperature other than the one in the reactor
[a] The temperature is an average value (more sources give a sensitivity analysis or a profile of temperatures)						
[b] Large- and small-scales belong to industrial scale						
[c] n.s. non-specified						
[d] K_{eq} is the equilibrium constant for a specific reaction						

2.2. Syngas desulphurisation

2.2.1. Introduction

During the gasification process, the sulphur content present in the carbonaceous material forms an appreciable amount of H_2S -with lesser amounts of other sulphur compounds (COS, CS_2)- in the syngas that is produced. This syngas is an important feedstock needed for post-gasification processes. Most of the syngas is utilized for conversion to liquid fuels and power generation. These processes include Fischer-Tropsch synthesis, syngas fermentation, mixed alcohols synthesis, methanol synthesis and Integrated Gasification Combined Cycle (IGCC). The presence of these sulphur containing compounds in the syngas have an adverse effect for the following reasons:

- When combusted, the syngas produces SO_2 which reacts in the atmosphere to form acid rain
- The deactivation of catalysts used for NO_2 emission control, water-gas shift (Equation 2-5) and Fischer-Tropsch synthesis
- Corrosion of turbines and other process equipment used in the IGCC

Hence there is a need for the syngas to be desulphurised to the required level before further processing. Table 2-6 shows the syngas sulphur requirements for Fischer-Tropsch synthesis, syngas fermentation, mixed alcohols synthesis and methanol synthesis.

Table 2-6: Syngas sulphur requirements for conversion to liquid fuel processes

Fischer-Tropsch	Methanol	Mixed alcohol	Fermentation
- <100ppb (most important poison)	- <100ppb - COS exists as a poison in the liquid phase	- Same as Methanol synthesis	- Tolerance (up to 2% H_2S) - Sulphur promotes organisms' growth

2.2.2. Conventional desulphurisation

Desulphurisation is not a new topic of research. It has been around for many years; however, some technologies are more researched than others. Known technologies for conventional desulphurisation include scrubbing processes and cold gas desulphurisation.

2.2.2.1. Scrubbing processes

2.2.2.1(a) Wet gas scrubbing

Wet gas scrubbing (WGS) technology provides SO_2 control of exhaust gases and combined particulates for refineries. The WGS process, which is essentially a saturated gas scrubber, is based on calcium or sodium reagent (referred to as alkaline particulates) for the control of SO_2 in a column designed to simultaneously capture particulate (Hamon Research-Cottrell, Inc., 2016).

The most common wet scrubbing installations make use of an absorbent containing limestone ($CaCO_3$) and gypsum ($CaSO_4.2H_2O$) in slurry. Limestone is cheap; however, control efficiencies for such systems are limited to approximately 90%. The limestone reacts with the sulphur to produce gypsum in the scrubber column; and is referred to as a reactive sorbent. The reaction proceeds as follows:

$$CaCO_3(s) + SO_2(g) + 0.5O_2(g) + 2H_2O(l) \rightarrow CaSO_4.2H_2O(s) + CO_2(g) \quad (2\text{-}7)$$

Within the reaction there are 4 main steps that occur (Nygaard et al., 2004):

- Absorption – SO_2 is absorbed into the slurry and proceeds to dissociate to HSO_3^- and SO_3^{2-}.
- Oxidation – HSO_3^- oxidises to form SO_4^{2-}.
- Dissolution – $CaCO_3$ dissolves in water to form aqueous Ca^{2+}, HCO^{3-}, CO_3^{2-} and CO_2.
- Crystallisation – Ca^{2+} and SO_4^{2-} combine and crystallise to form gypsum.

The absorbing reagent is inserted in the flue gas in a spray tower or directly into the duct. In a typical wet scrubbing system, the flue gas is sent to a spray column. In order to provide good contact between the waste gas and sorbent, the nozzles and injection locations are designed to optimize the size and density of slurry droplets formed by the system The density and size of the slurry droplets formed by the system are controlled by optimally designing the injection and nozzle positions (Cheremisinoff, 2016). This increases the contact between the sorbent and waste gas. Contained in the slurry droplets is the dissolved sulphur dioxide which reacts with the alkaline particulates to form alkaline sulphates. The slurry falls to the bottom of the absorber column where it is collected. A mist eliminator is positioned such that the treated flue gas is allowed to pass through it to remove whatever entrained slurry may exist before exiting the column. The solid is removed from the waste gas stream.

Depending on how the solids generated are handled, a scrubbing unit can be typically classified as "once-through" or "regenerable." Once-through'' systems either make use of the spent solids as a saleable by-product or dispose of it as waste; the former being the more obvious choice for economic and environmental reasons. The sorbent is recycled back into the system for a regenerable system. Currently, once-through processes are more financially feasible than regenerable processes (Copper and Alley, 2002).

The only downside to the use of alkaline particulates is the fact that their reaction with H_2S gas occurs at a much higher temperature of ~900°C (Woods et al., 1990). Therefore, the treatment of coal gas, to also remove any H_2S that may have formed, would require the use of non-reactive organic solvents. These are classified as physical solvents and perform depending on the solubility of the individual gaseous components into the solvent which follows Henry's law (Kohl and Riesenfeld, 1979). Hence, the solubility of the individual components into the solvent is directly proportional to their gas phase partial pressures. The non-reactive nature of this process makes the regeneration process simple and cost effective as it is only necessary to reduce the pressure to strip the acid gases from the solvent. Many organic solvents can be used but for them to be practically useful, they must have low vapour pressure to avoid loss of solvent, a high capacity for acid gases, low capacity for the main constituents of the syngas like hydrogen and methane, be thermal stability, non-corrosive and cheap (Ali, 2015).

2.2.2.1(b) Dry systems

As the name suggests, there is a pneumatic injection of the powdered sorbent into the downstream duct or furnace directly for a dry sorbent inject system. The dry waste product is removed from the (then cooled) flue gas with the aid of ESP filters. When inserting sorbent into the duct, it is required to have a good dispersion and small amounts of water can be added to improve SO_2 removal. Dry sorbent systems usually use sodium based alkaline reagents and calcium. Sufficient residence time at the proper temperature as well as an even distribution of sorbent across the reactor is crucial for high SO_2 removal rates (Cheremisinoff, 2016).

The advantage of using an entirely dry process is extremely high levels of sulphur control. It also provides medium control of nitrogen oxides in an adsorption process utilising an activated coke. The activated coke can be regenerated and produces sulphuric acid as a by-product which can be sold to greatly reduce the costs of reagent feed and disposal.

Advantages:

- Inexpensive and readily available reagents.
- Products of reaction may be reusable.
- High SO_2 removal efficiencies, from 50% up to 98% (Cheremisinoff, 2016).
- Lower annual and capital costs due ease of waste disposal.
- Require less water and has a simpler design than wet systems

Disadvantages:

- Limitations of use are for waste gas SO_2 concentrations in excess of 2000ppm (Cheremisinoff, 2016).
- Downstream equipment and absorber become scaled and deposited with wet solids.
- Higher operating cost due to the need for disposal of solid waste products.
- Like the reactive wet scrubbing, this system can only remove SO_2 and not H_2S.
- While high efficiencies are achievable, these are still lower compared to similar wet scrubbing systems.

This method can be combined with the Claus process. The Claus process removes H_2S by oxidising it to elemental sulphur. It may be used in this fashion or as a partial oxidation which would then convert the H_2S to SO_2 which could then be removed by the dry scrubber. The Claus process proceeds through the following chemical reaction:

$$H_2S + 1.5O_2 \rightarrow SO_2 + H_2O \quad (2\text{-}8)$$

$$2H_2S + SO_2 \rightarrow 3S + 2H_2O \quad (2\text{-}9)$$

$$H_2S + 0.5O_2 \rightarrow S + H_2O \quad (2\text{-}10)$$

The complete Claus process has an H_2S removal efficiency of up 95% and may be controlled to be partially oxidising by altering the oxygen to hydrogen sulphide ratio. The Claus process for large acid streams are in excess of 15% H_2S (Siefers, 2010).

2.2.3. Cold syngas desulphurisation

The sulphur compounds are extracted as H_2S from the syngas through a process called COS hydrolysis. In this process there is 99% conversion of COS to H_2S when the syngas moves through the catalytic hydrolysis reactor from the water scrubber (NETL, 2016). This process is governed according to the following reaction:

$$COS + H_2 \rightarrow CO + H_2S \tag{2.11}$$

This reaction is relatively pressure independent and occurs in an operating range of 350°F to 400°F over an activated alumina-based catalyst (NETL, 2016). Figure 2-6 shows a simplified diagram of a cold syngas desulphurisation process used for Acid gas removal (AGR).

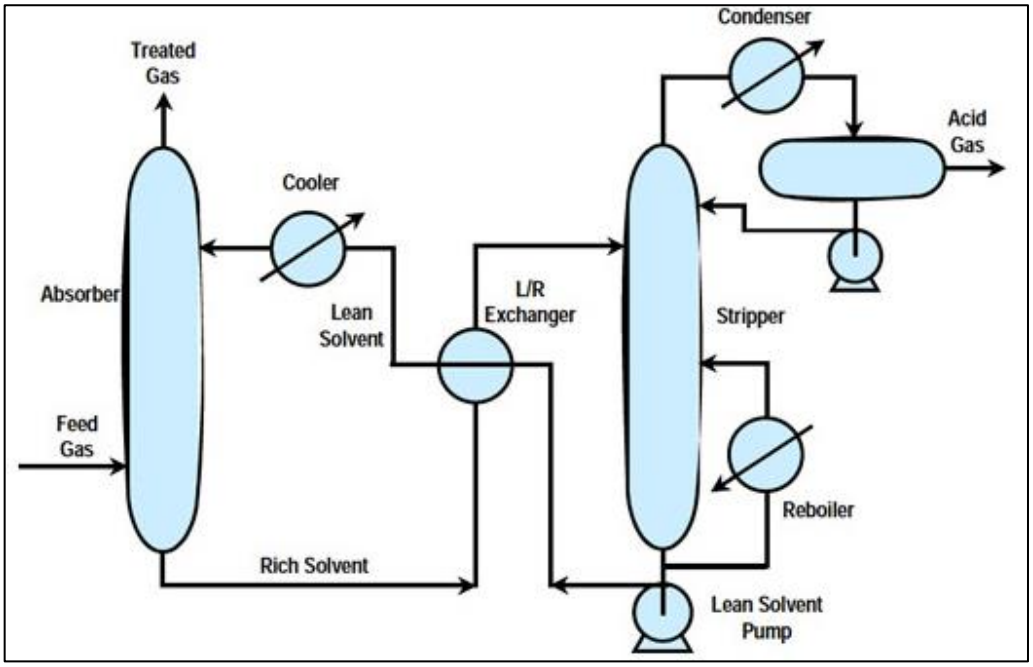

Figure 2-6: Simplified schematic of the cold syngas desulphurisation process (NETL, 2016)

The COS hydrolysis is followed by a countercurrent wet scrubbing process with liquid phase amine (lean solvent) to remove the H_2S (Gupta, Turk and Portzer, 2001). This is called a MDEA (Methyl-Diethanolamine) absorber. MDEA is a regenerable solvent used due to its high selectivity for hydrogen sulfide over carbon dioxide (Pacheco and Rochelle, 1998). In the absorption process the H_2S chemically dissociates as follows:

$$H_2S \leftrightarrow H^+ + HS^- \tag{2.12}$$

The MDEA solvent in turn reacts with the H^+ ions from the H_2S dissociation, governed by the following reaction:

$$MDEA + H^+ \leftrightarrow (MDEA)H^+ \tag{2.13}$$

The H_2S-free syngas exits at the top of the MDEA absorber. The rich solvent exits at the bottom of the absorber column and is heated, by a liquid-liquid heat exchanger to 90°C, before being passed to the stripper column. The stripper column acts as a regenerator in which the higher temperature gradient promotes the release of H^+ ions. These H^+ ions react with the HS^- in the solvent to form H_2S. The H_2S-rich stream then passes out the top of the stripper column through a condenser to separate the sorbent vapours and water from the acid gases which are sent for further treatment. The lean solvent from the stripper column bottom is then cooled and pumped back to the absorber column.

2.2.4. Hot syngas desulphurisation

Hot gas desulphurisation (HGD) is an improvement on conventional desulphurisation. There is no wastage of energy due to the syngas needing to be cooled down to nearly ambient temperatures. HGD is an efficient method which uses regenerable metal oxide sorbents to remove COS and H_2S from syngas at high pressure and high temperature (Yi et al., 2001). It is typically a dry process where the only moisture is present in the form of water vapour from the combusted fuel. Used for fuel and power utility flue gas cleaning, HGD mainly comprises of dry sorbents made of inorganic and metal oxides in a packed or fluidized bed reactor unit. The process usually occurs downstream of the gasifier and before being fed to the gas turbine (See Figure 2-1). Due to the ability of this process to occur at high temperatures, there is a higher associated thermal efficiency (as compared to wet and dry scrubbing techniques) and subsequently more efficient power generation. Typically HGD is carried out in fluidized bed reactors as they provide better gas-solid contact via vigorous agitation of the sorbent particles which effectively minimises the diffusional resistance giving rise to faster overall reaction kinetics (Gangwal, Harkins and Jain, 1990). Fluidized beds also make it possible to achieve a continuous, steady state within the reactor; eliminating any downtime required to replace sorbent as is the case with a fixed bed. When considering HGD, there are several key factors to consider:

- Ease of regeneration.
- Adsorption capacity (when the sorbent is saturated, metal sulphide will oxidize to SO_2).
- Its melting point and relative thermal stability.
- Cost of initialising and cost of continuous sorbent use should it not be regenerable.
- Reactive nature with the components of flue gas.
- Type of sorbent to be used.

Raharjo et al. (2010) studied the use of molten alkali carbonates for the purpose of both H_2S and CO_2 removal from hot gas. The results of this study showed that there was complete removal of both H_2S and CO_2 at high temperatures of ~900 °C. Parts of the spent molten were also found to be able to be regenerated at temperatures of ~380 °C using CO_2 as the regeneration agent.

Much research has been conducted with regards to the use of metal oxides and supported metal oxides for use in HGD. Yang (2007) showed that the optimum value for H_2S adsorption capacity was 33 wt. % ZnO loading. Thereafter there was a rapid decline up to a limit of 50 wt. % ZnO loading. Wang & Yang (2014) showed similar results, indicating that the optimum loading of ZnO on mesoporous silica lies between 10 and 30 wt. %.

Atimtay et al. (1993) demonstrated the use of copper and manganese oxides dispersed onto silica-rich zeolites. This was used to remove H_2S at temperature around 850 °C. The results showed that during HGD, there existed the possibility of a side reaction in the presence of zeolites where H_2S can be converted to carbonyl sulphide (COS) in the presence of carbon monoxide (CO). However, it can also occur that the metal oxide absorbent will convert the COS to CO_2.

The use of zinc-oxide based sorbent have been noted to be a low cost and highly efficient method to reduce the H_2S content in syngas to the ppm level (Sanchez, Ruiz and Otero, 2005). This is the basis for the experimental work that will be undertaken in this dissertation.

2.2.5. Sulfidation and sorbent regeneration

For regenerable hot gas desulphurisation to occur, the following two reactions are needed:
Sulfidation

$$ZnO_{(S)} + H_2S_{(g)} \rightarrow ZnS_{(S)} + H_2O_{(g)} \qquad (\Delta H = -79\ kJ/mol) \qquad (2.14)$$

Regeneration

$$ZnS_{(S)} + 1.5O_{2(g)} \rightarrow ZnO_{(S)} + SO_{2(g)} \qquad (\Delta H = -439.1\ kJ/mol) \qquad (2.15)$$

The raw syngas is passed through the zinc-oxide sorbent where it is desulphurised to form the sulfur-free syngas (Equation 2-14). The zinc-oxide is converted to zinc sulphide and is referred to as a spent sorbent. An oxygen gas reactant is passed through the spent sorbent to form the regenerated zinc-oxide sorbent and $S0_2$-rich gases (Equation 2-15).

2.3. Sorbents

2.3.1. Introduction

When choosing a sorbent there are many factors to be considered. Most especially regarding the ease of regeneration, likelihood of spalling and the temperatures at which the sorbent begins to activate and deactivate. A major concern with the selection of regenerable sorbents is the formation and accumulation of sulphates in the sorbent during use. Accumulation of sulphates is undesirable as it not only affects the efficiency with which sulphur can be removed by the sorbent, but may also be capable of causing spalling of the sorbent pellets. This results in fatal failures during the process; zinc oxide supported by titanium dioxide is an example of a sorbent which exhibits such a characteristic.

The chemical affinity of H_2S to metal cations promotes research into the removal of H_2S with the use metal oxide sorbents. Most research is focused on the reactive removal of H_2S using various supported and unsupported metal oxides.

2.3.2. Sorbent selection

2.3.2.1. Metal oxides

The removal of H_2S from syngas using metal oxides based sorbents is supported by the chemical affinity of H_2S to metal cations and surface metal sites (Wang and Yang, 2014). Properties of a good sorbent (Wang and Yang, 2014):

- Low toxic and low corrosive properties.
- Under the effects of moisture it should not degrade.
- Easy regeneration at relatively low temperatures.
- Easily producible for industrial scale processes.
- High selectivity and stability.
- Disposable as a non-hazardous material after its lifespan.
- High H_2S absorption capacity and uptake rates.

For each oxide, there exists a pH at which the surface will not be charged (Table 2-7). This pH is termed the isoelectric point (IEPS). At a pH above the IEPS, the surface becomes negatively charged and allows for the adsorption of cations; the converse applies at a pH below the IEPS (Pinna, 1998).

Table 2-7: Isoelectric points for different inorganic and metal oxides (Pinna, 1998)

Oxide	IEPS	Adsorption
Sb_2O_5	<0.4	Cations
WO_3	<0.5	
SiO_2	1.0–2.0	
U_3O_8	≈4	Cations or anions
MnO_2	3.9–4.5	
SnO_2	≈5.5	
TiO_2	≈6	
UO_2	5.7–6.7	
γ-Fe_2O_3	6.5–6.9	
ZrO_2 hydrous	≈6.7	
CeO_2 hydrous	≈6.75	
Cr_2O_3 hydrous	6.5–7.9	
α-, γ-Al_2O_3	7.0–9.0	
Y_2O_3 hydrous	≈8.9	Anions
Fe_2O_3	8.4–9.0	
ZnO	8.7–9.7	
La_2O_3	≈10.4	
MgO	12.1–12.7	

Choice of support material can play a significant role in the effectiveness of the prepared sorbent. The use of inert supports, commonly inorganic oxides such as silica and alumina, helps to alleviate the loss of surface area and reduce the effects of sintering and evaporation that occur when a pure metal oxide is used as sorbent (Wang & Yang, 2014). A support material is deemed acceptable based on some of its characteristics. These characteristics include (Perego and Villa, 1997):

- Inertness.
- Mechanical properties such as attrition resistance.
- Great stability and fortitude under regeneration and reaction conditions.
- High surface area without having the particle being too small.
- Pore size distribution, average pore size with respect to porosity.

Many unsupported and supported metal oxide based sorbents have been manufactured for the reactive absorption of H_2S at moderate to high temperatures (200-800°C). Higher temperatures favour higher equilibrium constants, hence better absorption. Fe, Mn, Zn, Ca, Ba, Co, Cu are among some of the most common metal oxides that are deemed thermodynamically feasible for high temperature desulphurisation applications such as coal gas desulphurisation (Wang and Yang, 2014).

To achieve a highly active sorbent it is required to have a sufficiently high metal dispersion. This is accomplished by depositing the metal oxide onto an inert support material with a large specific surface area. Alumina, silica, clay and zeolite supports are commonly used since they are thermo-stable and highly porous. Porous supports also favour the regeneration of the metal oxide and prevent the agglomeration of metal oxides particles (Yang and Tatarchuk, 2010). Metal oxides themselves are subject to surface area losses and sintering at high temperatures and pressures. It is believed that support materials can stabilize the active metal oxide and prevent metal reduction in the presence of hydrogen and carbon monoxide (Yang and Tatarchuk, 2010). In the temperature range of (200-800°C) silica is a better support than alumina for regenerable desulphurisation applications (Yang and Tatarchuk, 2010).

(Wang and Yang, 2014), showed that at high wt. % loading of zinc and copper oxide, the sorbents form clusters (agglomerate) which block the pores of the sorbent. This hinders the absorption of H_2S gas into the pores to react with the remainder of the dispersed metal oxides. This effectively only allows the larger metal oxide particles on the surface of the sorbent to react with H_2S. Conversely, lower loadings of metal oxide particles are relatively evenly dispersed and more metal oxide particles are capable of reacting with H_2S; Figure 2-7 shows these effects.

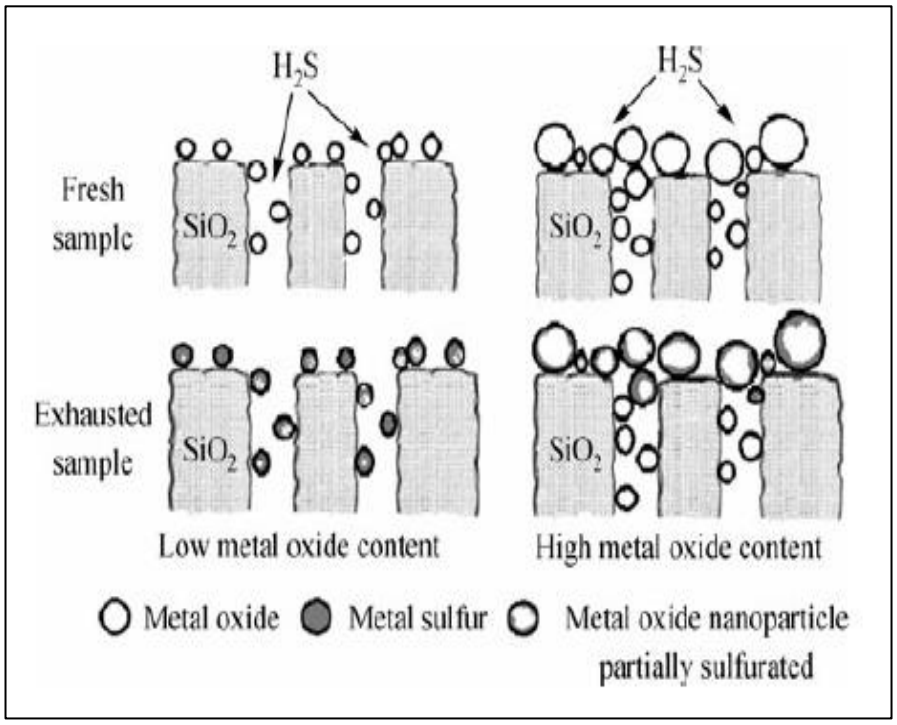

Figure 2-7: Schematic representation of the reaction process for low and high metal oxide content

2.3.2.2. Zinc-oxide based sorbents

ZnO has an elevated equilibrium constant and sulphur absorption capacity in the temperature range of 300-500°C. Due to these properties, it can be utilized in the removal of H_2S (Yang and Tatarchuk, 2010). The equilibrium limitation at low to moderate temperatures in the presence of excess water restricts sorbents (such as ZnO and regenerated sorbents) from removing H_2S below a concentration of 0.1 ppmv. The presence of carbon monoxide and carbon dioxide, which initiates the formation of carbonyl sulphide, also enhances the difficulty of removing sulphur. ZnO is not an efficient sorbent for absorbing the carbonyl sulphide formed.

CuO and ZnO based sorbents have been studied extensively for their regeneration capabilities in high temperature desulphurisation applications. Theoretically ZnO has a very high sulphur adsorption capacity, whereas CuO possesses an extremely high equilibrium constant which results in very low equilibrium concentrations of H_2S even in the presence of excess moisture.

ZnO supported on SiO_2 (ZnO/SiO_2), displayed an enhancement in high sulphur removing and breakthrough capacity at elevated temperatures (Figure 2-8). ZnO/SiO_2 sorbents demonstrated minimized intraparticle mass transfer resistance since most of the ZnO reacted (Yang and Tatarchuk, 2010)

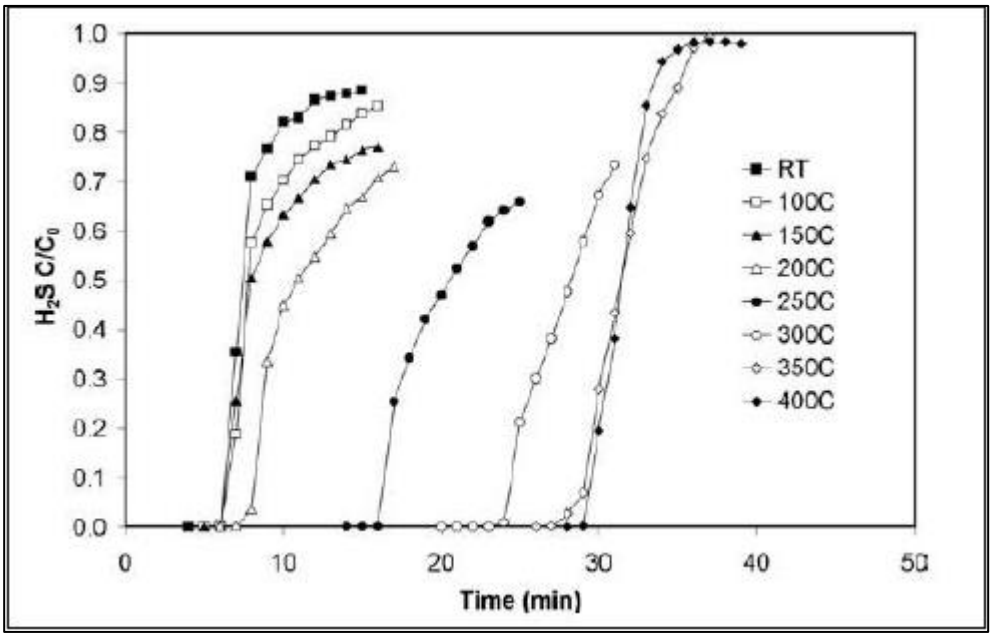

Figure 2-8: Breakthrough capacity of ZnO/SiO_2 at various desulphurisation temperatures (Yang and Tatarchuk, 2010)

The choice of metal oxide can be seen to depend on the operating temperature of the selected process. The research of Westmoreland and Harrison (1976) revealed the stability of various metal oxides over a temperature range of 0 – 1400 ℃ (Table 2-8). Zinc, cobalt and iron based sorbents were classified as medium temperature sorbents, operating in the range of 300 – 500 ℃. In order to achieve high adsorption, higher temperatures are preferred. By inspection of Table 2-8, it can be seen that barium, calcium and strontium will be unlikely to fulfill the low temperature requirement as they only begin to absorb sulphur at temperatures in excess of 800 °C. These metal oxides will form metal sulphides which can be converted to metal sulphates, thereby increasing the weight of the sorbent, which typically decompose at a temperature of 740 °C (Atimtay and Harrison, 2013).

Table 2-8: Metal oxides stability as a function of temperature in Hot Gas Desulphurisation (Westmoreland and Harrison, 1976)

Barium	**No Sulphiding**		BaS			**BaS Melts**
			$BaCO_3$			
Calcium	**No Sulphiding**		CaS			
			$CaCO_3$			
Cobalt	CoS				**CoS Melts**	
	$CoO \rightarrow Co$					
Copper	Cu_2S				**Cu_2S and Cu Melts**	
	Cu					
Iron	$FeS_2 \rightarrow FeS$					**FeS Melts**
	$Fe_3O_4 \rightarrow FeO, Fe_3C, Fe$					
Manganese	MnS					
	$MnCO_3$ MnO					
Molybdenum	MoS_2					**MoS_2 Melts**
	$MoO_2 \rightarrow$ Mo					
Strontium	**No Sulphiding**		SrS			
			$SrCO_3SrO$, $SrCO_3SrO$			
Tungsten	WS_2					**WS_2 Decomposes**
	$WO_3 \rightarrow WO_2 \rightarrow WO_2$, WC - WC					
Vanadium	V_2S_3		**V_2S_3 Melts**			
	V_2O_3					
Zinc	ZnS		**Zn(g) Becomes significant**			
	ZnO					
0	**400**	**600**	**800**	**1000**	**1200**	**1400**

Temperature °C

2.3.3. Sorbent preparation

The purpose of the preparation of supported sorbent materials is to obtain a product with a high selectivity for the component to be removed and stability. The active phase, the supported metal oxide, must be widely dispersed in order to achieve a large surface area and subsequently, a maximum activity. In order to achieve this objective the active metal is adsorbed onto the surface and absorbed into the pores of a highly porous and thermally stable support material. The preparation of dispersed metal oxides requires a combination of:

- Impregnation of the metal precursor onto the support material
- Drying
- Calcination

2.3.3.1. Impregnation

There are two types of impregnation techniques classified as the incipient wetness (or dry) impregnation technique and wet (or soaking) impregnation technique. The incipient technique involves using a volume of solution containing the metal precursor, which is less than the pore volume of the support. In this method the solution is sprayed onto a constantly stirred support. The wet impregnation technique was selected for this experiment. This method uses a volume of solution which is greater than the pore volume. The sorbent is the constantly stirred, filtered and oven dried. This technique is used for low-loading sorbents because multilayer adsorption is not possible.

The concentration of the metal precursors deposited onto the support is dependent upon the concentration of the solution and pore volume of the support, but also on the concentration of absorbing sites existing at the surface. Commonly used inorganic oxide support materials such as, Al_2O_3, SiO_2, MgO, tend to polarize and become surface charged when submerged into an aqueous solution. The charge is dependent on the pH of the solution. Another important characteristic of the support material is that it should be inert. While there is insufficient documented experiments using pure $Si0_2$ as the sorbent for desulphurisation, Yang (2007) has conducted experiments to quantify the inertness of this support. These experiments discuss the effect of diluting a fixed volume of $ZnO/Si0_2$ sorbent with progressively larger volumes of SiO_2 particles. The breakthrough results confirmed that the $ZnO/Si0_2$ sorbent packed bed and the diluted packed beds shared the same breakthrough curve. This confirmed that SiO_2 is an inert support.

The Ultrasonic-assisted Impregnation (UAI) technique is used to more evenly disperse the metal oxide onto the support material. This ultrasonic-assisted method is referred to as Sonochemistry. The ultrasonic sound waves cause the molecules to oscillate, during rarefaction and compression cycles, about their average positions (Bianchi et al., 1993). As the oscillations proceed, cavitation bubbles are formed in the liquid-solid slurry due to the critical molecular distance of the molecules being exceeded (Bianchi et al., 1993). Highly dense ultrasonic energy is generated when the cavitation bubbles implode releasing the stored energy rapidly (Bang and Suslick, 2010). These high velocity jets force the metal oxide precursor into the pores of the silica support by removing the passivating surface coatings (Bianchi et al., 1993). Research proves that the UIA technique gives rise to faster reaction times, increased uniformity of size distribution as well as higher surface area, for the metal oxide based sorbents (Bang and Suslick, 2010).

IEPS for SiO_2 is between 1 and 2. To prepare ZnO/SiO_2 sorbents it is suitable to use deionised water as the solution to ensure Zn^{2+} ions are attracted to the SiO_2 surface.

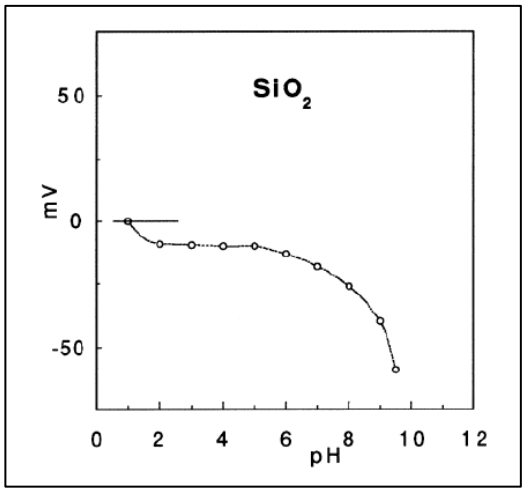

Figure 2-9: Zeta potential curve vs. pH for SiO_2 (Pinna, 1998)

2.3.3.2. Drying

After impregnation, the material undergoes drying at temperatures of 100 – 120 °C in order to evaporate and remove any of the solvent (typically water) used during impregnation step. The temperature of the oven, the period of drying, type of atmosphere can influence the rate of drying. The desired conditions are different for each system. Pinna (2014) showed that if the rate of drying is slow, the evaporation of the

solvent permits the diffusion of the salt into the liquid deeper in the pore. This results in an increased concentration of metal precursor at the bottom of the pore after precipitation. Too high drying rates cause temperature gradient to develop, which force the solution out of the pores to the outer surface where precipitation occurs (Pinna, 1998). In order to obtain a uniform distribution, the rate of drying has to be higher than the rate of homogenization of the solution. During this process, the wet metal precursor dispersed onto the support is usually converted into a hydroxide.

2.3.3.3. Calcination

This process mainly involves heating the sorbent in an oxidising atmosphere at a recommended temperature usually little higher than that which will be encountered during the reaction. Calcination decomposes hydroxide formed during drying in order to form the required metal oxide. The anions or the cations introduced during the impregnation step are also removed (Pinna, 1998).

CHAPTER 3: GAS-SOLID REACTION MODELLING

This chapter adapted from (Levenspiel, 1999) and (Ali, 2015) will cover the gas-solid reaction modelling of a packed-bed desulphurisation reactor.

3.1. Introduction

Gas-solid reactions are commonly used in chemical industries for coal gasification. In the field of extractive metallurgy the use of gas-solid reactions is prominent through a process called roasting. This process occurs at elevated temperatures and includes Sulfidation, Reduction and Oxidation of metal oxides as well as Calcination. It is therefore imperative to understand the mechanisms for gas-solid reactions to plan the experimental design and interpret the experimental results.

The general formula for gas-solid reactions:

$$aA_{(g)} + bB_{(s)} \leftrightarrow cC_{(g)} + dD_{(s)} \tag{3.1}$$

Szekely, Evans and Sohn (1976) based this mechanism on a gas stream passing over a single particle. This can be summarized by the following assumptions:

- Gaseous reaction product diffusion through the pores of the solid support.
- Chemical surface reaction on the solid support.
- Mass transfer from the bulk phase gas stream – to the solid particle exterior surface – of the gaseous reactant.
- Gaseous product desorption from the surface of the solid support.
- Mass transfer from the solid particle exterior surface – to the bulk phase gas stream – of the gaseous product.
- Gaseous reactant adsorption on the surface of the solid support.
- Gaseous reactant diffusion through the pores of the solid support.

The rate controlling step is determined by whichever of the above mechanisms shows the greatest resistance with respect to the reaction. The effect of the above mechanisms on a single particle is shown in Figure 3.1.

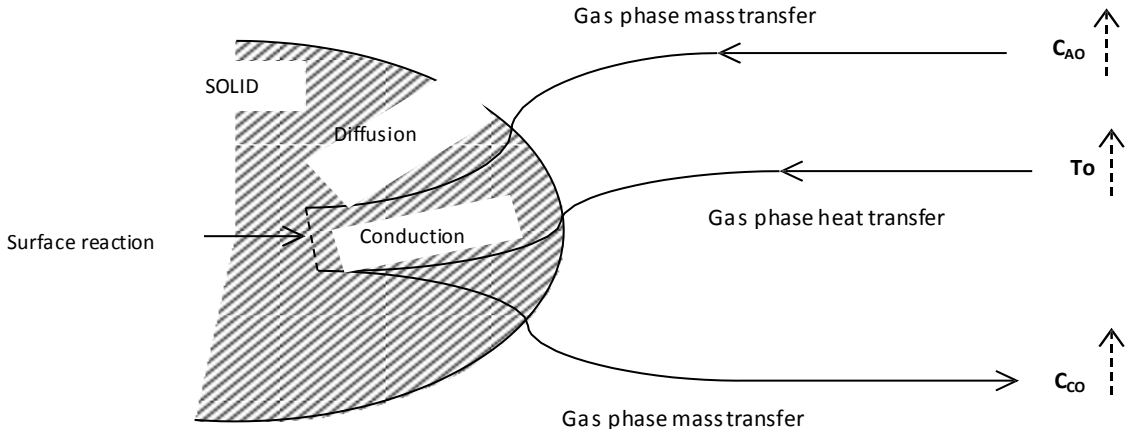

Figure 3-1: Reaction mechanism of a gas passing over a single solid particle (Szekely, Evans and Sohn, 1976)

3.2. Mathematical models

Mathematical models are predictive models for determining how gas-solid reactions will proceed at varying conditions. These models incorporate reaction kinetics, mass transfer and pore diffusion effects to simulate the conditions as close to reality as possible. In this section a single particle model, the shrinking core model, which is applicable to the HGD process will be discussed. Thereafter these single particle models will be integrated into a packed bed model. This resultant model will be used to describe the system used in this dissertation.

3.2.1. Shrinking Core Model

The establishment of the shrinking core model (SCM) was accredited to Yagi and Kunii (1955). This model was developed to describe how solid particles are consumed by either a reaction or dissolution. A gas film initially surrounds the non-porous solid. Thereafter mass transfer occurs between the bulk gas phase and solid particles. Due to the proceeding reaction, the solid particle 'shrinks' leaving an ash layer formation around the unreacted core (Gbor and Jia, 2004). SCM can be visualized by the following steps (Figure 3-2):

1. Reactant A in the gas phase diffuses through the gas film to the solids surface.
2. Further diffusion of reactant A as it passes through the ash layer to the unreacted core.
3. Gas-solid reaction between solid surface and reactant A (Equation 3.1).

4. Gaseous product C diffuses through ash layer to the solid surface exterior.
5. Further diffusion of gaseous product C as it passes back to the bulk fluid from the gas film.

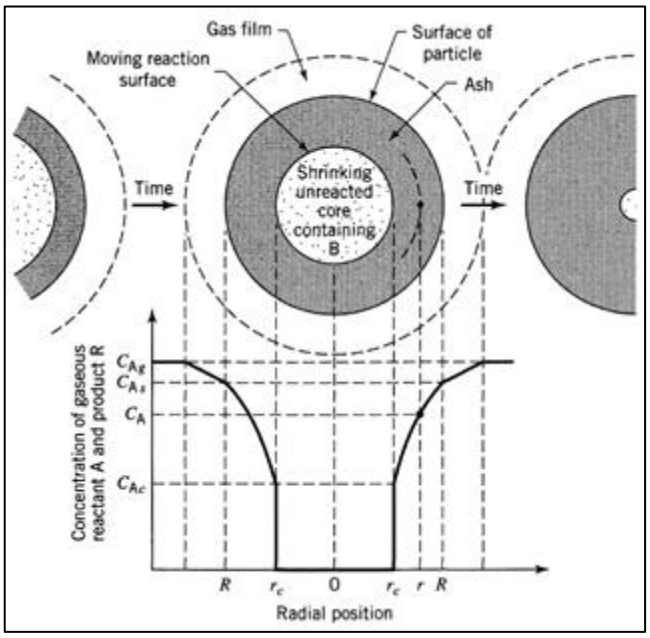

Figure 3-2: Representation of Shrinking Core Model (Levenspiel, 1999)

In some cases not all of the steps will occur. It is therefore important to determine the rate-limiting step to develop the rate equation. For this dissertation the step with the greatest resistance was considered as rate-controlling. Cases where steps 1, 2 and 3 were rate-controlling are detailed for solid spherical particles to develop the conversion equations (Levenspiel, 1999).

3.2.1.1. Gas film diffusion controlling

In the case where step 1 is rate-controlling, the concentration profile of reactant A in the gas phase is depicted by Figure 3-3. It is shown that there is no reactant A in the gas phase on the particle surface, hence, the concentration of the gas film (C_{Ag}) becomes the driving force. Below is the rate of reaction, based on a single particle, for the moles of reactant A in the gas phase diffusing per unit time:

$$\frac{dN_A}{dt} = -4\pi R^2 k_g C_{Ag} \tag{3.2}$$

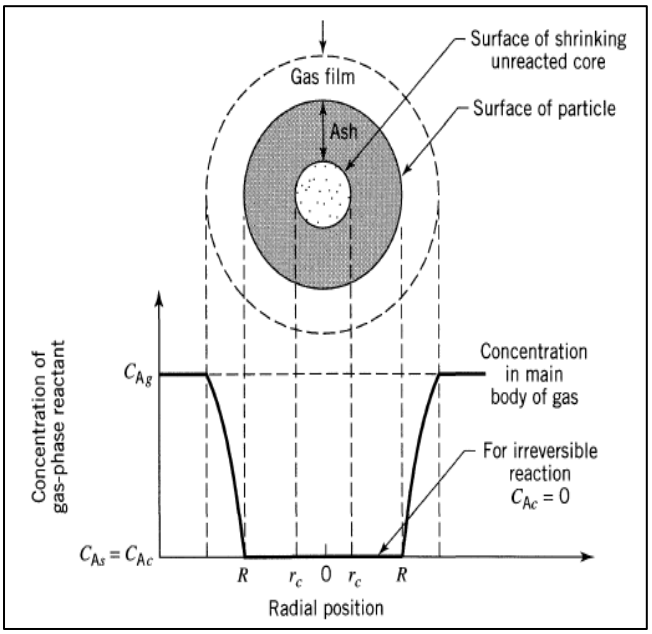

Figure 3-3: Representation of gas film diffusion rate-controlling in the SCM (Levenspiel, 1999)

The amount of moles of reactant B in the solid phase present in a particle is:

$$N_B = \rho_B V_p \tag{3.3}$$

The disappearance of reactant B in the solid phase as related to the decreasing radius of the unreacted core:

$$-dN_B = -\rho_B V_p = -\rho_B d\left(\frac{4}{3}\pi {r_c}^3\right) = (-\rho_B 4\pi {r_c}^2)dr_c \tag{3.4}$$

Using the stoichiometry of Equation 3.1:

$$-dN_B = -bdN_A \tag{3.5}$$

The rate of reaction with respect to the decreasing radius of the unreacted core is obtained by combining Equations 3.2, 3.4 and 3.5:

$$\frac{dr_c}{dt}\frac{-\rho_B {r_c}^2}{R^2} = C_{Ag} k_g b \tag{3.6}$$

Integrating this provides a relationship between the decreasing radius of the unreacted core and the time taken for this to occur:

$$t = \frac{R\rho_B}{3C_{Ag}k_g b}\left[1 - \left(\frac{r_c}{R}\right)^3\right] \tag{3.7}$$

Let X be the fractional conversion for a spherical particle:

$$X = \left[1 - \left(\frac{r_c}{R}\right)^3\right] \tag{3.8}$$

Hence, the relationship between the fractional conversion, reaction time and radius of the surface of the particle is given by:

$$t = \frac{R\rho_B}{3C_{Ag}k_g b}X \tag{3.9}$$

3.2.1.2. Ash layer diffusion controlling

In the case where step 2 is rate-controlling, the concentration profile of reactant A in the gas phase is depicted by Figure 3-4. For gas-solid systems in this regime, a steady-state is used to approximate the significantly higher flow rate of reactant A relative to the decreasing radius of the unreacted core. Below is the reaction, based on a single particle, for the rate of moles of reactant A in the gas phase diffusing through the ash layer per unit time:

$$\frac{dN_A}{dt} = -4\pi R^2 Q_A \tag{3.10}$$

The case of equimolar counterdiffusion in Fick's Law is used to express the flux of A:

$$Q_A = D_e \frac{dC_A}{dr} \tag{3.11}$$

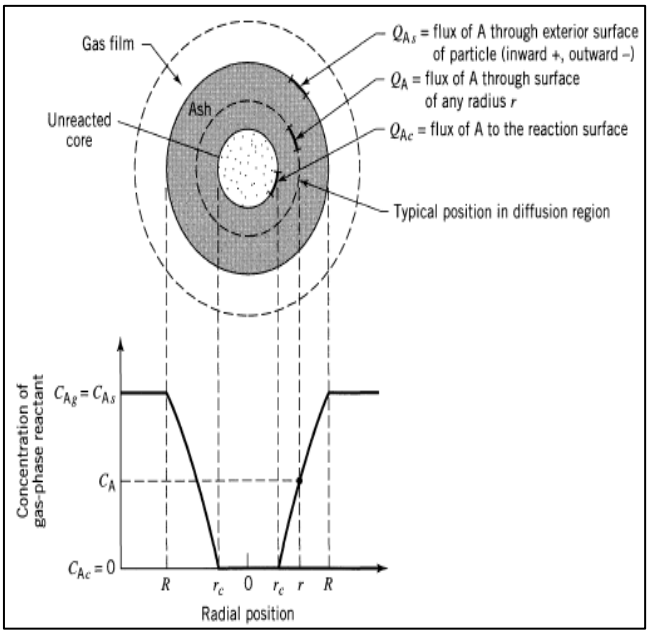

Figure 3-4: Representation of ash layer diffusion rate-controlling in the SCM (Levenspiel, 1999)

Integrating Equation 3.10 from R to r_c across the ash layer:

$$\frac{dN_A}{dt}\left(\frac{1}{r_c} - \frac{1}{R}\right) = -4\pi C_{Ag} D_e \tag{3.12}$$

To account for the decreasing radius of the unreacted core with time, Equations 3.4 and 3.5 are substituted into Equation 3.12 then integrated:

$$t = \frac{R^2 \rho_B}{6 C_{Ag} D_e b}\left[1 - 3\left(\frac{r_c}{R}\right)^2 + 2\left(\frac{r_c}{R}\right)^3\right] \tag{3.13}$$

Substituting Equation 3.8 into Equation 3.13 provides the relationship between the fractional conversion, reaction time and radius of the surface of the particle:

$$t = \frac{R^2 \rho_B}{6 C_{Ag} D_e b}\left[1 - 3(1-X)^{\frac{2}{3}} + 2(1-X)\right] \tag{3.14}$$

3.2.1.3. Chemical reaction controlling

In the case where step 3 is rate-controlling, the concentration profile of reactant A in the gas phase is depicted by Figure 3-5. The amount of available surface on the unreacted core influences the rate of reaction. Below is the rate of reaction, based on a single particle, for the rate of moles of reactant A in the gas phase reacting with the solid surface per unit time:

$$\frac{dN_A}{dt} = -4\pi {r_c}^2 C_{Ag} k \tag{3.15}$$

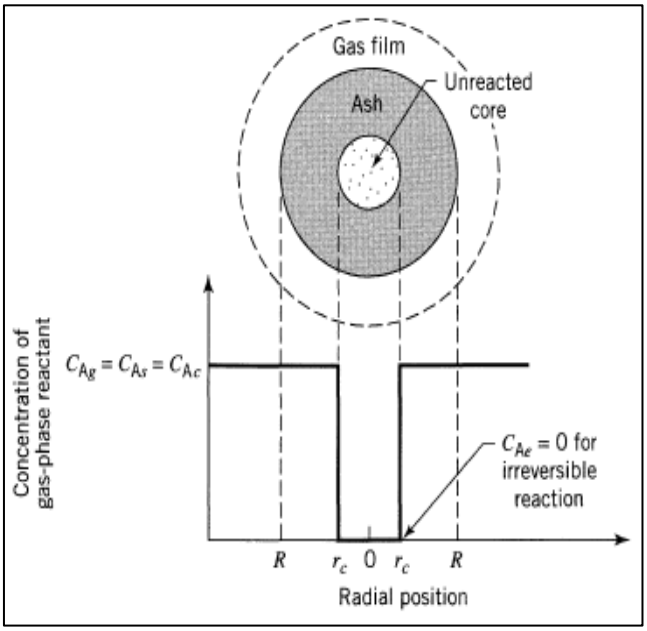

Figure 3-5: Representation of chemical reaction rate-controlling in the SCM (Levenspiel, 1999)

The disappearance of reactant B in the solid phase as related to the decreasing radius of the unreacted core:

$$-\rho_B \frac{dr_c}{dt} = C_{Ag} k b \tag{3.16}$$

Integrating Equation 3.16 from R to r_c:

$$t = \frac{\rho_B}{C_{Ag} k b}(R - r_c) \tag{3.17}$$

Substituting Equation 3.8 into Equation 3.17 provides the relationship between the fractional conversion, reaction time and radius of the surface of the particle:

$$t = \frac{\rho_B R}{C_{Ag} k b}(1 - (1 - X)^{1/3}) \tag{3.18}$$

It is seen that throughout the conversion of the particle, gas film diffusion controlling, ash layer diffusion controlling and chemical reaction controlling share a relative importance. Due to linearity of the concentrations for these three cases, the summation of the times needed for each resistance will be the overall conversion time for the particle:

$$t = \frac{R\rho_B}{3C_{Ag}k_g b} X + \frac{R^2 \rho_B}{6C_{Ag} D_e b}\left[1 - 3(1 - X)^{\frac{2}{3}} + 2(1 - X)\right] + \frac{\rho_B R}{C_{Ag} k b}(1 - (1 - X)^{1/3}) \tag{3.19}$$

Hence the overall rate of reaction can be simplified as:

$$-r_A = \frac{4\pi R^2 C_{Ag}}{\frac{1}{k_g} + \frac{(R - r_c)R}{D_e r_c} + \frac{R^2}{k {r_c}^2}} \tag{3.20}$$

3.3. Packed-bed reactor modelling

The shrinking core model was chosen as the basis of this reactor modelling. Variables that were otherwise unobtainable were sourced from experimental data of research with similar process variables (Yang, 2007). To ensure the simplicity of calculations, the following assumptions were made:

- Plug-flow conditions
- Equimolar counterdiffusion
- Isothermal conditions

Developing the mass balance for species A, where ε is the packed bed porosity (or void fraction) and u is the velocity of the gas mixture diffusing through the packed bed:

$$\varepsilon \frac{\partial C_A}{\partial t} = -u \frac{\partial C_A}{\partial z} - r_A \tag{3.21}$$

Due to the low pressure nature of species A in the system, a steady state assumption is made, which simplifies Equation 3.21 to:

$$u \frac{\partial C_A}{\partial z} = -r_A \qquad , C_A(z=0) = C_{A0} \tag{3.22}$$

Developing the mass balance for species B:

$$\frac{\partial C_B}{\partial t}(1-\varepsilon) = -b r_A \qquad , C_B(t=0) = C_{B0} \tag{3.23}$$

The rate of consumption of species A:

$$r_A = \frac{dN_A}{dt}\frac{1}{V} \tag{3.24}$$

The rate of consumption of species A based on a single spherical particle:

$$r_A = \frac{dN_A}{dt}\frac{3(1-\varepsilon)}{4\pi R^3} \tag{3.25}$$

By substituting Equation 3.20 in terms of fractional conversion into Equation 3.25, the overall rate of reaction is derived:

$$r_A = \frac{3(1-\varepsilon)}{R}\left[\frac{1}{k(1-X)^{\frac{2}{3}}} + \frac{1}{k_g} + \frac{R}{D_e}\left((1-X)^{-1/3} - 1\right)\right]^{-1} \tag{3.26}$$

The following equations were developed substituting the overall rate of reaction into Equation 3.21 and Equation 3.23:

$$\frac{\partial X}{\partial z} = -\frac{r_A}{uC_{A0}} \tag{3.27}$$

$$\frac{\partial C_A}{\partial z} = -\frac{r_A}{u} \tag{3.28}$$

$$\frac{\partial C_A}{\partial t} = -u\frac{\partial C_A}{\partial z} + D_e\frac{\partial^2 C_A}{\partial z^2} + r_A \tag{3.29}$$

This system of ODEs can be solved using an implicit numerical method (4th order Runga-Katta, ode 45 in *Matlab*) with the below initial conditions:

$$X(z, t = 0) = 0 \tag{3.30}$$

$$C_A(z = 0, t) = 1 \tag{3.31}$$

$$C_A(z, t = 0) = C_{A0} \tag{3.32}$$

CHAPTER 4: EXPERIMENTAL METHODS

4.1. Experimental design

Before the starting runs were conducted, the experiment was planned. This was done to determine exactly what data was desired from an experiment, how it was going to be obtained from the apparatus and how it realizes the goals of the study.

Experimental variables

The independent variables for this experiment should remain constant during each run. These variables are listed below:

- Pressure of gas mixture through the system (125 kPa discharge from tank).
- Gas composition (H_2S 1ppm, remainder N_2) and flowrate. The inlet concentration of H_2S in the gas mixture was10000 ppm (volume basis). This corresponds to 1 vol%.
- Desulphurisation and regeneration temperatures of the reactor.
- Sorbent
    - Surface area.
    - Type and preparation method.
    - Mass of ZnO loaded onto the silica support in reactor.
- Space velocity
    - In reactor: determined by flowrate and the volume of sorbent in the bed.
- Oxygen composition and flow rate.

The dependent variables depend on the values of the independent variables previously mentioned:

- The conversion of zinc oxide to zinc sulphide (Equation 2-14).
- The conversion of zinc sulphide to sulphur dioxide (Equation 2-15).
- The outlet concentration of H_2S: determined by the extent of reaction.
- The regeneration and desulphurisation time.
- The outlet volumetric flowrate of gas from the reactor.
- Sorbent saturation capacity.

This study involved the following sets of experimental work each having a specific objective:

1. Prepare ZnO/SiO_2 sorbents using the wet impregnation technique and an ultrasonically assisted wet impregnation technique. The aim was to increase the dispersion of zinc oxide onto silica.
2. Comparing the dispersion -of the zinc oxide on the surface of the silica support- of the different ZnO/SiO_2 sorbents using microscopy techniques.
3. The last step of the experimental work involved the hot gas desulphurisation of the gas mixture and regeneration of the ZnO/SiO_2 sorbents. The effect of the following variables on desulphurisation and regeneration time as well as sorbent capacity were investigated:
   - The wt. % ZnO loading onto silica
   - The reaction temperatures
   - The ultrasonically assisted wet impregnation technique sorbent compared to the conventional wet impregnation technique sorbent

The experiment was designed to be a 3^2 factorial design with two independent variables and three levels for each variable. The aim of the experimental design is to evaluate the effect of wt. % ZnO loading and desulphurisation temperature -both with and without sonication- on the breakthrough time achievable. The following general set up will be used:

Table 4-1: Summary of Experimental design

		Non-sonicated					Sonicated		
Loading	30%	Run 1	Run 2	Run 3	Loading	30%	Run 10	Run 11	Run 12
	20%	Run 4	Run 5	Run 6		20%	Run 13	Run 14	Run 15
	10%	Run 7	Run 8	Run 9		10%	Run 16	Run 17	Run 18
		350 °C	450 °C	550 °C			350 °C	450 °C	550 °C
		Temperature					Temperature		

A preliminary process design was considered based on the existing equipment set-up in the lab. Figure 4-1 depicts a process flow diagram of this preliminary process design.

4.2. Preliminary process design

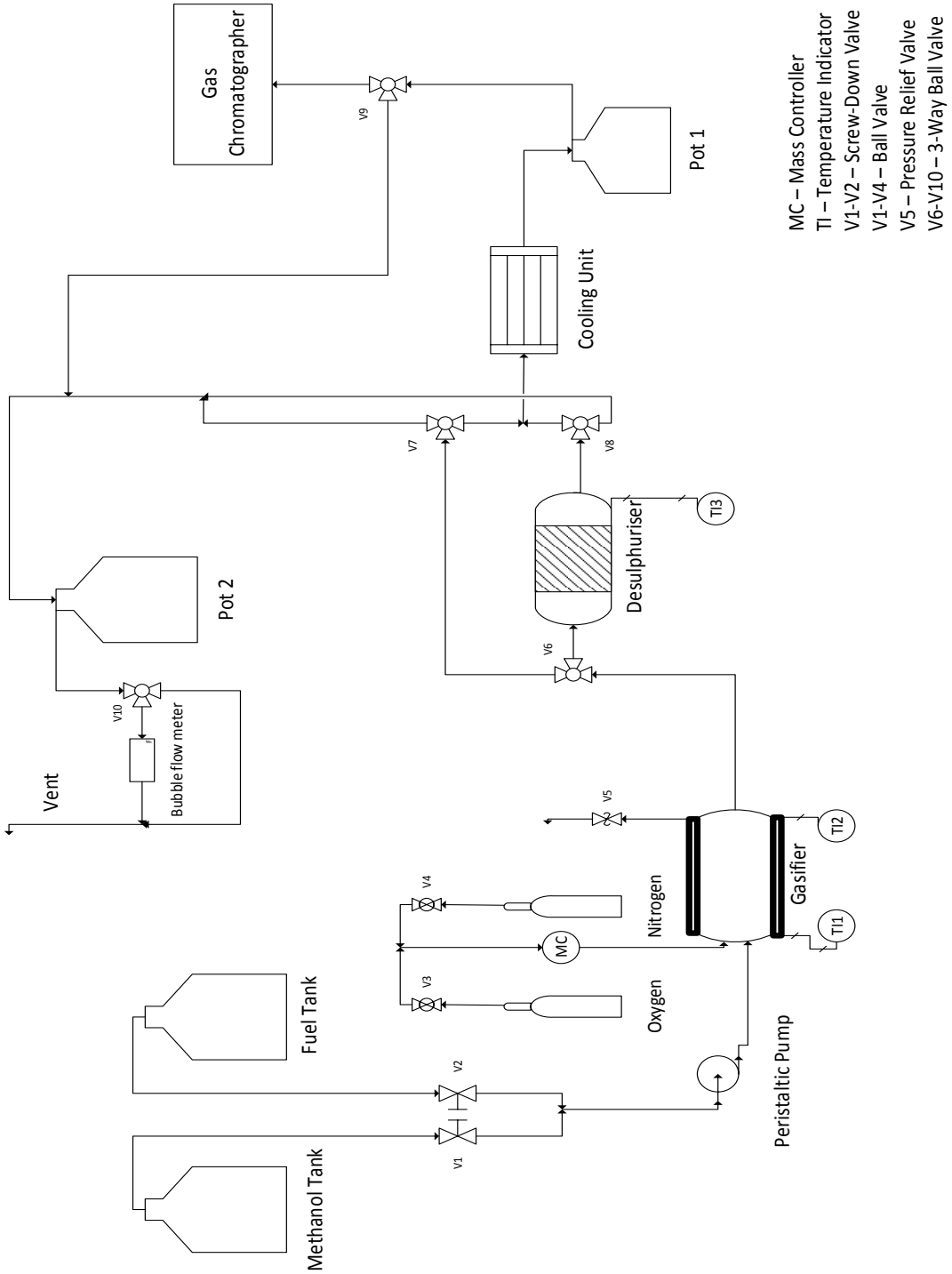

Figure 4-1: Process flow diagram of preliminary process design

4.2.1. Gasification process equipment

The gasification reactor was fabricated by GM Heating (Pty) Ltd and contains its own tubular furnace. The reactor is manufactured -using stainless steel 316- to withstand the corrosive nature of H_2S. The tubular reactor contains a 600 mm long tube with an I.D. of 37 mm. The reactor is fitted with 3 K-type thermocouples to measure the temperature at the inlet, centre and exit respectively. The thermocouples are connected to a temperature control panel with a set point of 830°C. This temperature was selected since all syngas components form at this temperature and don't vary with an increase in temperature. The furnace housing is stainless steel and insulated with glass wool.

The fuel (a mixture of methanol and propanethiol) was pumped using a Watson Marlow 101U/R peristaltic pump operating at 7 rpm. The oxygen did not require a pump since the cylinder was pressurised and the pressure was controlled using a gas regulator. Methanol and 1-propanethiol have relatively low boiling points of 64 and 67 °C respectively. Therefore, the fuel inlet tube was coiled around the reactor to use the heat of the reactor to vapourise the fuel. The purpose of this is to ensure efficient mixing between the oxidant and the fuel.

The fuel mixture was stored in a 3-litre sealed glass fuel tank and the inlet hole was fitted with an O-ring to which a pipe was connected and passed into the extractor to avoid the smell of propanethiol permeating throughout the lab. This also prevented a vacuum from being created through the pumping action. When refilling the fuel tank, the pipe was detached from the O-ring and the tank was taken into a fume-hood. Pure methanol was contained in a 1-litre sealed glass methanol tank. Conical pots filled half way with water served the purpose of cooling gas flows and condensing the steam. This prevented the backflow of water and excess condensate in the exit pipes.

4.2.2. Proposed change of process design

After considering the objectives of this study, it was determined that they could be met with a simpler, more energy efficient and less resource wasteful process design. The primary use of the gasifier was to form a syngas from the gasification of the fuel mixture. As this was not an objective of study in this dissertation, the gasifier was deemed unnecessary. In keeping with the primary objective of hot gas desulphurisation, a gas mixture of H_2S passed through a tubular furnace was sufficient to replace the fuel mixture and gasifier needed to form the syngas. Further justification for choosing an alternative process design, more specific to the achieving the desired results from this dissertation, can be found on the following page.

Reasons for choosing an alternative process design:

- Purging of the desulphuriser and gasifier was time intensive and not devoid of H_2S peaks on the gas chromatography analysis due to residue build-up from the fuel used.

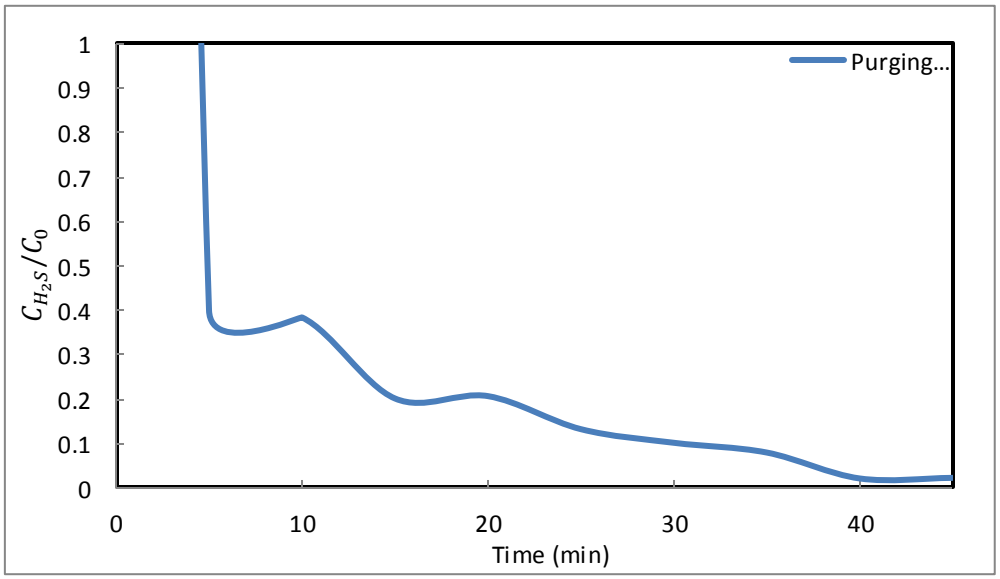

Figure 4-2: Purging cycle of test run

- Lack of consistency for the peaks in the outlet concentration of H_2S.

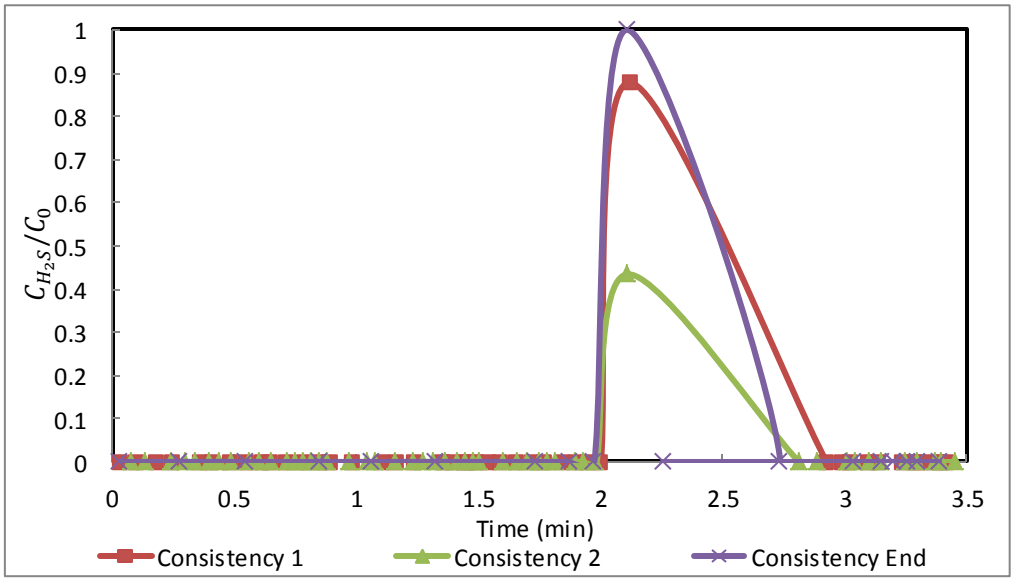

Figure 4-3: Consistency test of test run

- Erratic breakthrough curves during desulphurisation yielding inaccurate results.

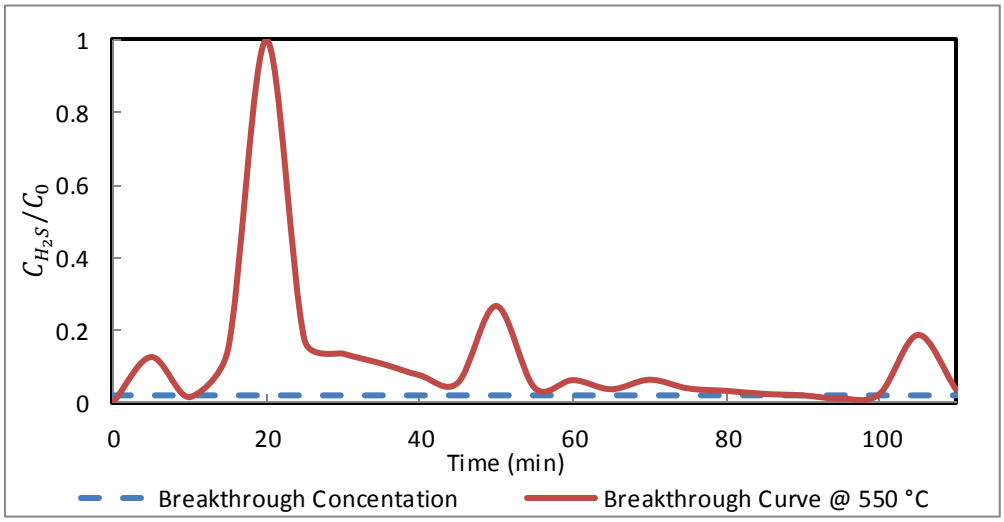

Figure 4-4: Breakthrough curve of test run

- The excessive cost of the fuel needed to produce the syngas as well as mitigating the dangers of using 1-propanethiol.
- Smaller cleaning time needed when loading the desulphurisation reactor.

Montgomery, Raymond and Christine, (2012) details the advantages of having a process design as:

- Smaller trial and error procedures thereby reducing the overall cost.
- A closer conformance to targeted requirements due to a reduction in the variation of results.
- Development of the process requiring a smaller time input.
- Improvement in the process yields.

As such, the proposed experimental process design in the following section utilizes these advantages as well as achieves the objectives of this study.

4.3. Experimental process design

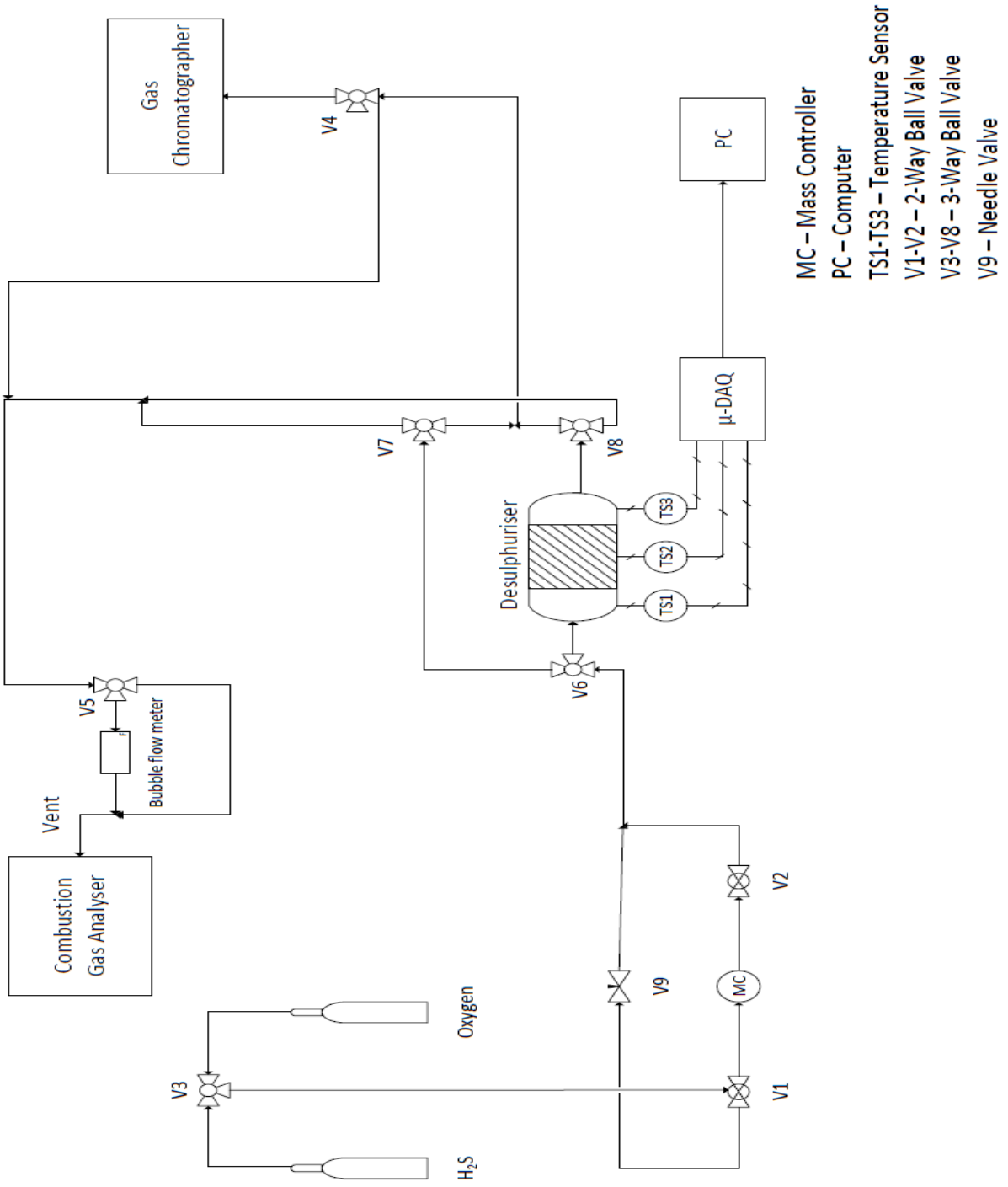

Figure 4-5: Process flow diagram of experimental process design

The following changes were made to the preliminary process design to form the experimental process design shown in Figure 4-5:

- The methanol tank used to flush out the residual fuel from the preliminary process design was removed
- A tank containing a gas mixture of H_2S replaced the fuel tank.
- The peristaltic pump and screw-down valves were removed as the experimental process design used a direct gas feed from the tank.
- The gasifier unit was removed (as previously explained) and consequently the cooling unit due to the lack of excessive hot exit gas flowing to the GC in the experimental process design.
- Pot 1 and pot 2 were removed as there was no liquid flowing in the system.
- A Combustion Gas Analyser was connected to the vent line for regeneration purposes.
- Three K-type thermocouples on the desulphurisation reactor were connected to a µDAQ to interface with the computer.
- The layout of the piping and positioning of the valves were changed.

The valves (V-1, V-2, V-3 and V-9) were adjusted to allow either the gas mixture of H_2S or the oxygen/nitrogen to flow through the system. The flow rate of the oxygen/nitrogen was controlled by an Alicat Scientific gas mass flow controller (GM). The flow rate of the gas mixture of H_2S was controlled with a needle valve (V-9) as well as the bubble flow meter. By adjusting valves (V-6, V-7 and V-8) the gas mixture was passed to either the desulphuriser, GC or bubble flow meter. A detailed description of the valve positioning is described later in this chapter (see Figure 4-8 and Table 4-3). As the gas mixture was desulphurised, the three K-type thermocouples (TS-1 To TS-3) passed signals to a µDAQ. This µDAQ interfaced with the PC to output temperature readings for the desulphuriser exit, desulphuriser inlet and sorbent during the desulphurisation process. When the desulphurised gas reached V-5 it was either passed through the bubble flow meter or vented to the extractors. The nitrogen was use to purge the system of residual H_2S. The oxygen tank replaced the nitrogen tank during regeneration. A Combustion Gas Analyser was connected to the vent line to determine the extent of sorbent regeneration via SO_2 present in the exit gas.

4.4. Equipment

Figure 4-6: Equipment setup

4.4.1. Desulphurisation reactor

A Carbolite (UK) manufactured tubular furnace (Figure 4-6 label A) served the purpose of heating the desulphurisation reactor. The tubular furnace is 400mm long (of which 100mm is the heating zone) with an I.D of 38mm. The reactor tube (400mm long with an I.D of 27mm) is fabricated from 316 stainless-steel to withstand corrosive properties of H_2S. It was inserted horizontally into the tubular furnace. A 200mm and 6mm thick K-type thermocouple was inserted co-axially into the reactor tube to measure the temperature of the fixed bed.

The sorbent loaded in the reactor had to form a fixed bed to prevent the channelling of the gas flow and to provide a well-defined reaction front. The bed was fixed by an adjustable grid (attached onto the thermocouple) which fits flush against a tubular spacer which holds the sorbent. A filter grid was placed on the lower end of the spacer to hold the sorbent in place. Another mesh grid was placed before the first mesh to form a bed of 20mm glass beds. The glass beads absorb any carbon in the gas mixture.

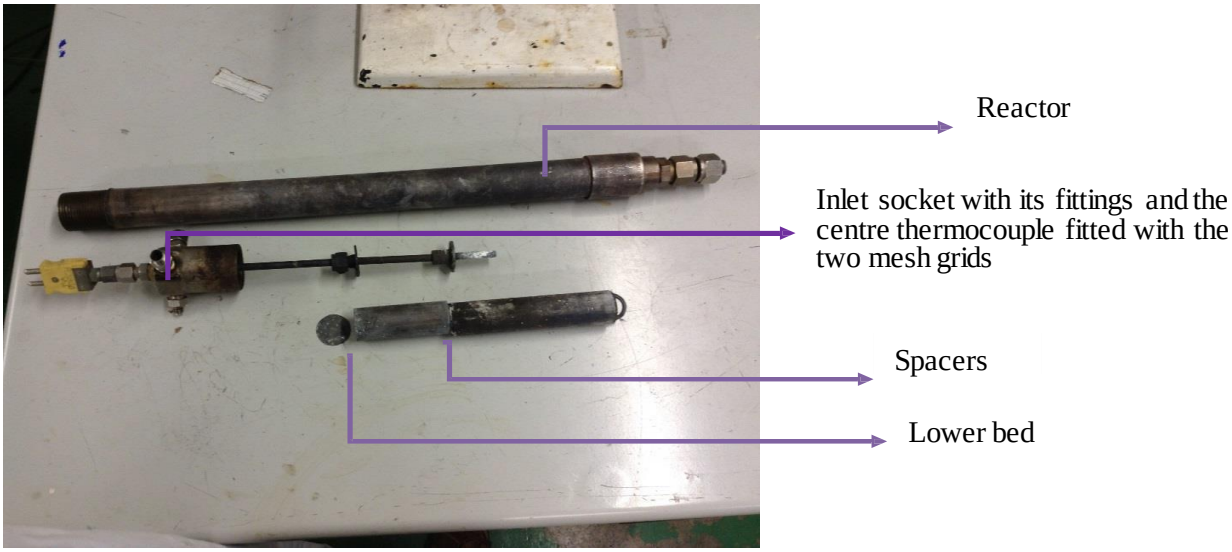

Figure 4-7: Reactor components

4.4.2. Gas sampling and analysis equipment

4.4.2.1. Gas Chromatograph

A Shimadzu GC 2014 (Figure 4-6 label B); equipped with a flame photometric detector (FPD) was used to determine the composition of H_2S in the inlet and exit gas. The FPD is sensitive to sulphur and phosphorus containing compounds only. This makes it applicable to this experiment.

The GC contained an Inertcap 5MS/NP capillary column of length of 30m, I.D. of 0.25mm with a wall thickness of 0.25µm.The carrier gas selected was helium, whereas the reference gases were zero air and hydrogen. These gases had to be pure to ensure no reactions take place with the column's stationary phase, which would inhibit the separation process. For optimum separation, the pressure for zero air and hydrogen on the GC gauges were set at 40 and 100 kPa respectively. Helium also serves as a make-up gas to increase the flow of gas across the detector; the pressure gauge was set at 20 kPa. The function of a split ratio is to prevent the formation of broad and tailing peaks as a result of high concentrations of H_2S in the gas mixture. The split ratio operates in such a way that the hot sample is mixed with the carrier gas and divided up into two streams depending on the specified ratio. The carrier gas flow enters the column and the split flow is vented. A split ratio of 72:1 was chosen as this was the maximum value that could be used to maintain the desired gas velocities required by the GC setup (Table 4-2).

Table 4-2: GC operating conditions

Detector temperature	250 °C
Split Ratio	1:72
Total flow	179.50 ml/min
Carrier gas	Helium
Injection temperature	200 °C
Carrier gas pressure	132 kPa
Oven temperature mode	Isothermal
Oven temperature	40 °C
Oven Hold Time	2 min

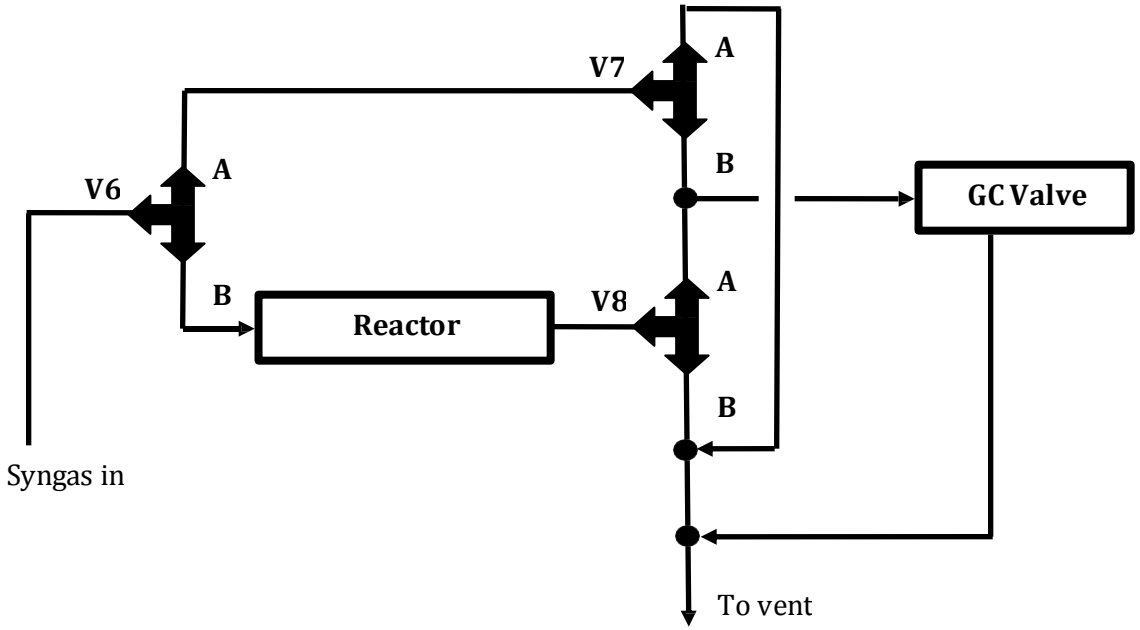

Figure 4-8: Valve positioning schematic (Botha, 2010)

The GC was directly connected to the experimental apparatus using an online sampling valve and thin stainless steel capillary tubing. An external sample loop of 1 ml was used and accessed by switching the position of the sample valve. To sample the inlet gas, valve V6 needs to be in position A with V8 closed and V7 in position B. To sample the exit gas, valve V6 needs to be in position B with V8 in position A and V7 closed. Table 4-3 shows the valve positions for the different actions with respect to the labels in Figure 4-8.

Table 4-3: Valve positioning

ACTION	V6	V7	V8
Bypass to vent gas and bubble flow meter	A	A	Close
Gas mixture to GC prior to desulphurisation	A	B	Close
Gas mixture to desulphurisation reactor and then to the GC	B	Close	A
Gas mixture desulphurisation reactor and then to the vent and bubble flow meter	B	Close	B

4.4.2.2. Combustion gas analyser

Figure 4-9: Combustion Gas Analyzer

The regeneration characteristics of the spent sorbent were determined from sulphur dioxide desorption measurements during high-temperature (550 °C) oxidative treatment of the material. For analysis of the SO_2 concentration in the exit gas during oxidative regeneration of the spent sorbent, a Bacharach ECA-450 Portable Combustion Gas Analyser was used. This unit has been specifically calibrated for the range of concentrations that would be expected in this study. The sulphur dioxide is detectable in the range of 0 to 4000 ppm SO_2. For sulphur dioxide the accuracy is $\pm$5% of readings or $\pm$5 ppm, whichever is greater, between 0 and 2000 ppm SO_2.

4.4.3. Sorbent preparation

The following equipment were used for the sorbent preparation:

- Glass beakers
- Ultrasonic probe (set to 30 W)
- Mass balance
- Buchner funnel and suction pump (used to filter the sorbent after stirring)
- Magnetic hot plate stirrer (used to agitate the mixture of SiO_2 and ZnO)
- Ceramic crucibles (used for calcination step)

4.5. Experimental procedure

4.5.1. Sorbent preparation

- High-purity grade, high surface area silica (300 m^2/g**)** is used from Sigma-Aldrich. This powdered silica has a particle size of 250-500 μm and a pore size of 1.15 cm^3/g pore volume.
- Prepare six batches of different wt. % ZnO loading (See Appendix for calculations and figures):
  - 30% loading ZnO, non-sonicated
  - 30% loading ZnO, sonicated*
  - 20% loading ZnO, non-sonicated
  - 20% loading ZnO, sonicated*
  - 10% loading ZnO, non-sonicated
  - 10% loading ZnO, sonicated*
- First the zinc chloride is weighed and dissolved with deionised water. This reaction is exothermic so the water is added slowly and performed in an ice bath.
- The silica is then weighed and added directly to the mixed solution of zinc chloride and water.
- Two methods are then followed: 1) standard wet impregnation, 2) ultrasonically assisted wet impregnation*. In both methods the beaker containing the slurry is placed on a magnetic stirrer (2.5 stirring setting) and allowed to stir for 4 hours. However, in the case of the ultrasonically assisted method, an ultrasonic probe is placed into the mixing slurry and set to a power output of 30 Watts. This is to ensure that the probe did not overheat during the wet impregnation.
- Once mixing is complete, the sorbent is allowed to settle before being decanted and filtered under suction.

*ultrasonically assisted wet impregnation

- The filtered sorbent is then oven dried at 105 °C overnight.
- The dried sorbent is then placed in a furnace to calcine at 450 °C for 4 hours.

4.5.2. Loading of the desulphurisation reactor

- With the use of a mass balance, 5g of the sorbent is weighed in a beaker.
- Clean the spacers and the desulphurisation reactor – with the aid of a steel brush and a soapy solution while adding acetone at the end – to remove any deposits of carbon.
- Return the mesh and two spacers back into the reactor tube in their correct positions (See Figure 4-7).
- Pour the 5g of the sorbent into the reactor tube.
- Apply anti-seize grease around the reactor tube inlet thread. This step is necessary to ensure the easy off-loading of sorbent through the reactor opening.
- Fill the remaindering area of the reactor tube with glass beads and then screw the socket in slowly. The glass beads will collect any carbon as well as improve the residence time of the flow through the reactor.
- Screw in the socket completely and wipe off any excess anti-seize grease along the edges.
- Slot the reactor tube into the desulphurisation reactor furnace.
- Also apply the anti-seize grease around the reactor tube outlet thread before reconnecting it to the system.
- The desulphurisation reactor inlet is then reconnected to the gas feed line.

4.5.3. GC setup

- Open the tanks for the helium, zero air and hydrogen and switch on the GC.
- Switch on the *GC Solutions* program and click 'System ON'.
- Wait for the FPD to reach 250 °C at which point it will ignite.
- Manually inject a test sample using a gas syringe and proceed if peaks are present.

4.5.4. Purging the system

- This is done to ensure that there is no residual hydrogen sulphide present from any previous runs.
- A nitrogen line replaces the oxygen line which flows through an Alicat Scientific gas mass flow controller (GM). The flow rate is set at 500 cm^3/min.
- Open the nitrogen tank and allow it to flow through the bypass line.
- After about an hour, send the first sample for GC analysis. Complete purging is characterised by the lack of any substantial peaks on the GC.
- Samples are then sent every 30 minutes to the GC until purging is complete.
- Once complete, the gas line from the oxygen tank is reconnected.

4.5.5. Desulphurisation

- Switch on the desulphurisation reactor furnace allowing it to heat up to the desired set-point.
- Switch on the *Waveview* program. This allows the three K-type thermocouples on the reactor to interface with the µDAQ to output temperature readings to the PC.
- Adjust the valve positions to the desulphurisation bypass (see Table 4-3).
- Open the valve on the H_2S tank and set the regulator to 125 kPa.
- After 30 minutes the first sample is sent for GC analysis.
- After 10 minutes, a second sample is taken and the concentrations of the first and second samples are compared for consistency. If the concentration of hydrogen sulphide is not consistent, sampling of the gas mixture will continue until consistency is attained.
- Once consistency is established, the bypass is switched off, directing the gas mixture to flow to the desulphurisation reactor (see Table 4-3). The time at which this occurs is noted – this marks the start of the breakthrough curve.
- The gas exiting the desulphurisation reactor is sampled every 5 minutes until the exit concentration of hydrogen sulphide exceeds 1% of the inlet concentration (breakthrough concentration) and this time is noted. This concentration limit for sulphurous compounds coincides with its use as a syngas in the IGCC.
- Gas flow is measured with the aid of a bubble flow meter in intervals of 30 minutes until the completion of the run.

- At the point where breakthrough concentration is exceeded, turn off the desulphurisation reactor furnace and switch back to the bypass flow.
- Another sample is then taken and sent to the GC for analysis after a 10 minute interval to compare the initial concentration with the end consistency.
- Close the valve on the H_2S tank and save the output file from *Waveview*.
- Allow the desulphurisation reactor to cool and slot it out of the desulphurisation reactor furnace.
- Unscrew the socket and pull the thermocouple out slowly.
- Collect the glass beads in a beaker.
- Lower the reactor and pour the sorbent into a beaker.
- Inspect the inside of the reactor tube with a flashlight to determine if any sorbent is trapped within.
- Collect and weigh sorbent.
- Clean and reload the reactor with the now 'spent sorbent'.
- Reinitialize the *GC Solutions* and *Waveview*.

4.5.6. Regeneration

- Switch on the Desulphurisation reactor furnace allowing it to heat up to the desired set-point (550 °C).
- Adjust the valve positions for the gas mixture to flow through the desulphurisation reactor and then to the vent (see Table 4-3).
- Connect the probe of the Bacharach ECA-450 Portable Combustion Gas Analyser to the vent line.
- Open the valve on the oxygen tank which flows through the Alicat Scientific gas mass flow controller (GM). The flow rate is set at 500 cm^3/min.
- The first sample is sent for combustion gas analysis. The time at which this occurs is noted – this marks the start of the regeneration curve.
- The gas exiting the reactor is sampled every 5 minutes until the exit concentration of SO_2 reaches 50ppm (Useable Regeneration Concentration limit) and this time is noted. The 50 ppm concentration was chosen since it is the minimum limit required for a sorbent to be deemed regenerable.

- After the exit concentration of SO_2 reaches a limiting final value, the time is recorded and the run is stopped.
- Close the valve on the oxygen tank and save the output file from *Waveview*.
- Switch off the Bacharach ECA-450 Portable Combustion Gas Analyser.
- Close the tanks for the helium, zero air and hydrogen and switch off the GC.
- Allow the reactor to cool and slot it out of the reactor furnace.
- Unscrew the socket and pull the thermocouple out slowly.
- Collect the glass beads in a beaker.
- Lower the reactor and pour the regenerated sorbent into a beaker.
- Inspect the inside of the reactor tube with a flashlight to determine if any regenerated sorbent is trapped within.
- Collect the regenerated sorbent.

4.6. Methods of analysis

4.6.1. Gas Chromatography

The Gas Chromatograph (GC) is comprised of a stationary and mobile phase. Helium is the inert carrier gas used for the mobile phase. The packed column (with packing or a liquid coating) in the GC acts as the stationary phase. The GC may be seen as a separation column. The highly sensitive detectors need only a minimal amount of sample to generate a detectable signal. In most cases, the detector and column are prevented from overloading by operating in split-mode.

The stationary phase is responsible for separating the compounds via interactions with different magnitudes of strength. Compounds with a stronger magnitude of strength interact with the stationary phase for a longer period of time, hence resulting in a longer retention time.

Lower boiling point compounds have a shorter retention time and a higher vapour pressure. Similar polarities between the compound and the stationary phase increases the retention time due to the strength of interaction between the both of them. Therefore if the column as well as the compound is polar, then the retention times will be longer at the same temperature. If the compound and column have opposite polarities, then the converse is true. An excessively large flow rate and column temperature is not favorable for the operation of the GC. The shorter retention time results in a weak separation as the individual components remain in the gas phase. Inability of the compound to interact with the column results in a decrease in retention time. The variation in the retention times causes the quality of the separation to deteriorate. Ideally, the chromatogram peaks have a smooth symmetric shape where the area under the curve is representative of the concentration of a compound and different retention times and peak intensities represent different compounds (Bacher, 2016).

It is often the case that a GC would need to have the peak areas calibrated to the concentration values. This is done by manual injection of prepared samples of known concentration and correlating the peak area to the concentration.

4.6.2. Scanning Electron Microscope

Scanning Electron Microscopy (SEM) refers to a process in which a high-energy focused beam of electrons is used to generate a variety of signals as the energy is dissipated by the interactions between the electrons and the sample. The signals produced may then be used to generate low or high resolution topographic images of the sample giving information such as the chemical composition, external texture, structure and orientation and, for the purposes of this experiment, the surface dispersion. SEM can be used to generate images of molecules as small as 50 nm (Swapp, 2016). The capabilities of this equipment, however, are dependent on what the additional detectors can accommodate.

Energy-Dispersive X-ray Spectroscopy (EDX) makes use of the dispersion of x-rays of characteristic elements into an energy spectrum. This energy spectrum is analysed to determine the occurrences of specific elements. EDX can be used to determine the chemical composition of individual points to map out an elemental composition distribution over the imaged area (Goodge, 2016). It is a semi-quantitative method for determining this chemical composition via peak-height ratio. The output from this method is a graph showing x-ray counts vs. energy, with the peaks linked to the specific elements. An example of this is shown in Figure 4-10.

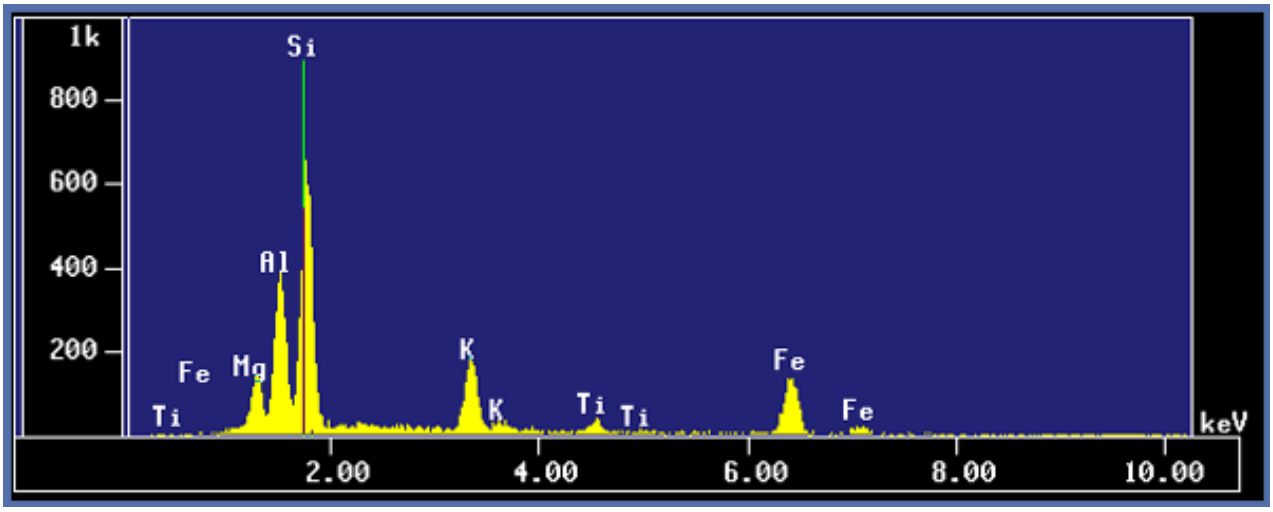

Figure 4-10: Biotite EDX spectrum (Goodge, 2016)

4.6.3. Transmission Electron Microscopy

The Transmission Electron Microscope (TEM) uses an electromagnetic lens to focus electrons into a thin beam that penetrates the specimen. Unlike light-transmitted microscopes, almost all of the incoming electrons are transmitted through the specimen. The TEM is capable of displaying images of the specimen in the magnification range of mm to μm (Egerton, 2005). The most important application of TEM's is to provide crystalline, topographical, and morphological information of the specimen. TEM produces an electron diffraction pattern of the specimen on camera viewing system (Egerton, 2005). An example of this is shown in Figure 4-11.

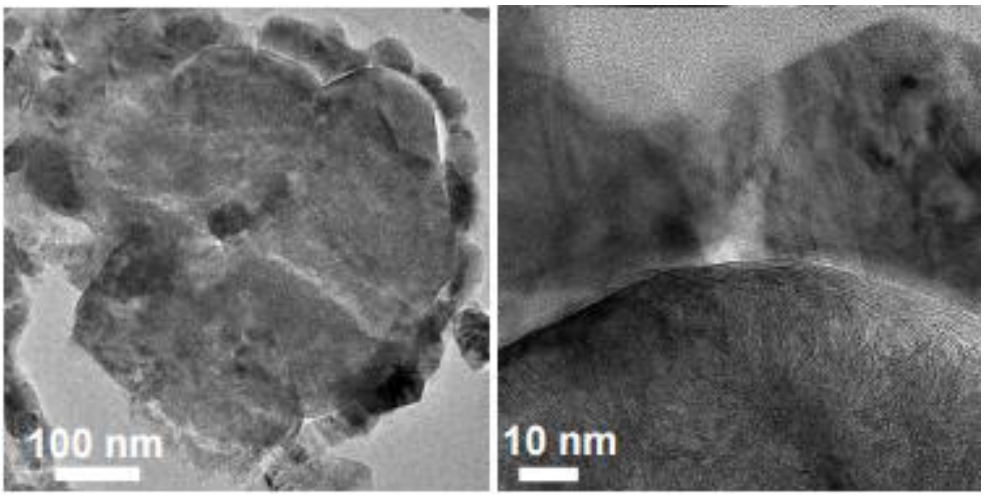

Figure 4-11: TEM micrograph of sulfided $ZnMoO_4$ mixed oxide (Girard et al., 2015)

CHAPTER 5: RESULTS AND DISCUSSION

5.1. Calibration

The GC calibration was difficult to undertake since only 1% and 5% H_2S gas mixtures were available. The following strategy was adopted. Three different sample loops (0.15 ml, 0.2 ml, 1 ml) and two different split ratios were used to simulate different concentrations of H_2S. Below are two examples:

Suppose we have a 1% tank (corresponding to 10000 ppm) and a 0.2 ml sample loop for the calibration. The standard split ratio used here is 72:1, the same as the desulphurisation experiments. In the actual desulphurisation experiments we use a sample loop volume of 1 ml. In this case the GC actually recognizes the following H_2S concentration:

$$\frac{0.2}{1}\times 1\% \times \left(\frac{72}{72}\right) = 0.2\%$$

This is a volume % which corresponds to 2000 ppm. We can also report it as a volume fraction of 0.002.

Suppose we have a 1% tank (corresponding to 10000 ppm) and a 0.15 ml sample loop for the calibration. The split ratio used here is 36:1, half of the value used in the desulphurisation experiments. In the actual desulphurisation experiments we use a sample loop volume of 1 ml. In this case the GC actually recognizes the following H_2S concentration:

$$\frac{0.15}{1}\times 1\% \times \left(\frac{72}{36}\right) = 0.3\%$$

This is a volume % which corresponds to 3000 ppm. We can also report it as a volume fraction of 0.003.

The following combinations were used to simulate different concentrations of H_2S (what the GC recognises as such):

1% tank, 0.2 ml loop, 72:1 split $\rightarrow$ 0.2 % or 0.002 vol fraction

1% tank, 0.15 ml loop, 72:1 split $\rightarrow$ 0.15 % or 0.0015 vol fraction

1% tank, 0.15 ml loop, 36:1 split $\rightarrow$ 0.3% or 0.003 vol fraction

1% tank, 1 ml loop, 72:1 split $\rightarrow$ 1% or 0.01 vol fraction

1% tank, 1 ml loop, 36:1 split $\rightarrow$ 2% or 0.02 vol fraction

5% tank, 1 ml loop, 72:1 split $\rightarrow$ 5% or 0.05 vol fraction

The actual recorded calibration data is presented in Appendix A. Plotting this data results in the following two graphs for high range (Figure 5.1) and low range (Figure 5.2):

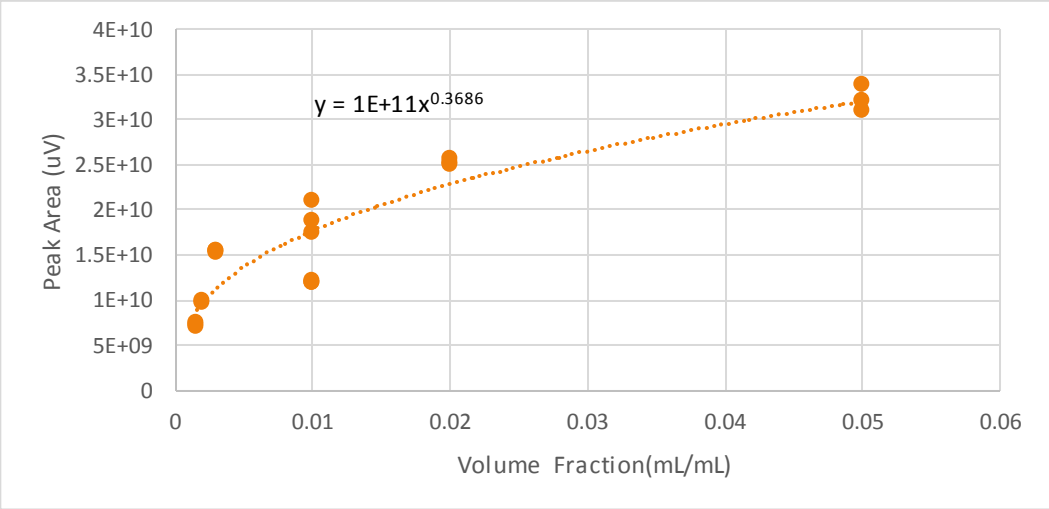

Figure 5-1: Full range calibration curve of H_2S

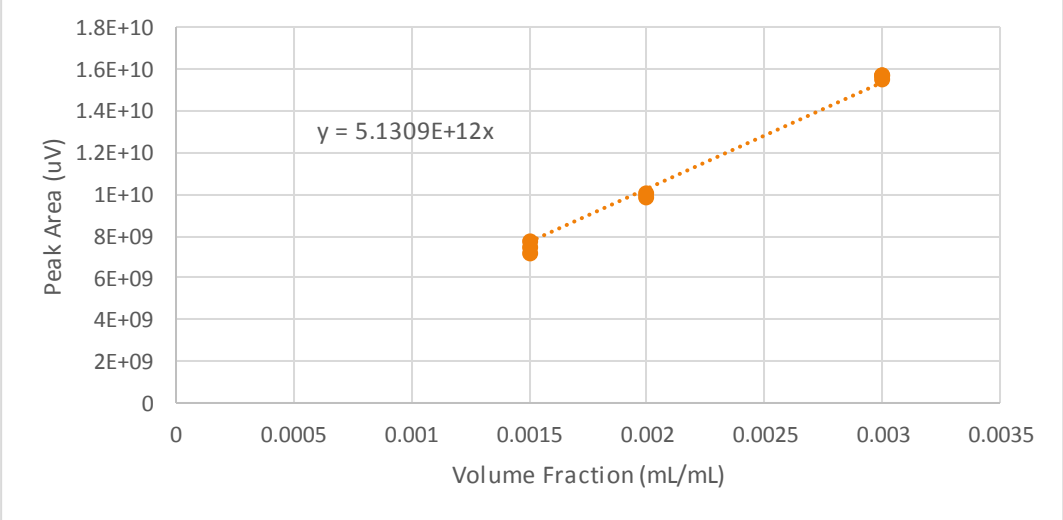

Figure 5-2: Experimental range calibration curve of H_2S

These can be used to determine the H_2S concentration of any injected sample (either inlet of exit).

5.2. Sorbent preparation

In order to commence with experimental runs it was first necessary to prepare the sorbent for use. High-purity grade, high surface area silica (300 m^2/g**)** was used from Sigma-Aldrich. This silica was then mixed with zinc chloride to form the sorbent precursor. As previously mentioned, six batches of different wt. % ZnO loading were prepared. During the ultrasonic wet impregnation technique the probe overheated and switched off, a cooling period of 20 minutes was allowed before switching it back on. The volume of water required to completely dissolve zinc chloride was insufficient to form a slurry with silica. An excess of up to 130ml of water was added per batch to ensure sufficient agitation upon stirring. The reaction of zinc chloride with water is exothermic and the beaker had to be placed in an ice bath. When dried and calcined, the silica gel produced a fine white powder of sorbent. There was concern that the powder was too fine and may pass through the mesh of the fixed-bed desulphuriser; however, the mesh used was sufficiently small to allow only the H_2S gas to permeate through. The sorbent remaining in the sieve would then be used for subsequent experimental runs. Figure 5-3 shows the prepared non-sonicated and sonicated sorbents. It was noted that the lower wt. % ZnO loading produced a finer sorbent, with non-sonicated sorbents being finer still.

Figure 5-3: Non-sonicated sorbents (left) and sonicated sorbents (right)

There are, however, methods to improve the preparation of this sorbent. In reaction B-2, HCl forms as a side product and lowers the utilization of ZnO. A possible method for removing this HCl from the liquid mixture is batch azeotropic distillation. This method is used for this system of chemicals due to different separations being required at different times. The H_20 and HCl form a maximum boiling azeotrope at

108.8 °C while the ZnO in solution is entrained. In the first cycle the HCl is removed as the overhead product, while in the second cycle the H_20 is removed. When there is enough H_2O left for the ZnO to serve as an entrainer, the process is stopped. The HCl removed from this procedure as well as the $S0_2$ formed during sorbent regeneration (Equation 2.15) are referred to as acid gases. These acid gases can be removed by passing them through $NaHCO_3$ and $Ca(OH)_2$ sorbents (Hemmer et al., 2002) . Alternatively these products can be sold to gas companies or valorized into hydrochloric acid and sulphuric acid.

5.3. Quantitative and Qualitative analysis of sorbent surface characteristics

This section contains the micrographs for the respective forms of microscopy as well as some statistical analysis of the results that were obtained.

5.3.1. Transmission Electron Microscopy

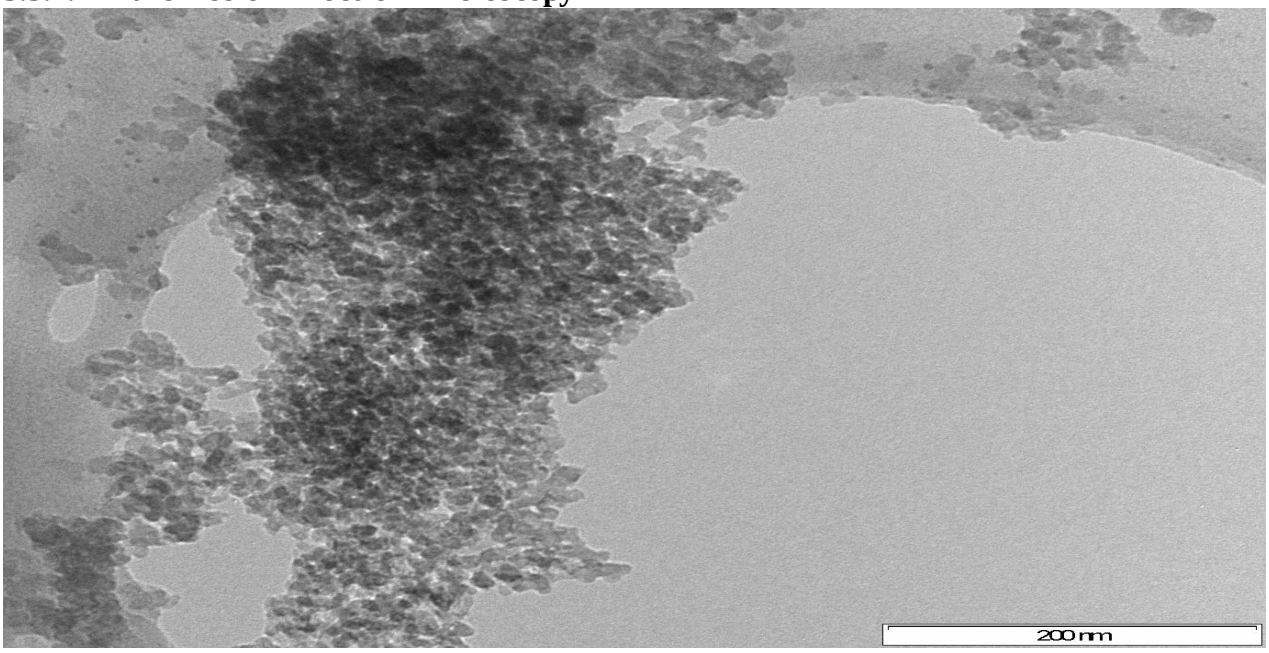

Figure 5-4: TEM micrograph of 10% loading ZnO, non-sonicated sorbent at 200,000x magnification

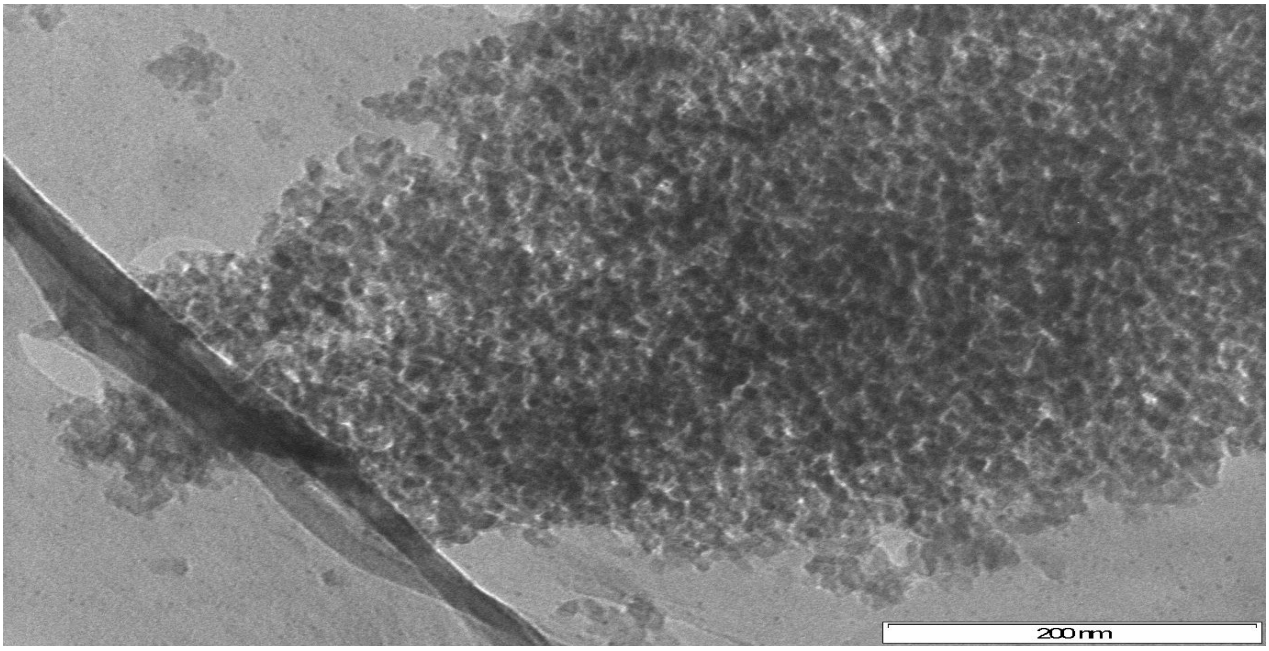

Figure 5-5: TEM micrograph of 20% loading ZnO, non-sonicated sorbent at 200,000x magnification

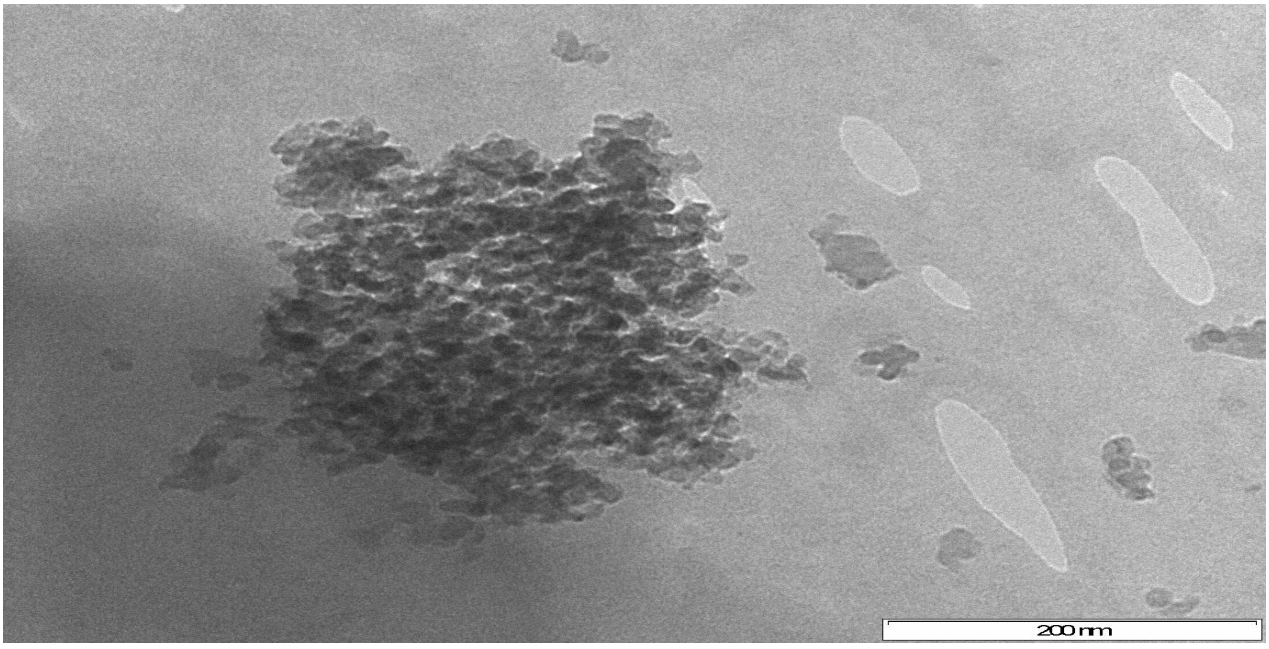

Figure 5-6: TEM micrograph of 30% loading ZnO, non-sonicated sorbent at 200,000x magnification

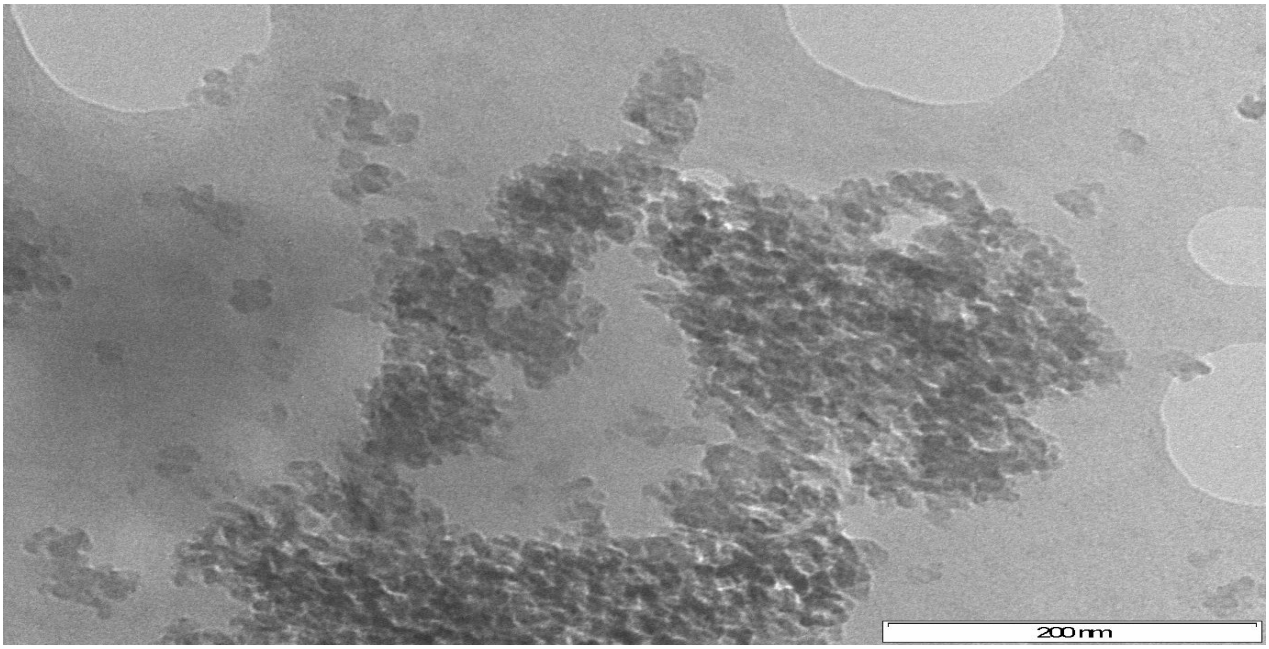

Figure 5-7: TEM micrograph of 10% loading ZnO, sonicated sorbent at 200,000x magnification

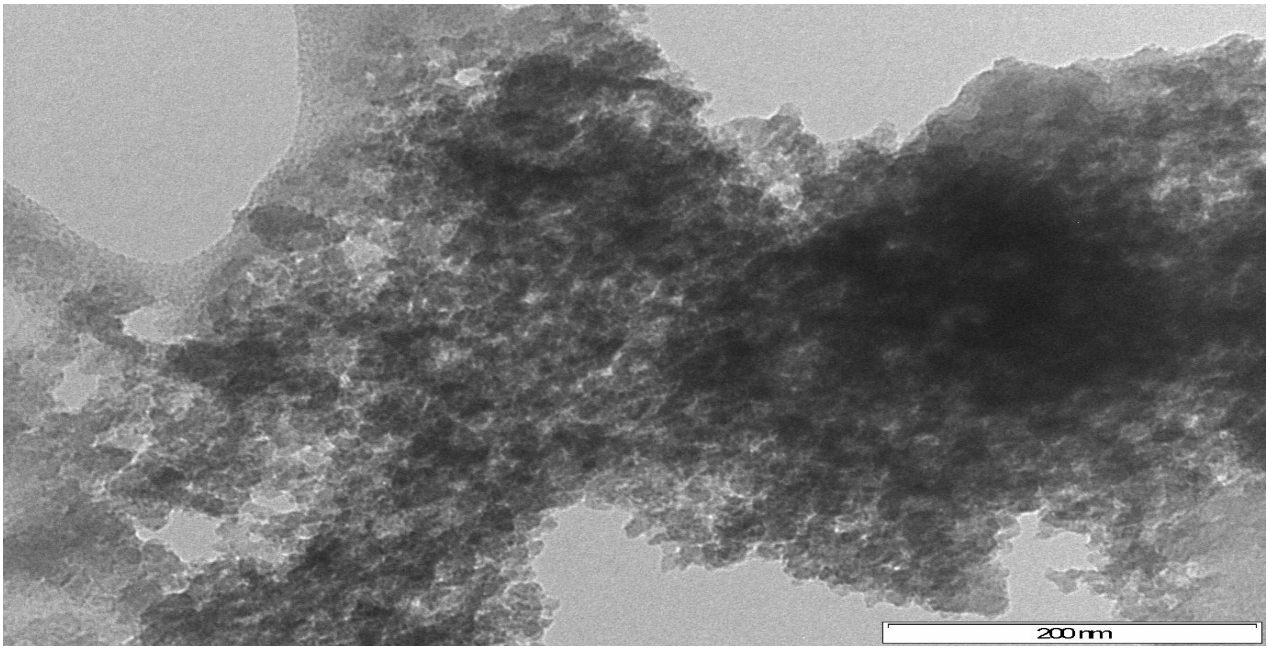

Figure 5-8: TEM micrograph of 20% loading ZnO, sonicated sorbent at 200,000x magnification

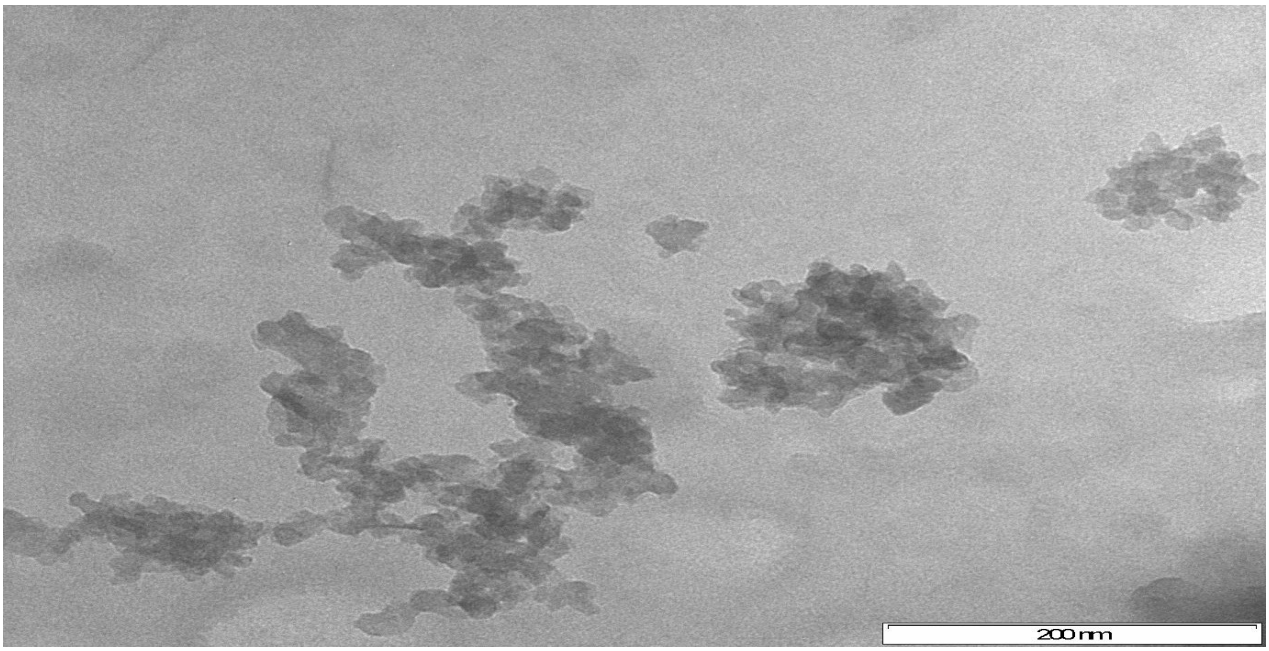

Figure 5-9: TEM micrograph of 30% loading ZnO, sonicated sorbent at 200,000x magnification

From the above TEM micrographs, the crystalline nature of the sorbents was noted. These TEM micrographs were taken over the surface of the silica and are visually based. The lack of metal oxides on the surface of the silica suggests a greater dispersion of the metal oxides through the pores. There were large aggregations of crystals with rounded edges which contained the crystallites. For the non-sonicated sorbents (Figure 5-4 to Figure 5-6) there was a greater presence of metal oxide agglomeration. For the sonicated sorbents (Figure 5-7 to Figure 5-9) there was a greater dispersion of the metal oxide over the surface of the silica support. As expected, when the wt. % ZnO loading was increased, for both non-sonicated and sonicated sorbents, the length of the particle size increased. The ultrasonically assisted wet impregnation technique results in a greater number of larger particles being forced through the pores of the silica. A higher magnification analysis is needed to penetrate the silica pores and quantify these agglomeration and dispersion effects.

Wang and Yang (2014) showed similar findings noting that the higher wt. % ZnO loading resulted in greater agglomeration and hence more pore blockage in the silica. Hence, the larger metal oxide particles were present on the surface of the support while the smaller particles were evenly dispersed in the pores of the silica.

5.3.2. Scanning Electron Microscopy (EDX)

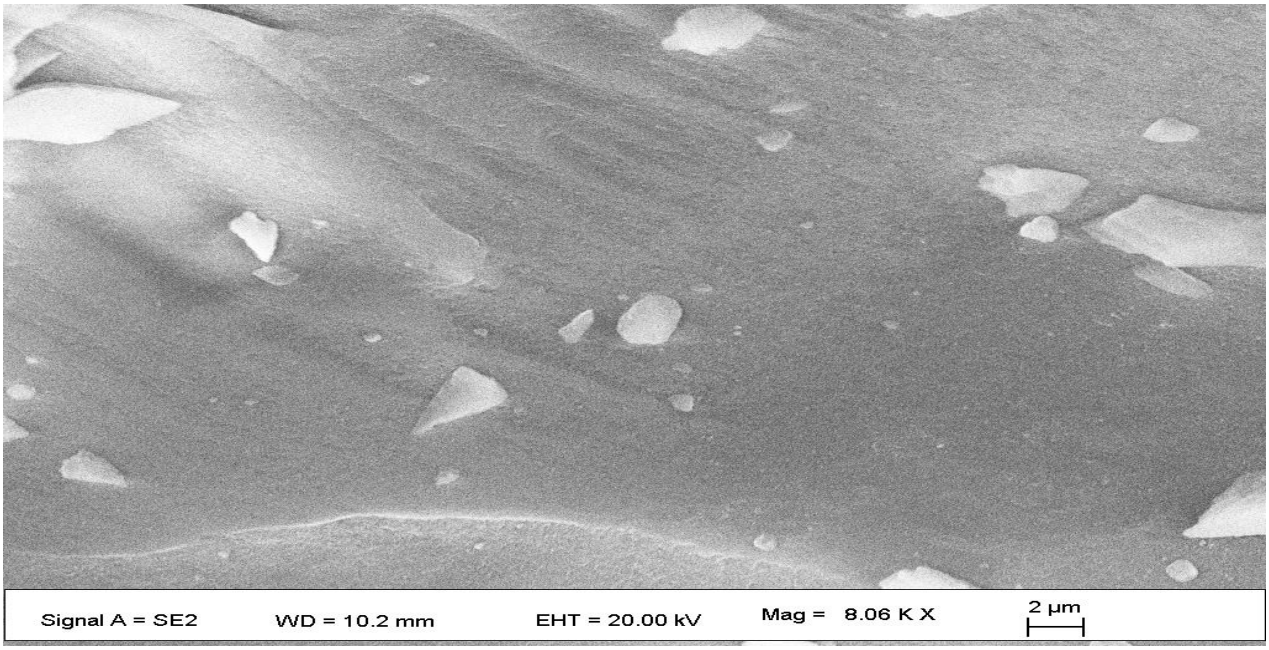

Figure 5-10: SEM micrograph of 10% loading ZnO, non-sonicated sorbent

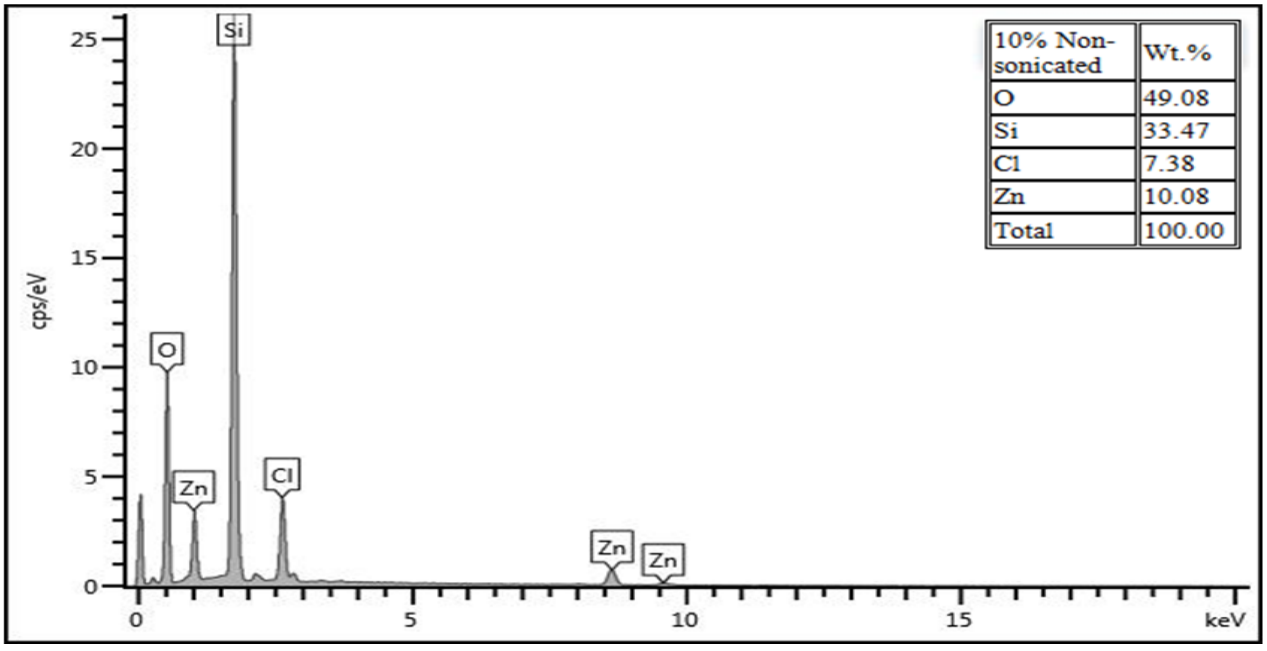

10% Non-sonicated	Wt.%
O	49.08
Si	33.47
Cl	7.38
Zn	10.08
Total	100.00

Figure 5-11: EDX analysis of 10% loading ZnO, non-sonicated sorbent

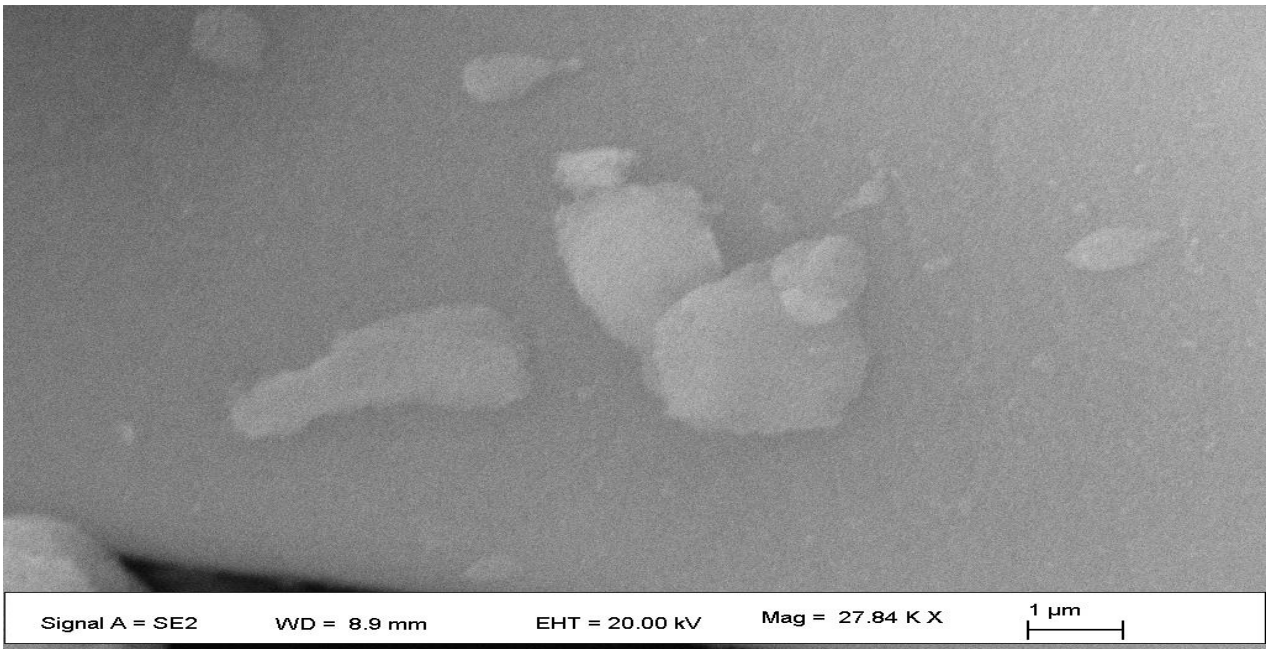

Figure 5-12: SEM micrograph of 20% loading ZnO, non-sonicated sorbent

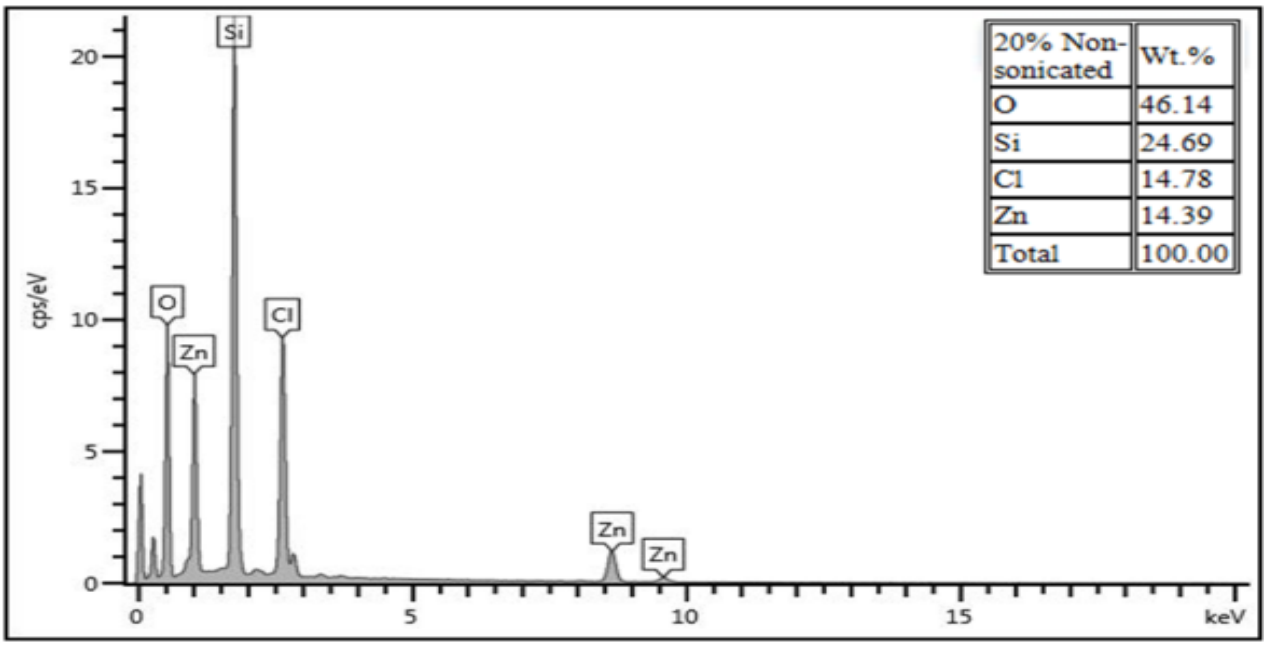

Figure 5-13: EDX analysis of 20% loading ZnO, non-sonicated sorbent

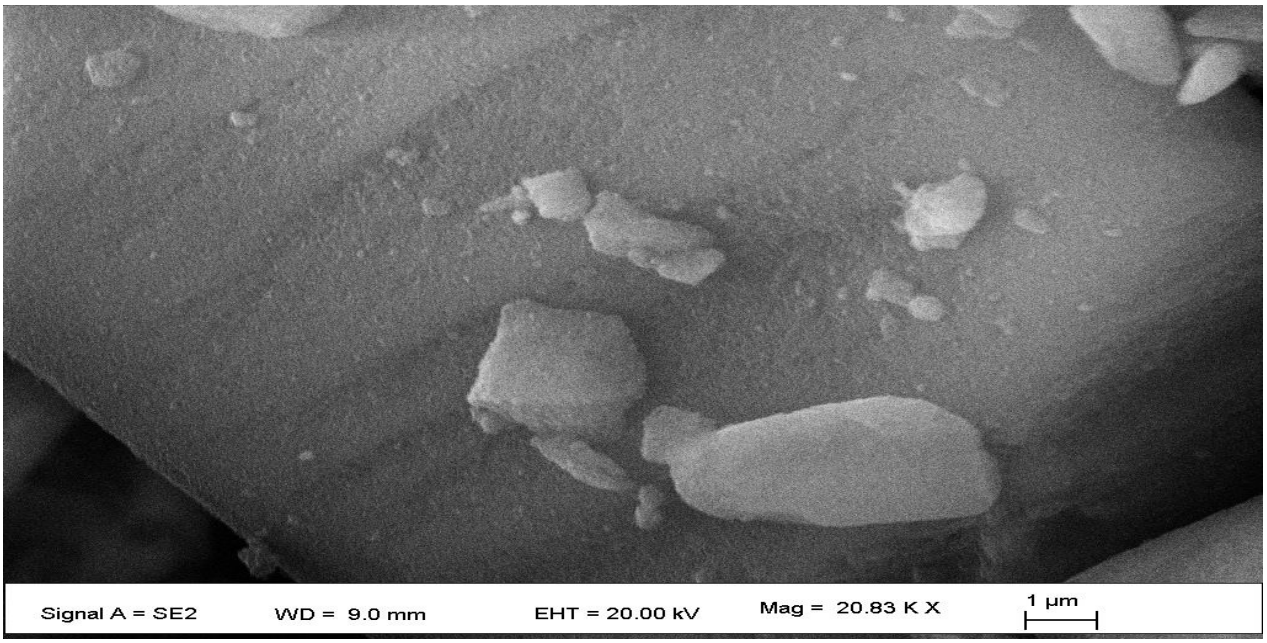

Figure 5-14: SEM micrograph of 30% loading ZnO, non-sonicated sorbent

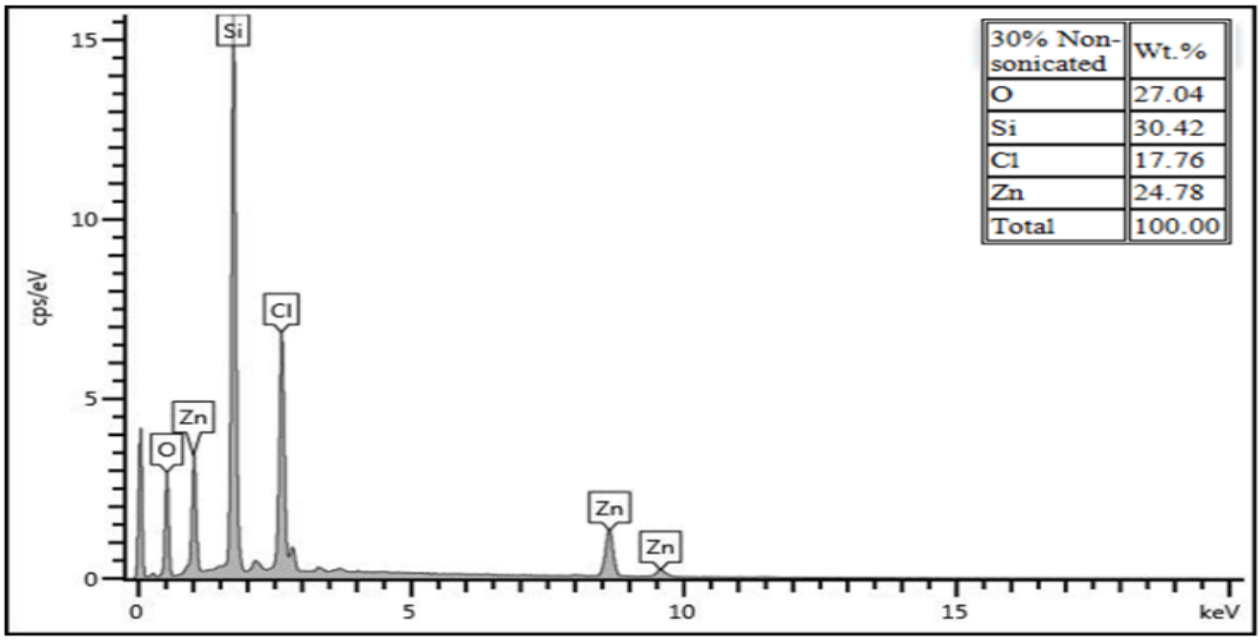

Figure 5-15: EDX analysis of 30% loading ZnO, non-sonicated sorbent

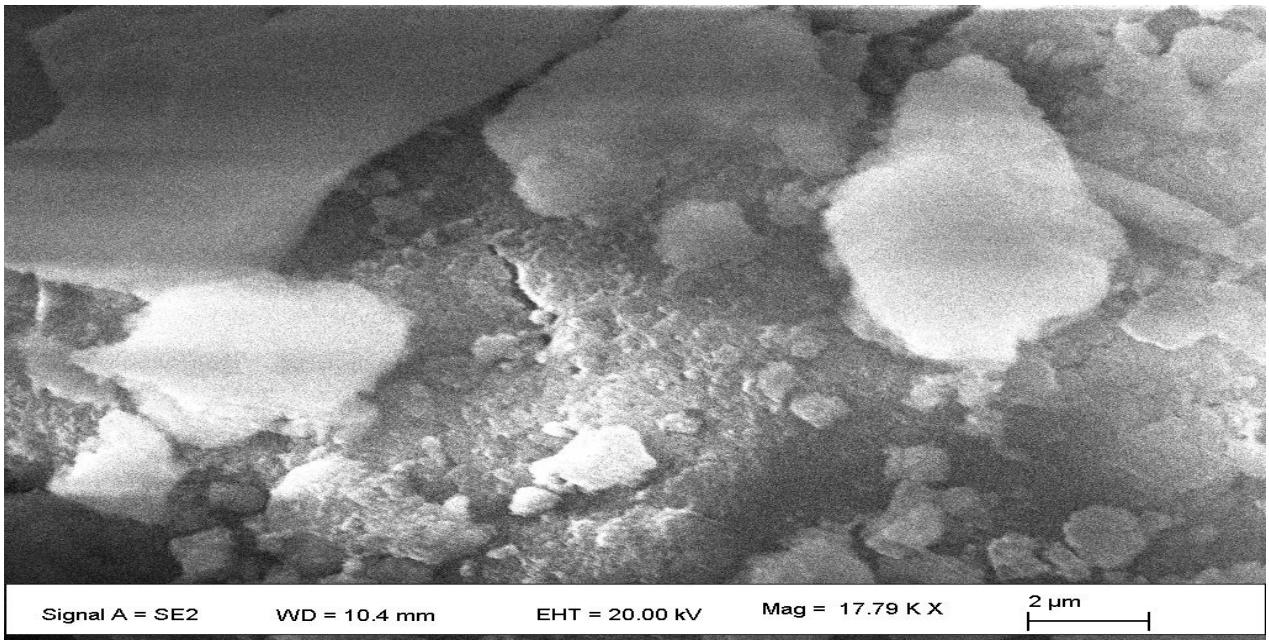

Figure 5-16: SEM micrograph of 10% loading ZnO, sonicated sorbent

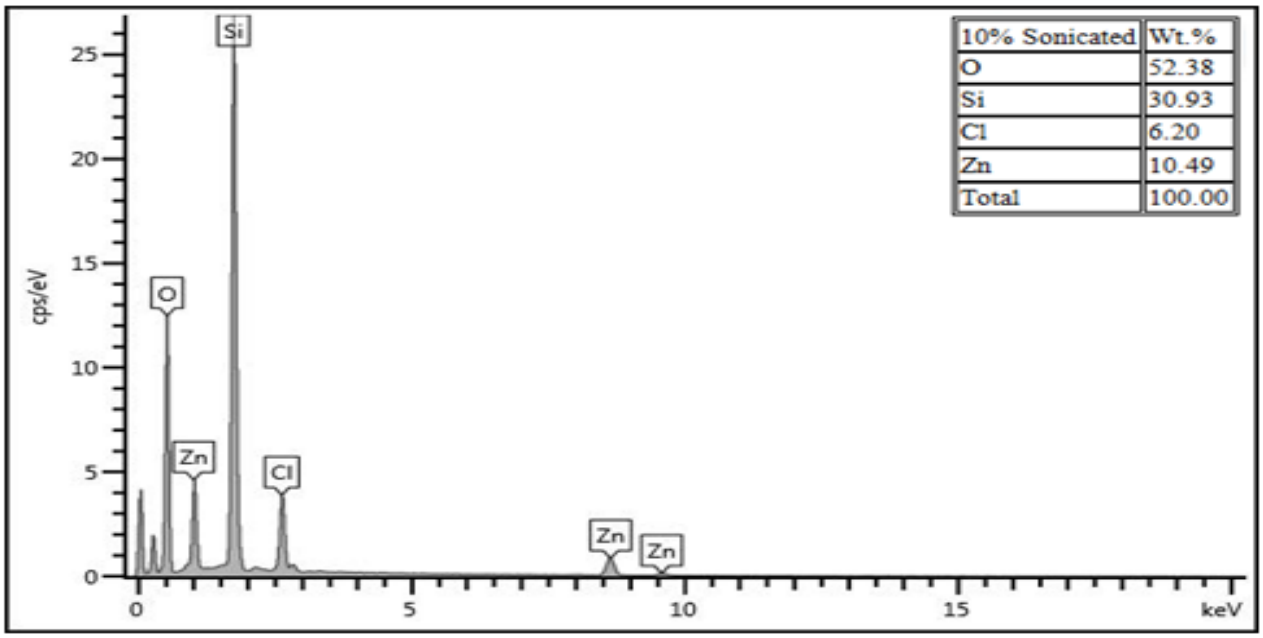

10% Sonicated	Wt.%
O	52.38
Si	30.93
Cl	6.20
Zn	10.49
Total	100.00

Figure 5-17: EDX analysis of 10% loading ZnO, sonicated sorbent

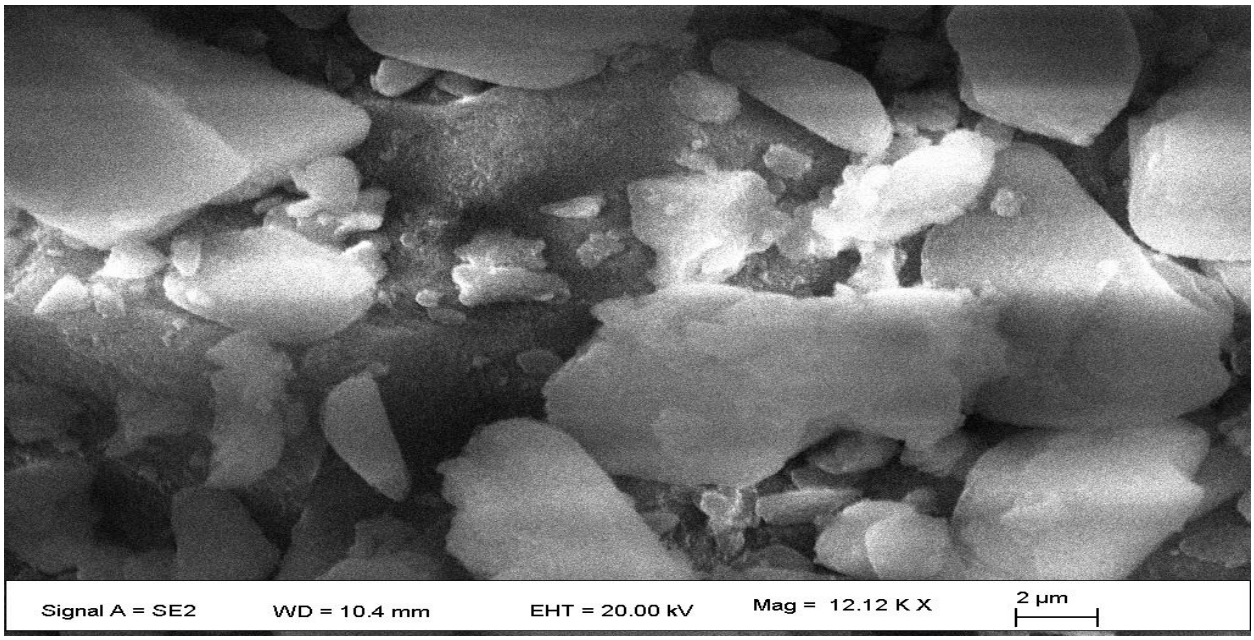

Figure 5-18: SEM micrograph of 20% loading ZnO, sonicated sorbent

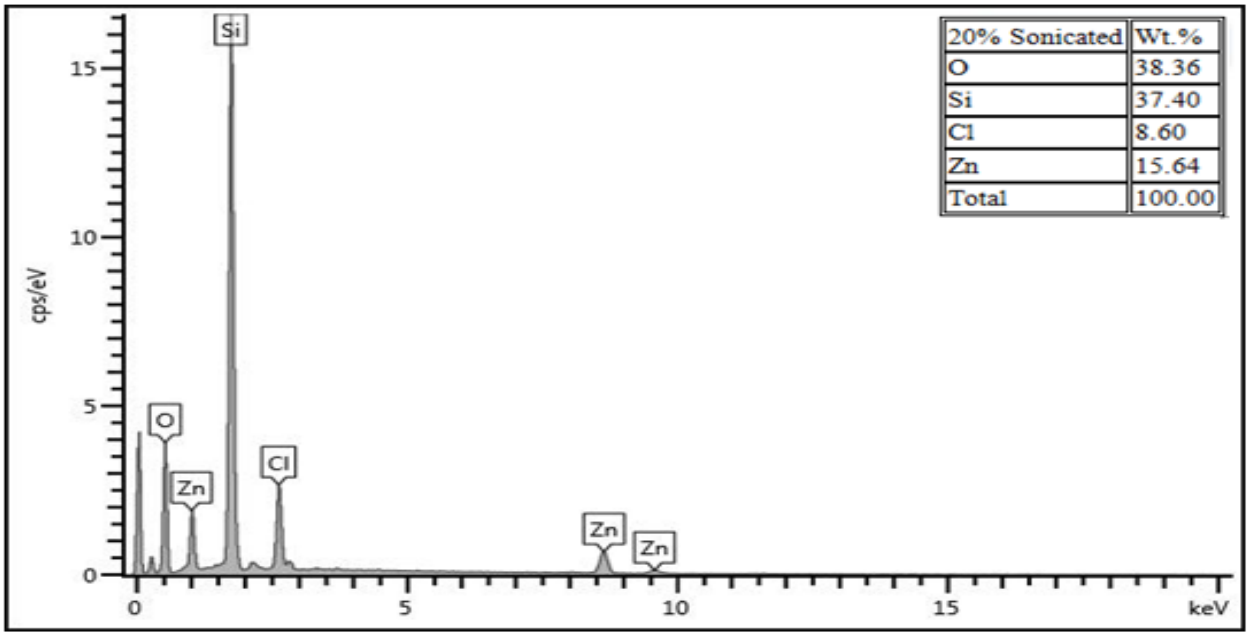

Figure 5-19: EDX analysis of 20% loading ZnO, sonicated sorbent

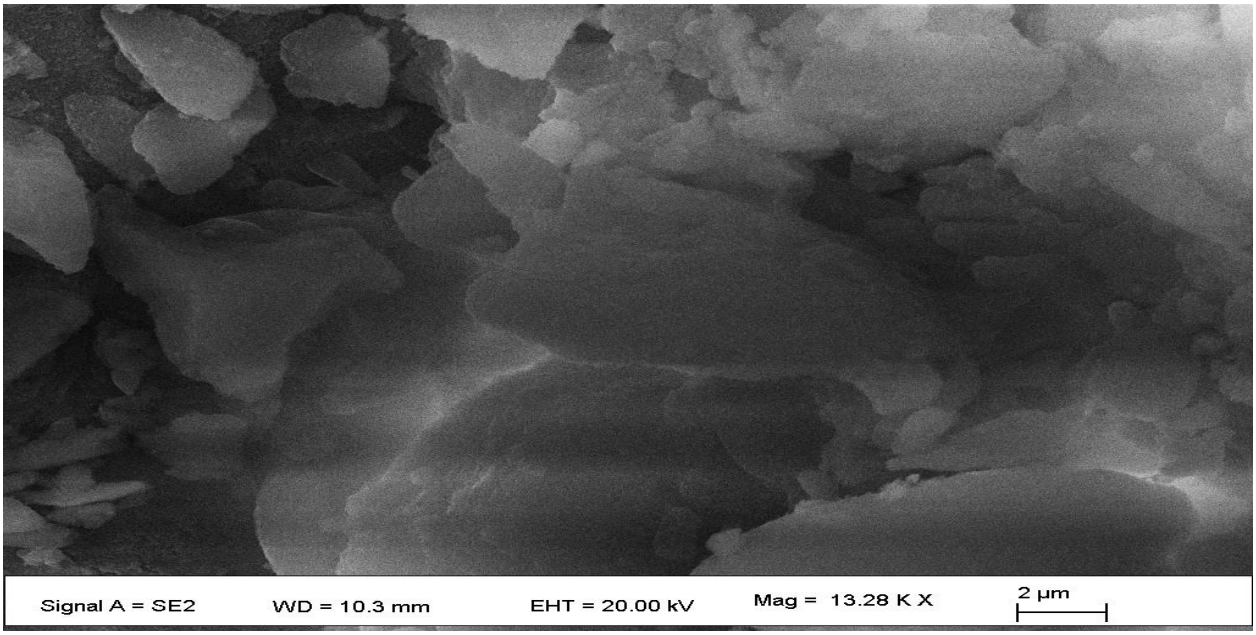

Figure 5-20: SEM micrograph of 30% loading ZnO, sonicated sorbent

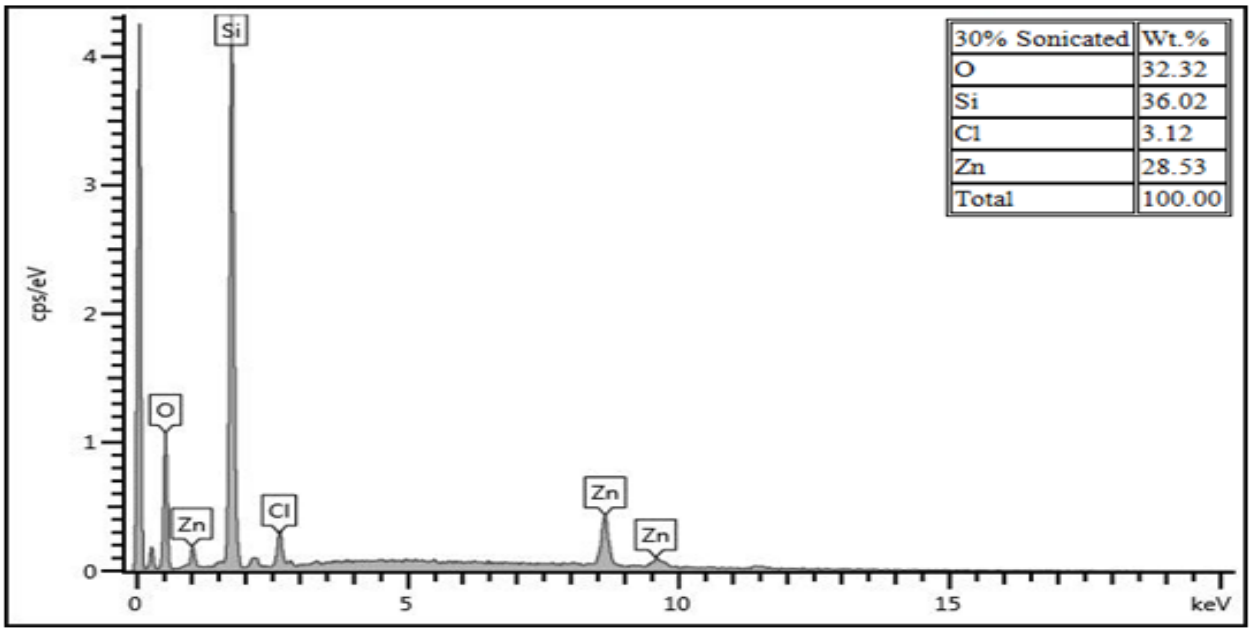

30% Sonicated	Wt.%
O	32.32
Si	36.02
Cl	3.12
Zn	28.53
Total	100.00

Figure 5-21: EDX analysis of 30% loading ZnO, sonicated sorbent

From the above SEM micrographs, the surface structure of the sorbents was noted. For the non-sonicated sorbents (Figure 5-10, 5-12 and 5-14) there was a random distribution of metal oxides on the surface of the silica. For the sonicated sorbents (Figures 5-16, 5-18 and 5-20) the distribution of the metal oxides showed greater uniformity. As expected, there was a greater dispersion for sonicated sorbents as compared to the non-sonicated sorbents.

As aforementioned, EDX is a semi-quantitative method used to determine the chemical composition of individual points to map out an elemental composition distribution over the imaged area. Samples were gold-coated to improve the conductivity of the sorbents and thereafter, the chemical compositions were limited to oxygen, silicon, chlorine and zinc. The chlorine component was as a result of the reaction (Equation B-2) needed for the wet impregnation technique to prepare the sorbents. Theoretically this reaction should proceed to 100% conversion. The problem lies with the solid zinc chloride reacting with excess water. The result is a change from a binary $ZnCl_2$-H_20 system to a ternary ZnO-H_20-HCl system, owing to the reactivity of the residual chlorine (Sorrell, 1977). This system readily forms zinc oxychlorides which lower the conversion of zinc chloride to zinc oxide in Equation B-2.

For both non-sonicated and sonicated sorbents the increase in wt. % ZnO loading resulted in a greater ratio of zinc to oxygen elements dispersed of the surface of the silica support. For the non-sonicated sorbents (Figure 5-11, 5-13 and 5-15) the EDX analysis showed a greater amount of chlorine present than in sonicated sorbents at equivalent wt. % ZnO loading. For the sonicated sorbents (Figure 5-17, 5-19 and 5-21) the EDX analysis showed a greater amount of zinc present than in non-sonicated sorbents at equivalent wt. % ZnO loading. From the results presented in this section it can be concluded that the ultrasonically assisted wet impregnation technique improves the dispersion of zinc loaded onto the surface of a silica carrier. Furthermore, the sonication actually improved the efficacy of the wet impregnation technique. This may be due to the improved access to the deeper pore network due to the action of the ultrasonic-assisted impregnation technique (refer to Section 2.3.3.1).

5.3.3. Statistical analysis

In order to quantitatively explain the results from the microscopy, a statistical analysis was done with respect to the lengths of particles (Table 5-1). The length of the particles was determined using a TEM analysis program to measure the size of the metal oxides within the pores of the silica. For the non-sonicated sorbents, the effect of higher wt. % ZnO loading was noticeable. This was due to the wet impregnation technique increasing the amount of metal oxides entering the pores, with a slight increase in the size of the particles entering, as wt. % ZnO loading increased. For the sonicated sorbents, however, the effect of higher wt. % ZnO loading was more profound. There was a greater increase in all statistics analysed in Table 5.1 for sonicated sorbents, when comparing them to the non-sonicated sorbents at equivalent wt. % ZnO loading. This was due to the ultrasonically assisted wet impregnation technique increasing the amount of metal oxides entering the pores and the size of the particles entering, as wt. % ZnO loading increased. From the Chebyshev inequality (Appendix B.4), at least 88% of particle lengths lay within three standard deviations from the mean length.

Table 5-1: Results of statistical analysis

	Mean length (nm)	**Variance (nm)**	**Standard deviation (nm)**	**95% Confidence interval (nm,nm)**
10% ZnO loading, Non-sonicated	9.31	4.40	2.10	(8.04, 10.58)
20% ZnO loading, Non-sonicated	9.56	2.34	1.53	(8.64, 10.49)
30% ZnO loading, Non-sonicated	9.72	3.78	1.94	(8.55, 10.90)
10% ZnO loading, Sonicated	11.29	4.73	2.17	(9.97, 12.60)
20% ZnO loading, Sonicated	12.42	14.70	3.83	(10.11, 14.74)
30% ZnO loading, Sonicated	13.88	19.59	4.43	(11.21, 15.56)

5.4. Desulphurisation and regeneration results

The experiment was designed to be a 3^2 factorial design with two independent variables (wt. % ZnO loading and temperature) and three levels for each variable. Table 5-2 shows a summary of the main results for the desulphurisation aspect of this study. As previously mentioned, a bubble flow meter was used to measure the volumetric flowrate of the H_2S containing gas flowing through the sorbent bed. The average bubble flow meter time for all runs was 1.4 seconds. The Alicat Scientific gas mass flow controller could not be used for the H_2S gas. The gas hourly space velocity (GHSV) is a standard measure used in packed bed reactors to relate the volumetric flow rate of reactant gas to the volume of the packed bed. The average GHSV for all runs was 67500 hr^{-1}. When the sorbent pores become saturated and can no longer adsorb the H_2S, it is referred to as the saturation capacity (SC) of the sorbent. This was calculated from the mass before and the mass after the desulphurisation, at which point the sorbents had reached saturation. Theoretically, a higher SC relates to a longer breakthrough time. Table 5-3 shows a summary of the main results for the regeneration aspect of this study. The other results presented will be discussed later.

Table 5-2: Summary of desulphurisation results for ZnO/SiO_2 sorbents

Run	Meaning	Breakthrough Time (min)	Average % increase in Breakthrough Time (%)	Saturation Capacity (g S/g ZnO)	Average % increase in Saturation Capacity (%)
1	30% loading ZnO, non-sonicated at 350 ℃	7	74.42	0.103	0.86
2	30% loading ZnO, non-sonicated at 450 ℃	34		0.112	
3	30% loading ZnO, non-sonicated at 550 ℃	45		0.117	
4	30% loading ZnO, sonicated at 350 ℃	13		0.104	
5	30% loading ZnO, sonicated at 450 ℃	59		0.113	
6	30% loading ZnO, sonicated at 550 ℃	78		0.118	
7	20% loading ZnO, non-sonicated at 350 ℃	4	73.07	0.099	9.62
8	20% loading ZnO, non-sonicated at 450 ℃	10		0.107	
9	20% loading ZnO, non-sonicated at 550 ℃	12		0.116	
10	20% loading ZnO, sonicated at 350 ℃	9		0.115	
11	20% loading ZnO, sonicated at 450 ℃	14		0.118	
12	20% loading ZnO, sonicated at 550 ℃	22		0.120	
13	10% loading ZnO, non-sonicated at 350 ℃	2	39.13	0.106	3.65
14	10% loading ZnO, non-sonicated at 450 ℃	7		0.115	
15	10% loading ZnO, non-sonicated at 550 ℃	14		0.122	
16	10% loading ZnO, sonicated at 350 ℃	5		0.115	
17	10% loading ZnO, sonicated at 450 ℃	9		0.118	
18	10% loading ZnO, sonicated at 550 ℃	18		0.122	

Table 5-3: Summary of regeneration results for ZnO/SiO_2 sorbents

Run	Regeneration time @ 50 ppm (min)	Final SO_2 Concentration (ppm)
1	30	30
2	15	8
3	12	6
4	-*	68
5	40	43
6	17	0
7	6	27
8	10	29
9	4	0
10	-*	83
11	37	38
12	12	18
13	11	0
14	8	0
15	6	0
16	-*	63
17	6	0
18	4	0

*Runs 4, 10 and 16 did not reach the useable regeneration concentration limit of 50 ppm.

Figure 5-22: Fresh sorbent (left) and spent sorbent (right), Run 18

Figure 5-23: Fresh sorbent (left) and regenerated sorbent (right), Run 18

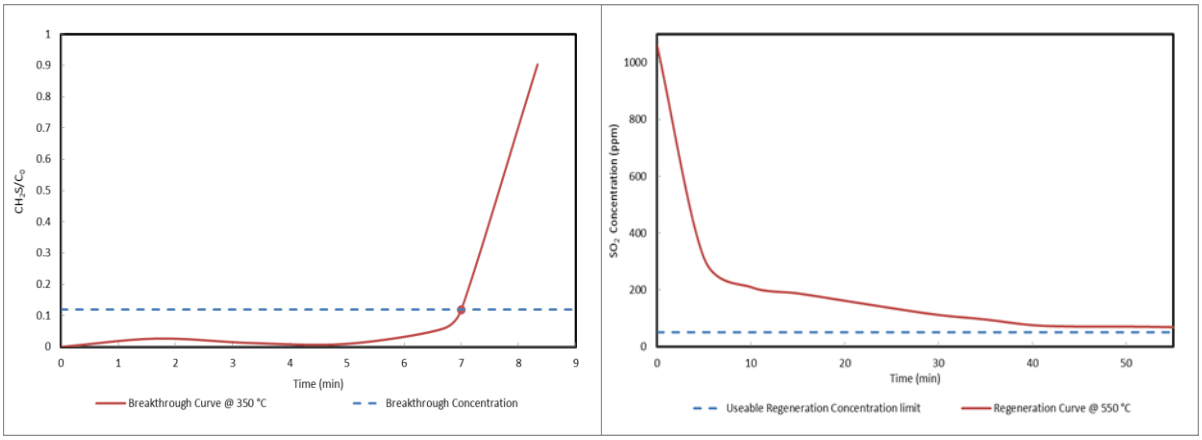

Figure 5-24: Breakthrough curve and regeneration curve, run 1

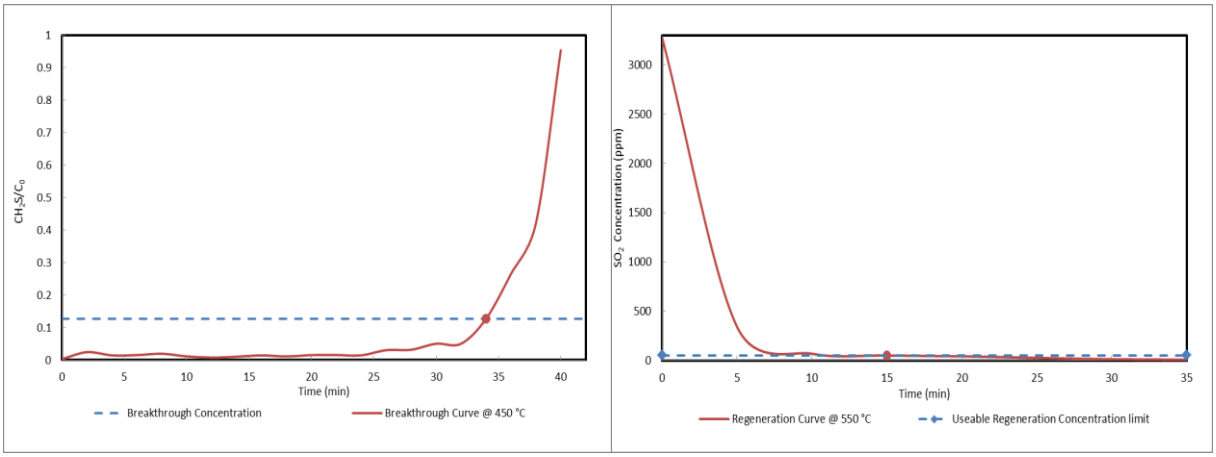

Figure 5-25: Breakthrough curve and regeneration curve, run 2

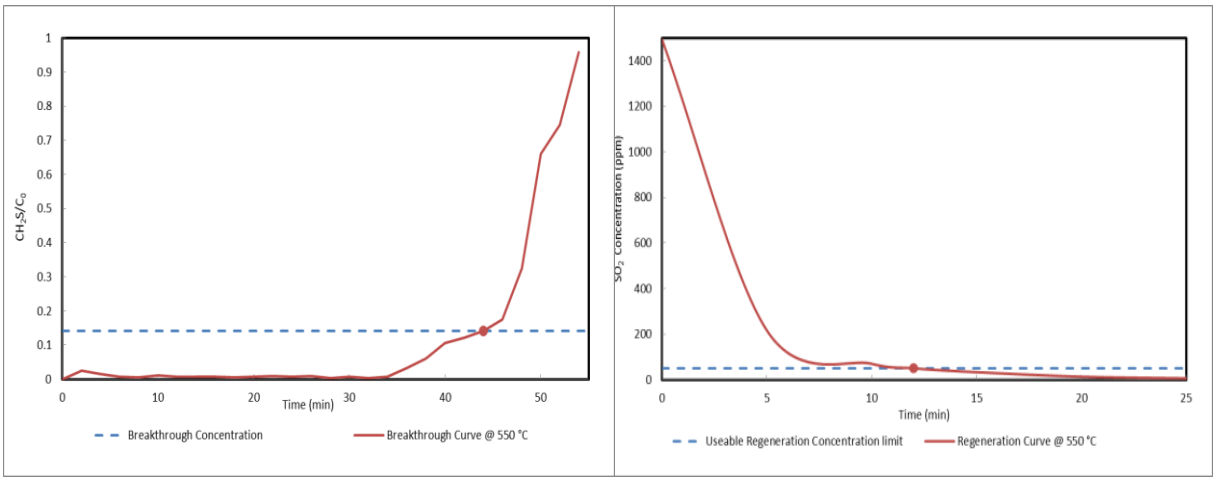

Figure 5-26: Breakthrough curve and regeneration curve, run 3

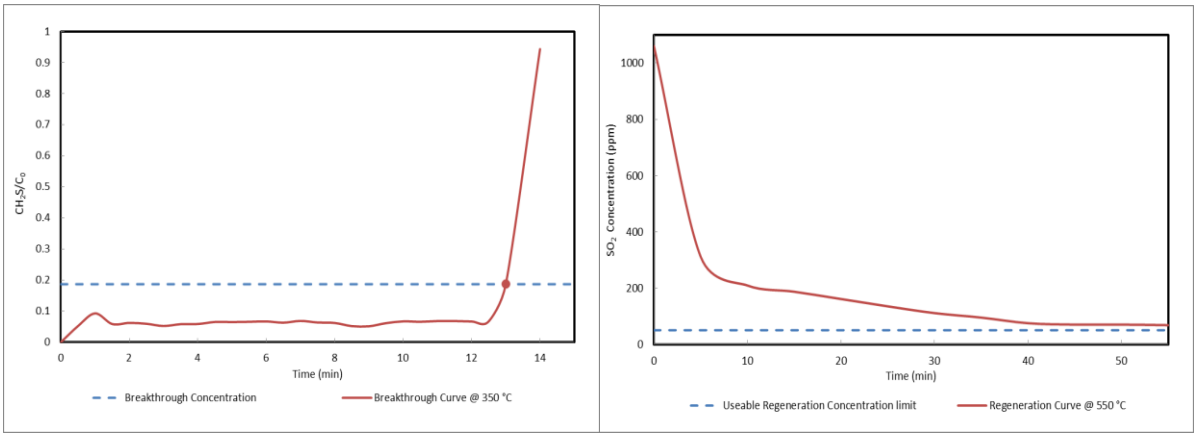

Figure 5-27: Breakthrough curve and regeneration curve, run 4

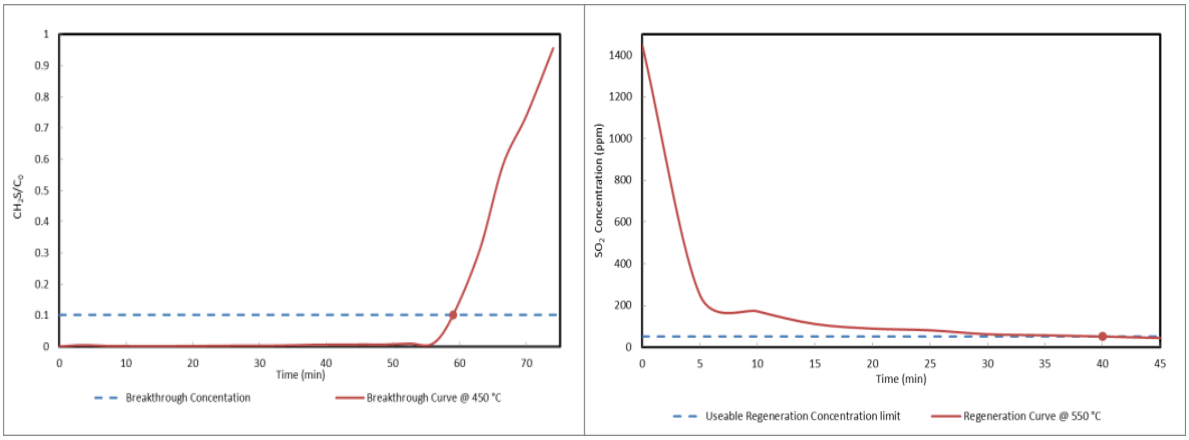

Figure 5-28: Breakthrough curve and regeneration curve, run 5

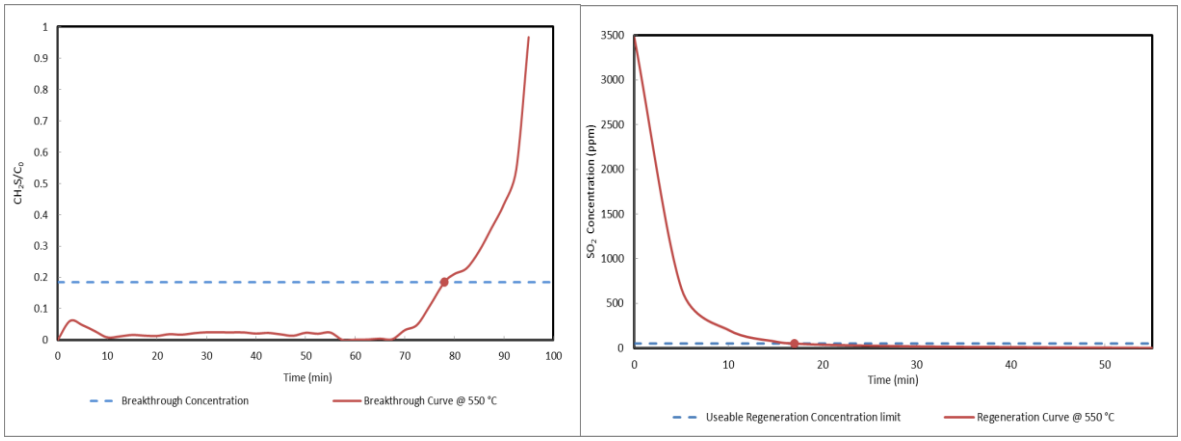

Figure 5-29: Breakthrough curve and regeneration curve, run 6

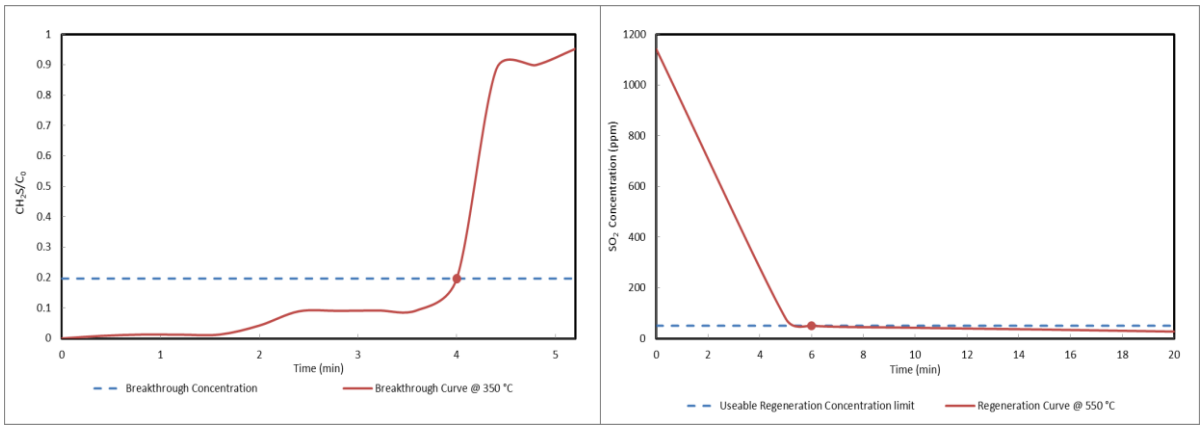

Figure 5-30: Breakthrough curve and regeneration curve, run 7

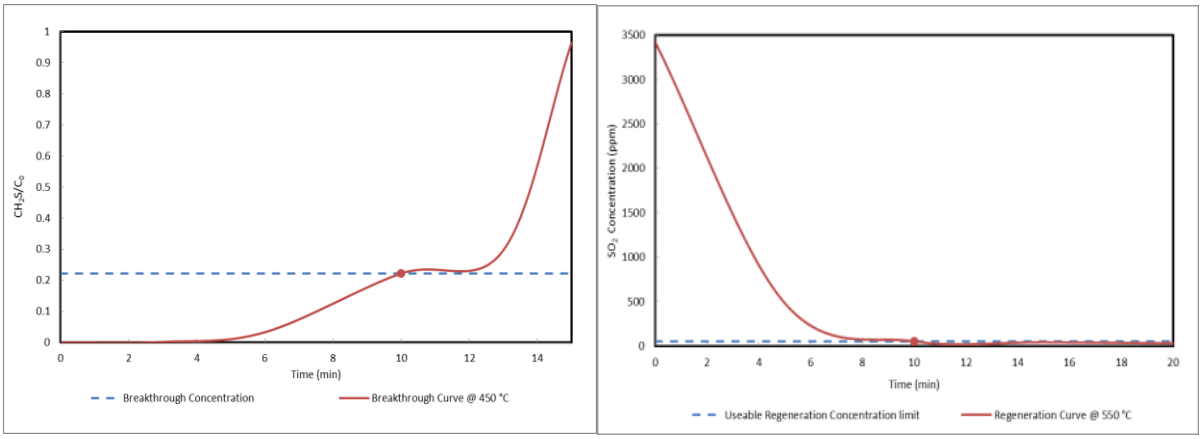

Figure 5-31: Breakthrough curve and regeneration curve, run 8

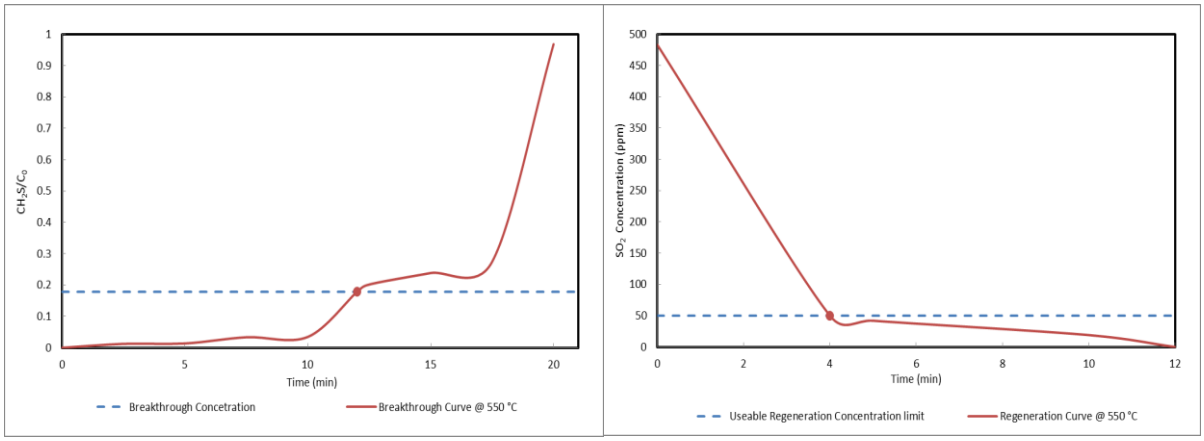

Figure 5-32: Breakthrough curve and regeneration curve, run 9

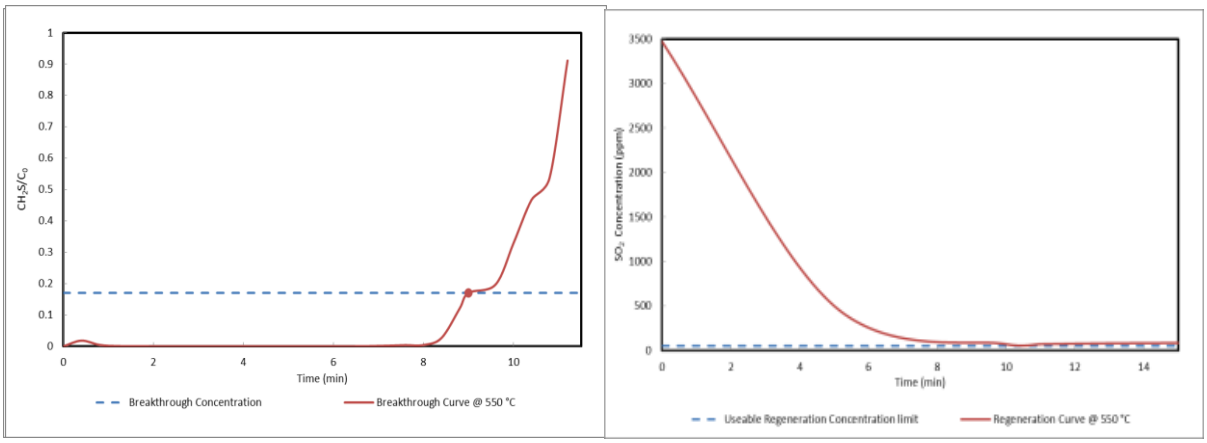

Figure 5-33: Breakthrough curve and regeneration curve, run 10

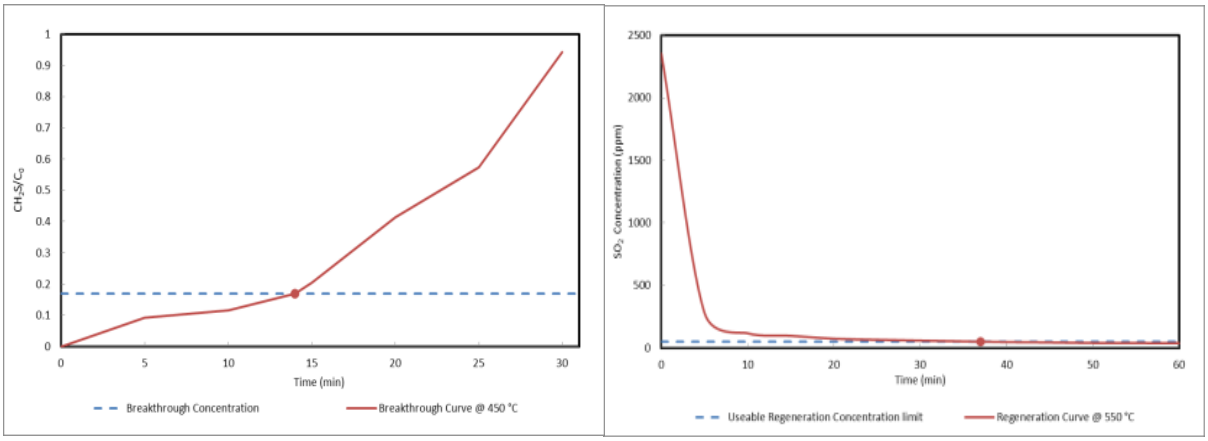

Figure 5-34: Breakthrough curve and regeneration curve, run 11

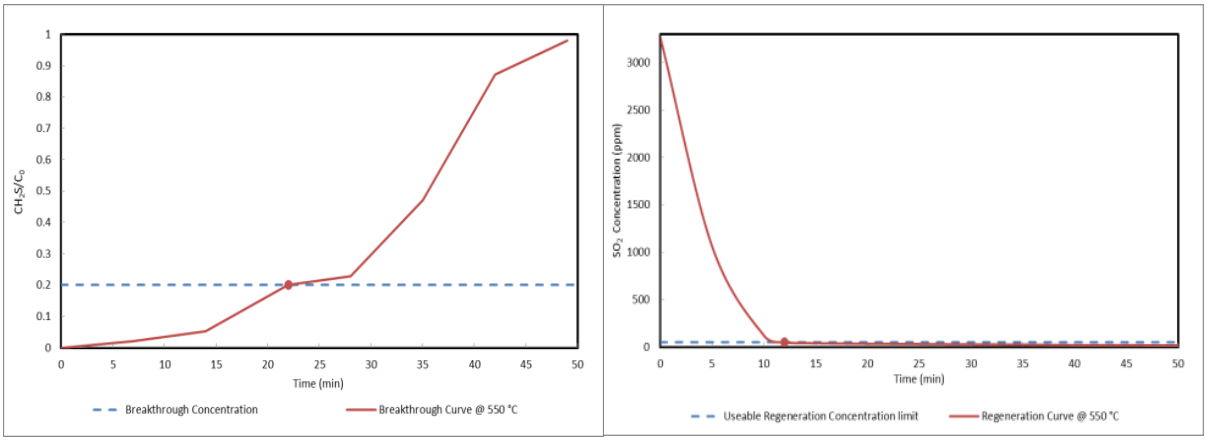

Figure 5-35: Breakthrough curve and regeneration curve, run 12

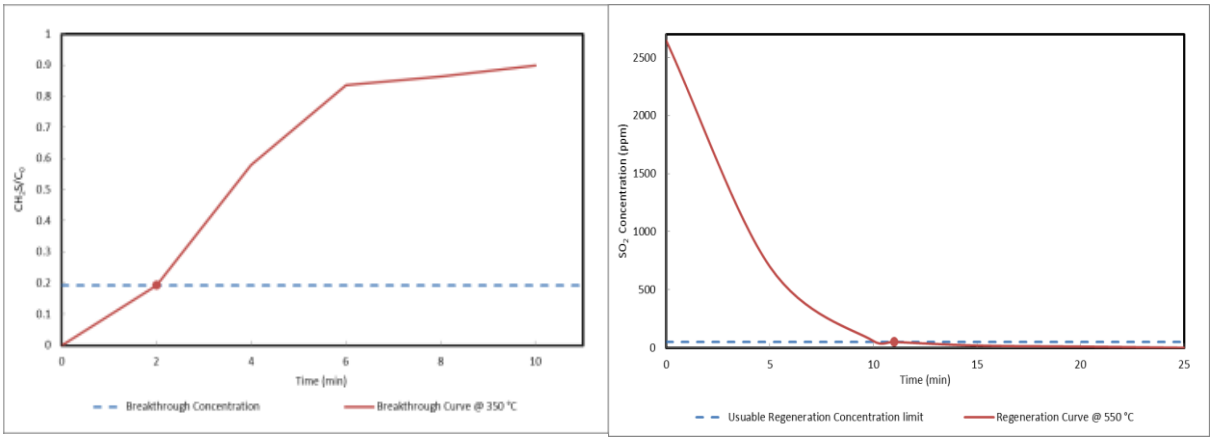

Figure 5-36: Breakthrough curve and regeneration curve, run 13

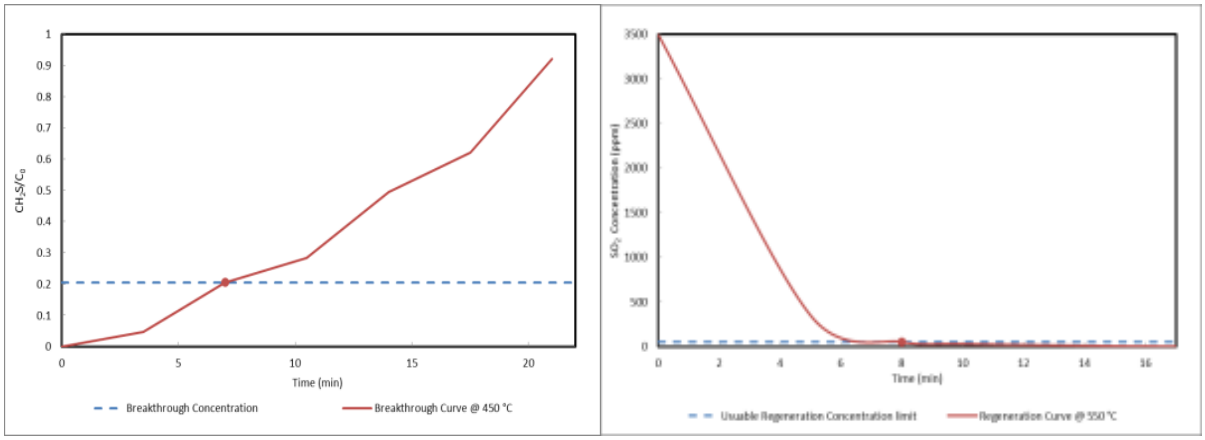

Figure 5-37: Breakthrough curve and regeneration curve, run 14

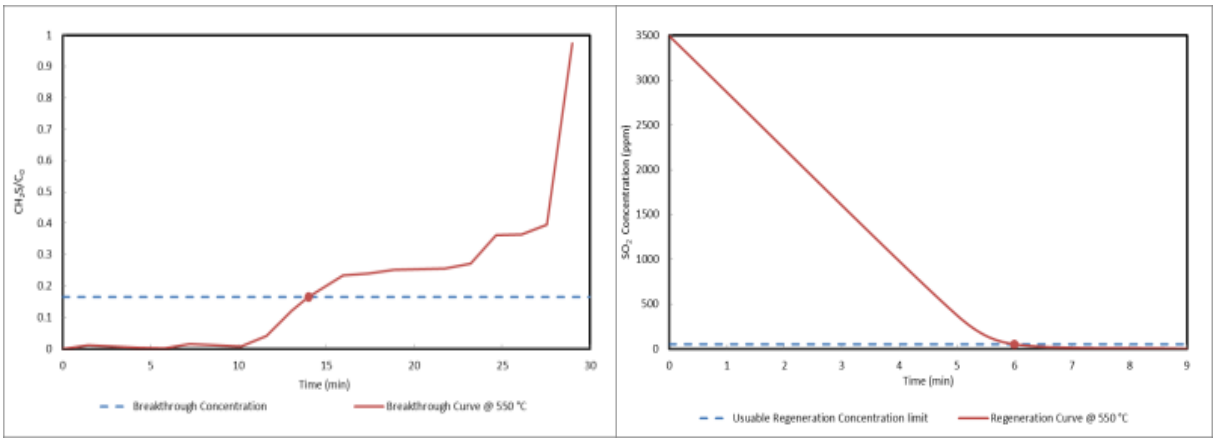

Figure 5-38: Breakthrough curve and regeneration curve, run 15

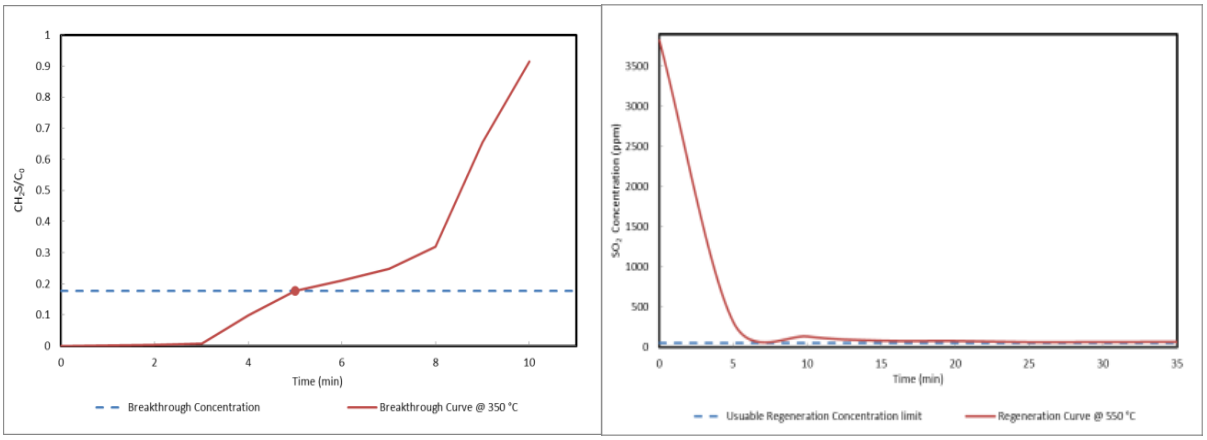

Figure 5-39: Breakthrough curve and regeneration curve, run 16

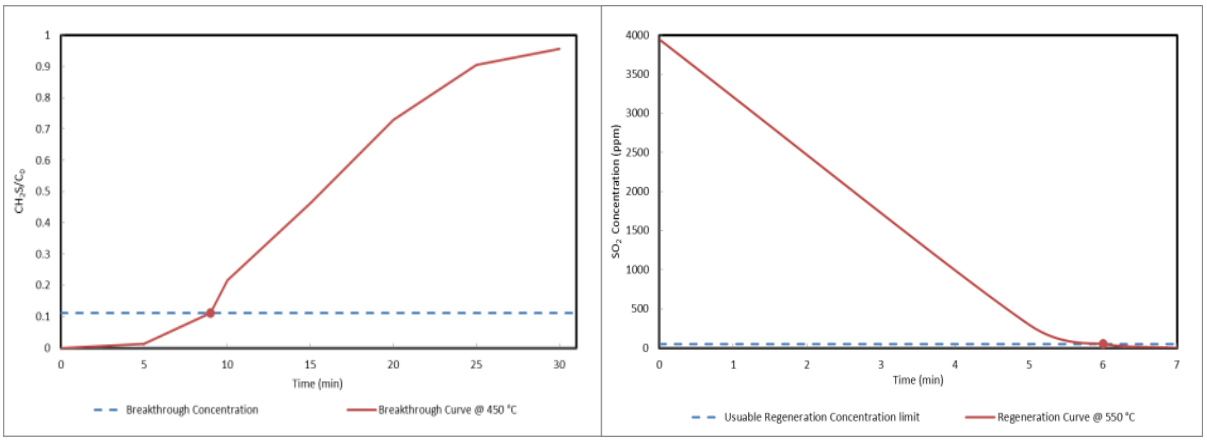

Figure 5-40: Breakthrough curve and regeneration curve, run 17

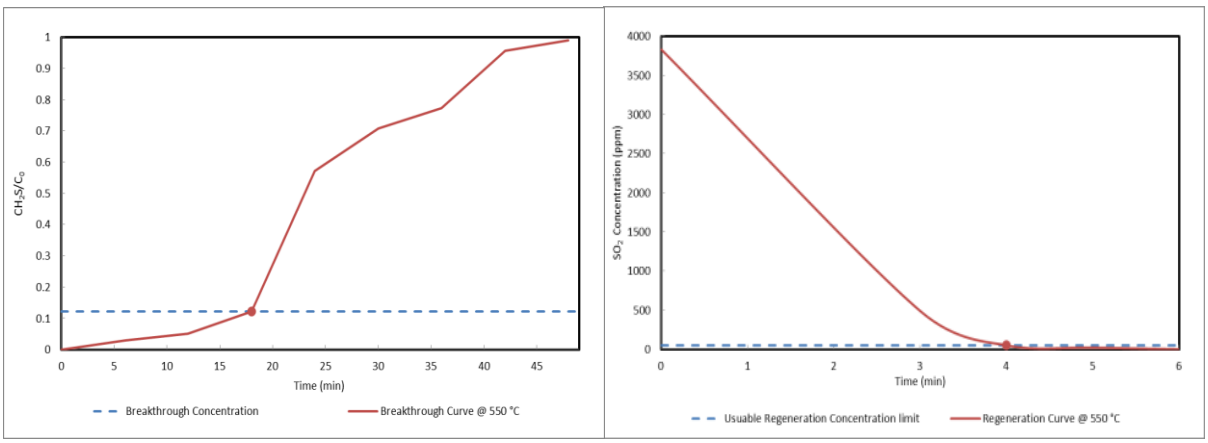

Figure 5-41: Breakthrough curve and regeneration curve, run 18

5.4.1. Desulphurisation

5.4.1.1. The effect of temperature on desulphurisation

The experimental range for desulphurisation temperature in this study was 350 °C - 550 °C, which was noted by Yang and Tatarchuk (2010) as the optimal range. Temperature profiles were plotted for all 18 runs and are shown in Appendix C (left). These temperature profiles depict the changes in temperature of the desulphuriser exit (blue dotted line), desulphuriser inlet (red dotted line) and sorbent (green solid line) during the desulphurisation process. A greater variation is noted in the sorbent temperature due this being the active site for reactions in the process. At the start of the runs, the temperature rise is due to the exothermic nature of the sulfidation reaction (See equation 2.14). Thereafter the temperatures stabilize due the sorbent reaching saturation forming isothermal conditions. At the point of sorbent saturation, the temperature of the sorbent starts to decrease to indicate the end of the sulfidation reaction. The averaged sorbent temperatures from the profiles show a great correlation to the temperatures required for the runs.

Figures 5-42 to 5-44 show that sonicated and non-sonicated sorbent samples of 5g revealed longer desulphurisation breakthrough times at elevated temperatures. At equivalent wt. % ZnO loading and varying temperature, sonicated sorbents had a longer breakthrough time. Moreover, at higher temperatures both sonicated and non-sonicated sorbents take longer to reach maximum sorbent saturation capacity which results in a longer useable sorbent. The higher operating temperatures would however require more energy input, so operating at lower temperatures is advisable if possible.

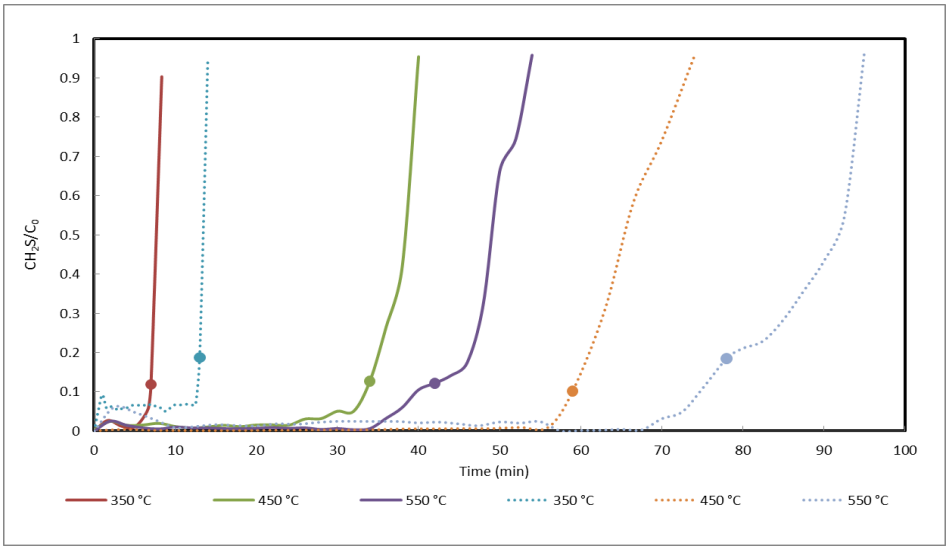

Figure 5-42: Breakthrough curves of 30 wt. % ZnO loading runs, non-sonicated (solid line) and sonicated (dotted line)

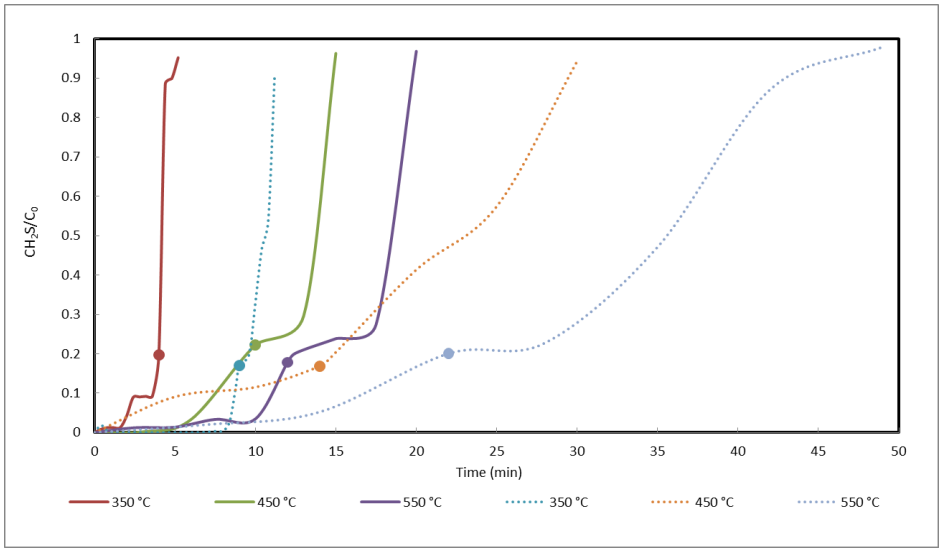

Figure 5-43: Breakthrough curves of 20 wt. % ZnO loading runs , non-sonicated (solid line) and sonicated (dotted line)

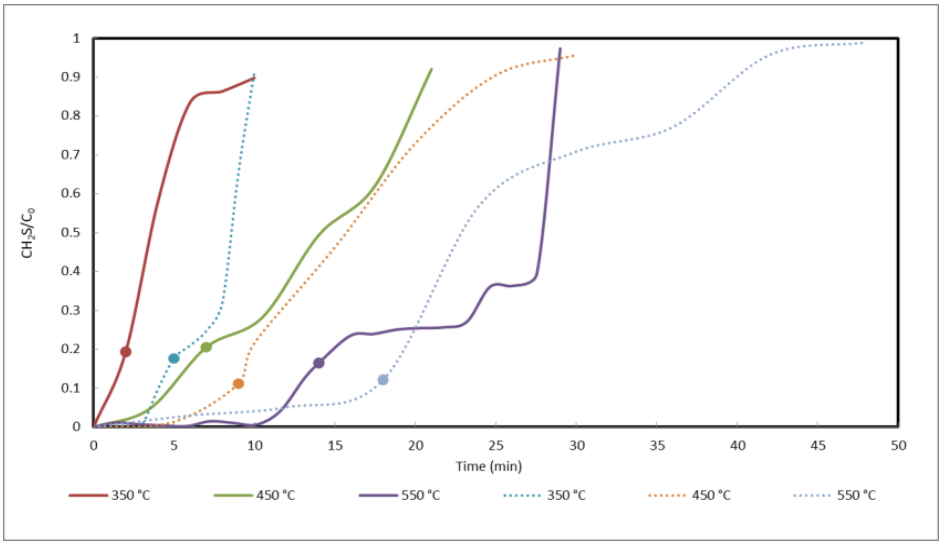

Figure 5-44: Breakthrough curves of 10 wt. % ZnO loading runs, non-sonicated (solid line) and sonicated (dotted line)

N.B. - The dotted lines denote the sonicated runs while the solid lines denote the non-sonicated runs. The solid dot on each line represents the breakthrough point.

5.4.1.2. The effect of wt. % ZnO loading on desulphurisation

The experimental range for wt. % ZnO loading in this study was 10% - 30%. The 10 wt. % ZnO loading non-sonicated sorbent showed better results than the equivalent 20 wt. % ZnO loading non-sonicated sorbent at 550 ℃. This could be due to the lower loading of metal oxide particles being relatively evenly dispersed and more metal oxide particles were capable of reacting with H_2S (see Figure 2-6). Wang and Yang (2014) further verified the importance of good dispersion of small metal oxide particles. They discovered that higher metal oxide loading resulted in larger particles and less dispersion, resulting in decreased sorbent capacity. They compared prepared sorbents of 10 wt. %, 20 wt. %, 30 wt. % ZnO dispersed onto mesoporous silica molecular sieve (MSU-1) using an incipient wet impregnation technique.

Figures 5-45 to 5-47 show that sonicated and non-sonicated sorbent samples of 5g revealed longer desulphurisation breakthrough times at higher wt. % ZnO loading. At equivalent temperature and varying wt. % ZnO loading, sonicated sorbents had a longer breakthrough time. Furthermore, by inspect of Table 5-2 (with respect to breakthrough times) it can be seen that there is a lesser variation in both sonicated and non-sonicated sorbents at low wt. % ZnO loading (10%-20%) and a greater variation in both sorbents at high wt. % ZnO loading (30%). This is a crucial result as it implies that differences in wt. % ZnO loading of the sorbent only become appreciable at a high wt. % ZnO loading range. Therefore the optimum range for appreciable breakthrough times for both sorbents lies in a range of 450 ℃ - 550 ℃ at 30 wt. % ZnO loading.

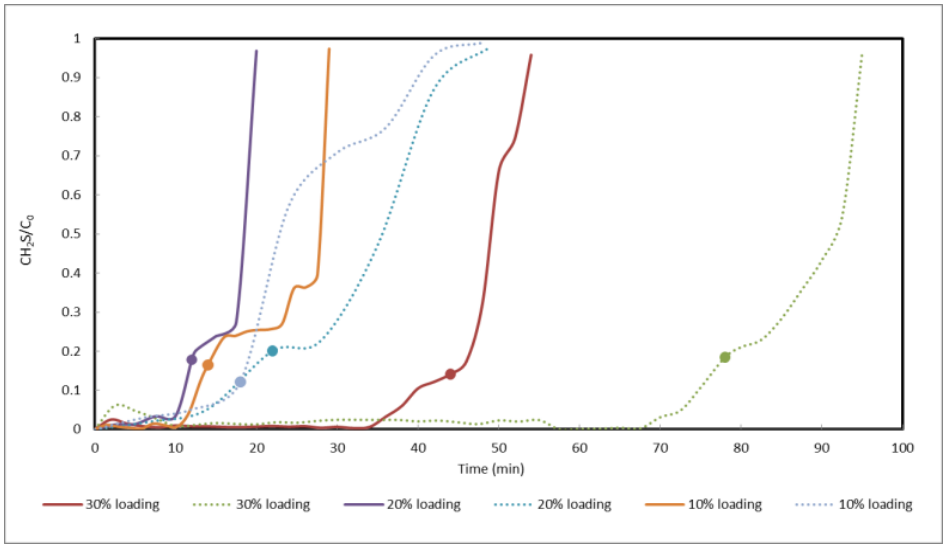

Figure 5-45: Breakthrough curves of 550 ℃ temperature runs, non-sonicated (solid line) and sonicated (dotted line)

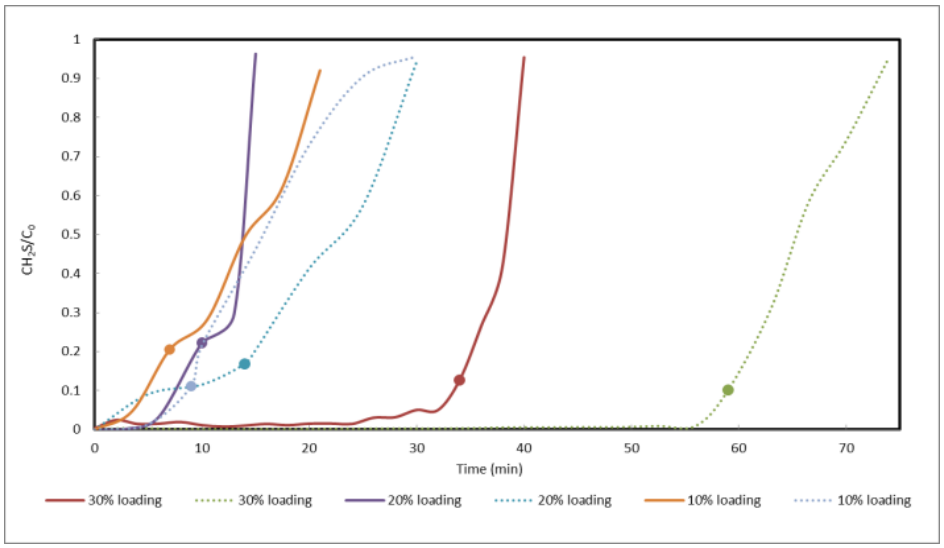

Figure 5-46: Breakthrough curves of 450 ℃ temperature runs, non-sonicated (solid line) and sonicated (dotted line)

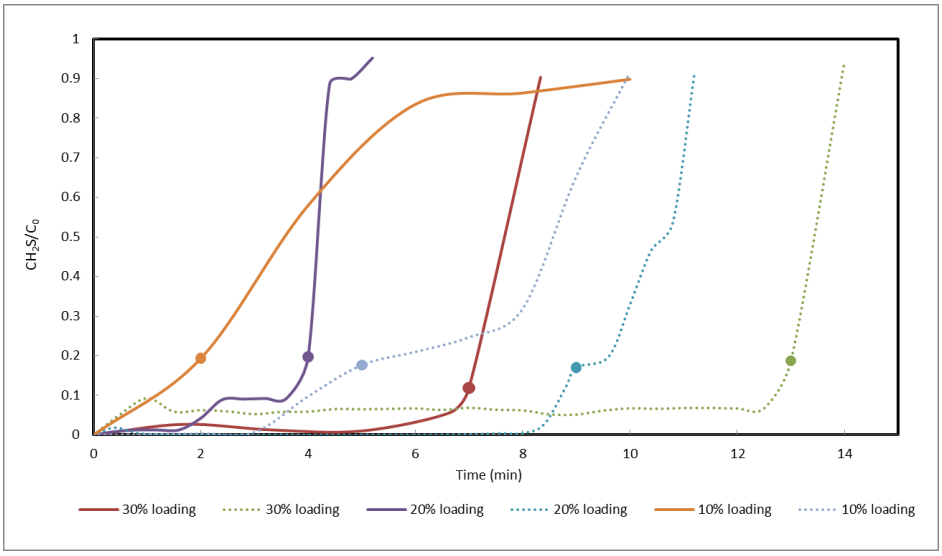

Figure 5-47: Breakthrough curves of 350 ℃ temperature runs, non-sonicated (solid line) and sonicated (dotted line)

5.4.1.3. The effect of other factors on desulphurisation

For this study the sorbent was prepared using high-purity grade, high surface area silica as the support material onto which the zinc-oxide was dispersed. This resulted in a fine white powder of sorbent. After desulphurisation the sorbent becomes saturated with H_2S forming a greyish zinc sulphide sorbent (see Figure 5-22). The mass increase can be attributed to the fact that zinc sulphide has a higher molecular mass than zinc oxide. Alternatively, a low surface area supported sorbent was also prepared.

Taking the best conditions for the runs in this study (30 wt. % ZnO loading sonicated sorbent at 550 °C), two runs were done using the low surface area sorbent at these conditions. Figure 5-48 shows the results of these runs:

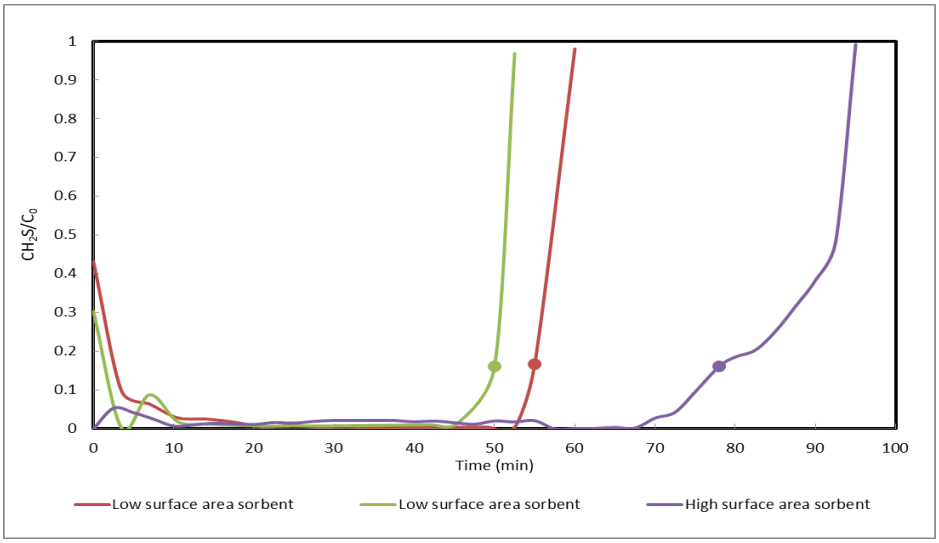

Figure 5-48: Breakthrough curves of high and low surface area sorbents

The high surface area sorbent had a longer breakthrough time than the low surface area sorbent at these conditions. The higher readings for the initial peaks of the lower surface area sorbent on Figure 5.48 were most likely due to some bypassing of the sorbent bed inside the reactor. It is however evident that a sorbent with a higher surface area has better desulphurisation characteristics. An average % increase in the breakthrough times for sonicated sorbents over non-sonicated sorbents was calculated. There was an average % increase in breakthrough time of of 39.13%, 73.07% and 74.74% for the (10, 20 and 30wt. %) ZnO loading sorbents respectively (See Table 5-2). In particular, as the wt. % ZnO loading of sorbents increased, the effect of sonication had a greater impact in improving breakthrough times.

From Table 5-2 it was seen that a higher saturation capacity did infact relate to a longer breakthrough time. An average % increase in the saturation capacity for sonicated sorbents over non-sonicated sorbents was calculated. There was an average % increase in saturation capacity of 3.65%, 9.62% and 0.86% for the (10, 20 and 30wt. %) ZnO loading sorbents respectively (See Table 5-2). This result highlighted that the improvement in saturation capacity was due to the sonication of sorbents. The saturation capacities for all runs were close in comparison to the value of 0.113 g S/g ZnO quoted by Yang and Tatarchuk (2010). This further validates the results achieved through all of the desulphurisation runs.

5.4.2. Regeneration

5.4.2.1. The effect of temperature on regeneration

The experimental regeneration temperature in this study was at 550 ℃ for all of the saturated sorbents (referred to as spent sorbents). A clear distinction should be made that it was the gas mixture that was desulphurised and not the sorbent itself. It is important to note that while the desulphurisation temperatures varied from 350 ℃ - 550 ℃, all spent sorbents were regenerated at 550 ℃ only. Temperature profiles were plotted and are shown in Appendix C (right) for all 18 runs. A similar trend was noticed between regeneration and desulphurisation with respect to the sorbent being the active site for reactions in the process, and the shape of the temperature profiles due to the exothermic nature of the regeneration reaction (See equation 2.15).

Figures 5-49 to 5-51 show that at elevated desulphurisation temperatures for the sonicated and non-sonicated spent sorbent samples of 5g, regeneration times were shorter. Furthermore, by inspect of Table 5-3 (with respect to regeneration times) it can be seen that the sonicated spent sorbents, desulphurised at 350 °C, were not regenerable to the useable limit. Hence, the desulphurisation temperature range of regenerable zinc-based spent sorbents for this study laid in the range of 450°C to 550 °C. Having now obtained the desulphurisation range for regenerable zinc-based spent sorbents at a fixed temperature regeneration (550 °C), a further run was done to test the effect of a lower fixed temperature regeneration at 350 °C (see Figure 5-52). The spent sorbent (at run 5 desulphurisation conditions) was not regenerable to the useable limit and the rate of sorbent regeneration was significantly lower.

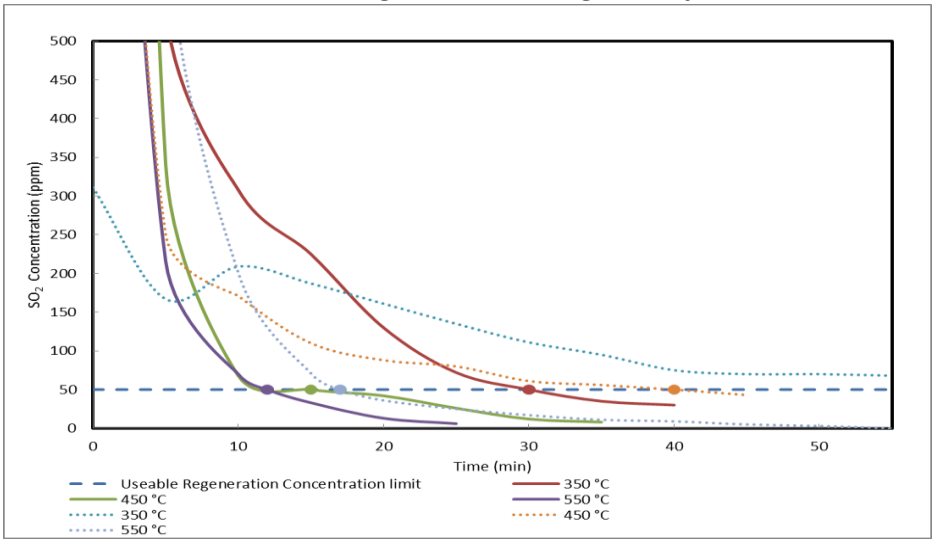

Figure 5-49: Regeneration curves of 30 wt. % ZnO loading runs, non-sonicated (solid line) and sonicated (dotted line)

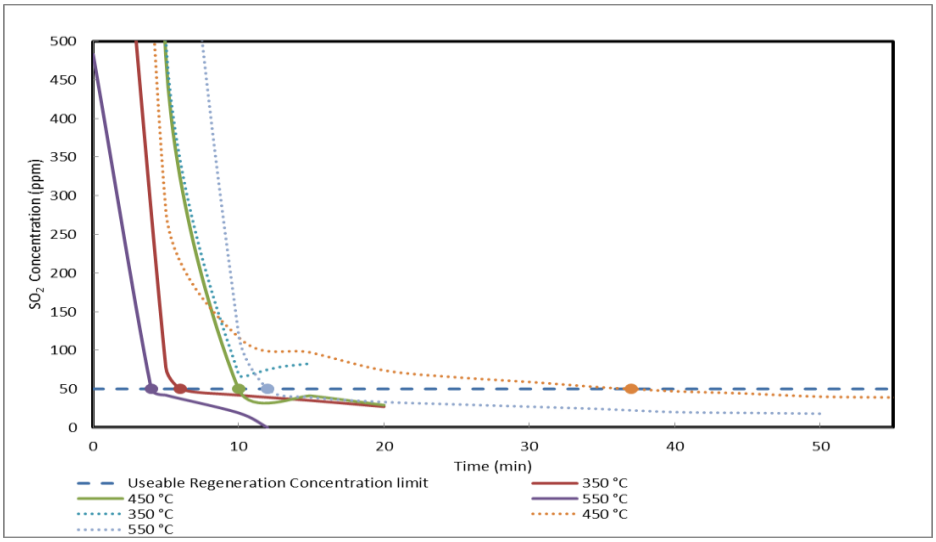

Figure 5-50: Regeneration curves of 20 wt. % ZnO loading runs, non-sonicated (solid line) and sonicated (dotted line)

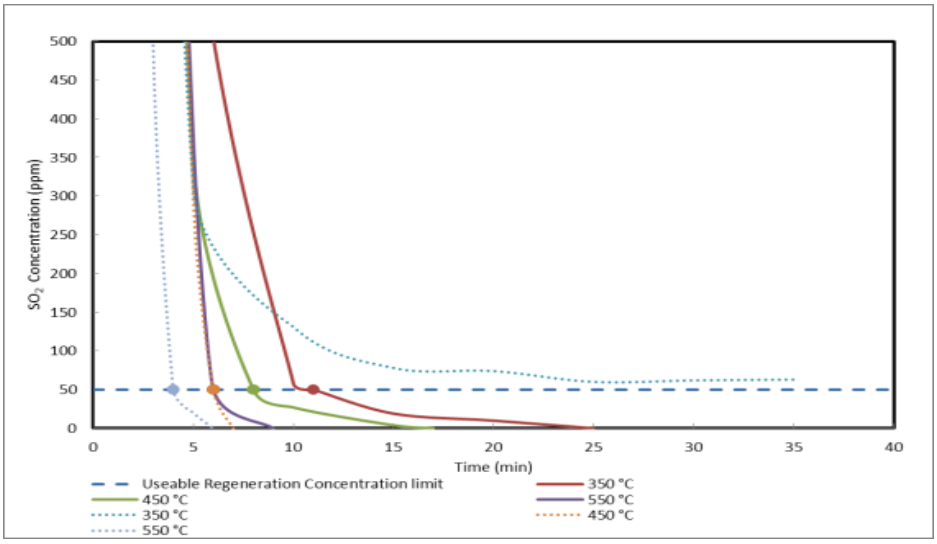

Figure 5-51: Regeneration curves of 10 wt. % ZnO loading runs, non-sonicated (solid line) and sonicated (dotted line)

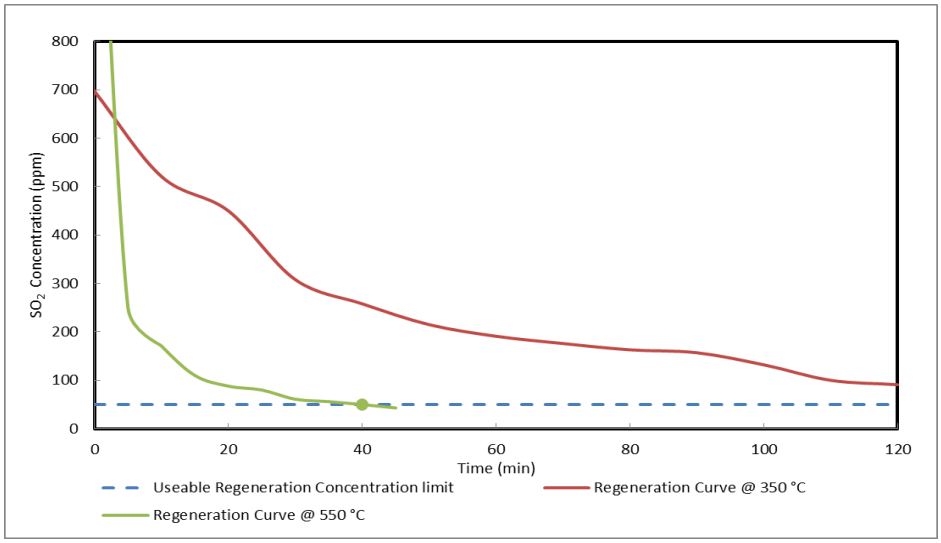

Figure 5-52: Comparison of lower and higher fixed temperature regeneration

5.4.2.2. The effect of wt. % ZnO loading on regeneration

The experimental range for wt. % ZnO loading in this study was 10% - 30%. Figures 5-53 to 5-55 show that at lower wt. % ZnO loading for the sonicated and non-sonicated spent sorbent samples of 5g, regeneration times were shorter. For higher wt. % ZnO loading (30%-20%) at equivalent desulphurisation temperature, sonicated sorbents had a longer regeneration time than non-sonicated sorbents. However, for lower wt. % ZnO loading (10%) at equivalent desulphurisation temperature, the converse was true. As aforementioned this could be due to the lower loading of metal oxide particles being relatively evenly dispersed and more metal oxide particles were capable of reacting with H_2S (see Figure 2-6). Furthermore, by inspection of Table 5-3 (with respect to regeneration times) it can be seen that all of the spent sorbents were regenerable to a useable limit within ~60 min in the desulphurisation temperature range of 450°C to 550 °C. There was also a general trend relating the lower wt. % ZnO loading to a lesser Final SO_2 concentration.

Hence, by taking the desulphurisation and regeneration results into consideration, the 30 wt. % ZnO loading sonicated sorbent employed at 550 °C showed the best overall performance.

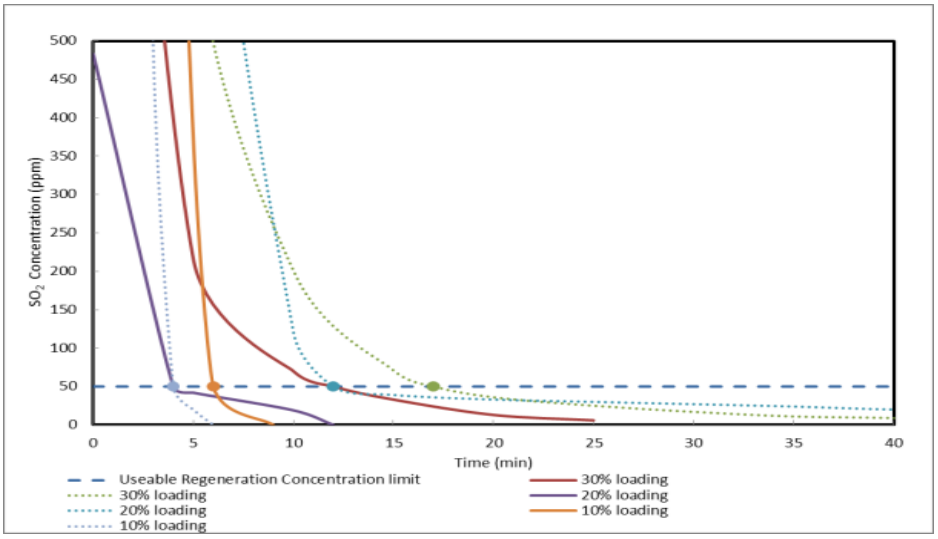

Figure 5-53: Regeneration curves of 550 ℃ temperature runs, non-sonicated (solid line) and sonicated (dotted line)

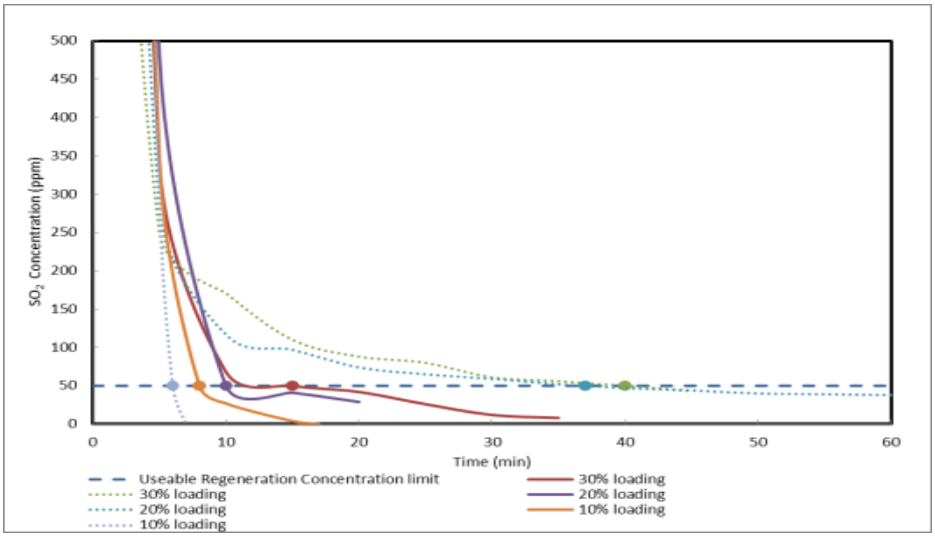

Figure 5-54: Regeneration curves of 450 ℃ temperature runs, non-sonicated (solid line) and sonicated (dotted line)

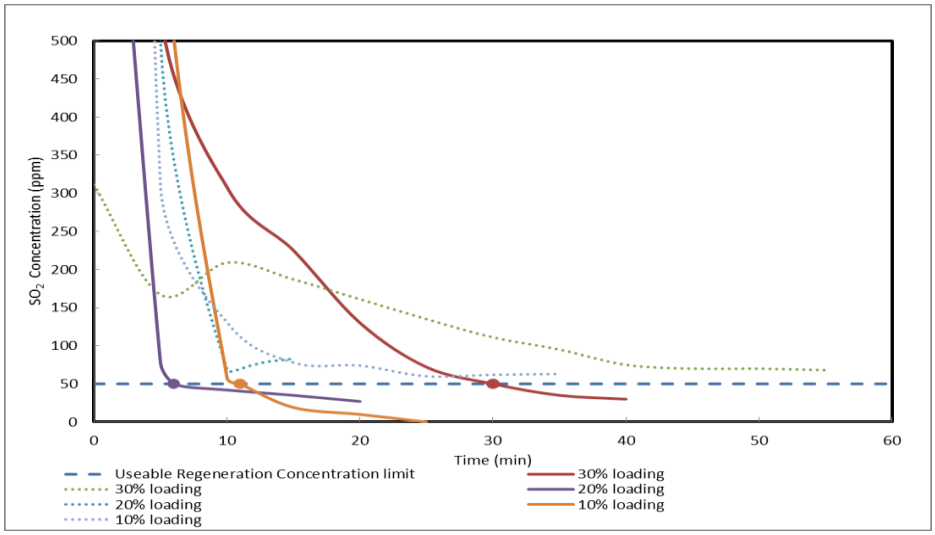

Figure 5-55: Regeneration curves of 350 ℃ temperature runs, non-sonicated (solid line) and sonicated (dotted line)

5.4.3. Repeatability

Tests for repeatability were carried out for the 30 wt. % ZnO loading sorbent since this was the best performing sorbent. The experiments were carried out at exactly the same operating conditions to determine how close of an agreement there was between the results of the successive runs.

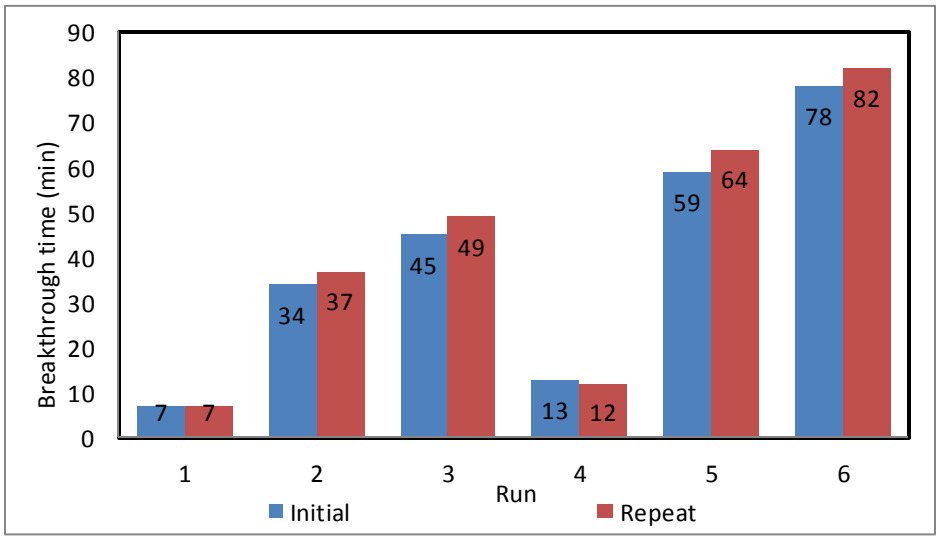

Figure 5-56: Comparison between runs for desulphurisation

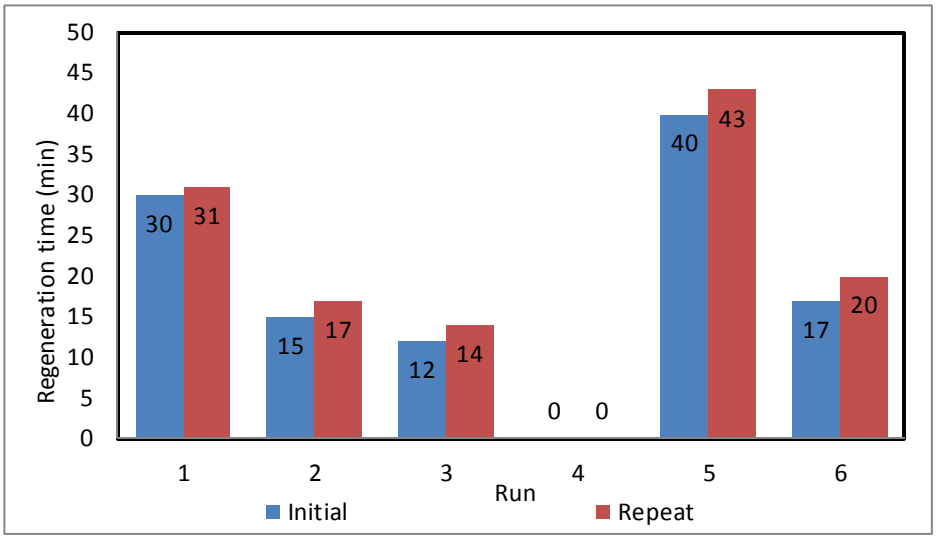

Figure 5-57: Comparison between runs for regeneration

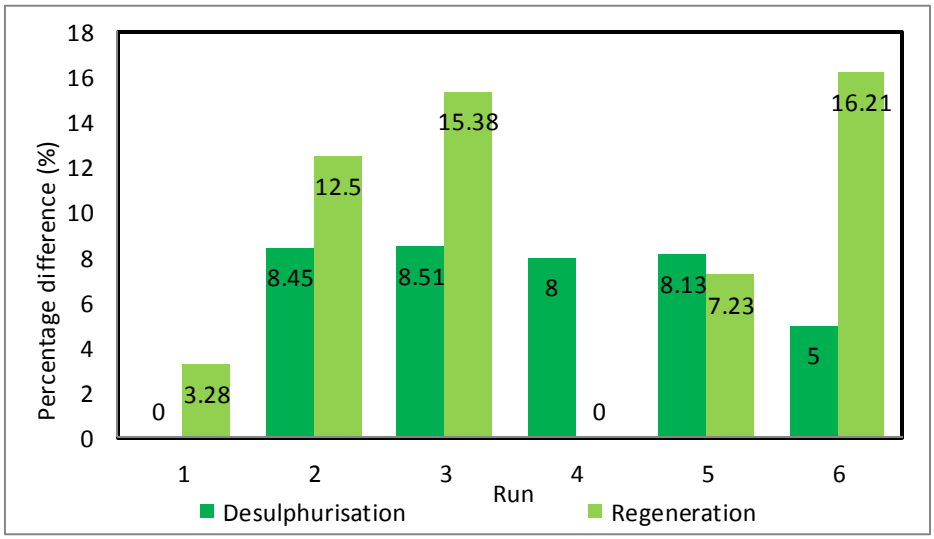

Figure 5-58: Percentage difference between the initial and repeated runs for desulphurisation and regeneration

From the desulphurisation comparison (Figure 5-56) it can be seen that the results are similar. The regeneration results (Figure 5-57) show more of a variation. The is a lesser variation in the low temperature range (350 °C), as compared to the higher temperature range (450 °C - 550 °C), for both regeneration and desulphurisation. The percentage difference between the initial and repeated runs was calculated for both desulphurisation and regeneration (Figure 5-58). In most experiments a percentage difference of about 10% is deemed acceptable (Appalachian State University, 2016). There are fundamentally three types of errors that affect this result:

- Personal error
  - This is as a result of the bias of the person performing the experiment and is usually termed as "Human-error".

- Random error
  - These errors usually occur due to factors that are considered indeterminate or unknown. For this experiment, there will be a delay between when a sample is sent for GC analysis and the time of actual breakthrough. Taking this variable analysis time into account would greatly increase the accuracy of results as well as decrease the percentage difference.

- Systematic error
  - Implicit errors caused by the system itself. These accuracies affect all measurements hence; a correction factor is needed to compensate for the constant deviation.

In order to determine the root cause for differing results between successive runs, there needs to be an independent assessment of measurement uncertainty. In these experiments there were two such factors. Firstly the mass of the sorbent used. There could have been loss in the mass of sorbent between successive runs while loading the reactor. The final factor was the volumetric flowrate of the gas mixture. As aforementioned, the Alicat Scientific gas mass flow controller could not be used for the H_2S gas. The volumetric flowrate was therefore controlled with a needle valve and bubble flow meter. The chances of fluctuations in the volumetric flowrate are highly likely. In these cases, the differing mass of sorbent and volumetric flowrate of the gas mixture would directly affect results between successive runs.

5.4.4. Comparative study

In this section the results from this dissertation was compared to the results of a similar experiment from literature. An attempt was made to relate the saturation capacities and breakthrough times for both experiments despite differing conditions. Yang and Tatarchuk (2010) prepared a ZnO/SiO_2 sorbent using an incipient wet impregnation technique. Their apparatus used quartz tubing of 1 cm inner diameter. An average saturation capacity for all runs of the non-sonicated and sonicated sorbents was compared to the values achieved by Yang and Tatarchuk (2010), in Table 5-4:

Table 5-4: Comparison table of saturation capacities

Sorbent	Average Saturation Capacities for all runs (g S/g ZnO)
Non-sonicated ZnO/SiO_2	0.111
Sonicated ZnO/SiO_2	0.116
Literature ZnO/SiO_2	0.113

From the results in Table 5-4, the values of the average saturation capacities for the non-sonicated and literature ZnO/SiO_2 sorbents were relatively close. From studies by Yang (2007), this points to the intraparticle diffusion resistance being minimal during the preparation of these sorbents via their respective techniques. The sonicated ZnO/SiO_2 sorbent with an average saturation capacity of 0.116 g S/g ZnO had the highest saturation capacity. This proves that the sorbents prepared via the Ultrasonic-assisted Impregnation (UAI) technique enhance saturation capacity. It is important to note, however that these average saturation capacities were lower than the theoretical value. At 100% conversion of Equation 2.14, the saturation capacity would be 0.329 g S/g ZnO. The difference in these values could be explained by under-utilization of the ZnO. As the ZnO particles are loaded onto the surface of the silica, there is a possibility of them piling on top of each other. This would result in a smaller surface area available, at the active sites, for desulphurisation. This unreacted ZnO would account for the differences between experimental and theoretical values.

To compare the breakthrough times, the Table 5-5 was first generated to summarize the differences between experimental conditions.

Table 5-5: Comparison between experimental conditions

	(Yang and Tatarchuk, 2010)	This dissertation
Mass of sorbent (g)	0.5	5
Volumetric flowrate of gas (cm^3/s)	1.667	142.857
H_2S inlet concentration (ppmv)	8000	10000
wt. % ZnO loading	17	20

A ratio of the volumetric flowrate of gas to the mass of sorbent used was compared for both cases (See Appendix B.6). From the value of these two ratios a normalizing factor was calculated to compare the results from literature to this study. The literature value for desulphurisation is 30 min at 350 °C. Taking

this breakthrough time and dividing by the normalizing factor, a normalized value of 3.5 min was attained. This normalized breakthrough time however is for a 17 wt. % ZnO loading. Figure 5-59 was plotted from the results of this dissertation in order to interpolate to 17 wt. % ZnO loading for comparison. A 2nd order polynomial trend-line was fitted to both sets of data for greater accuracy. After interpolating for 17 wt. % ZnO loading from these dissertations results, the non-sonicated sorbent breakthrough time was 3.42 min. This was very close to the normalized value from literature of 3.5 min, which shows an excellent correlation between desulphurisation results despite differing experimental conditions. The sonicated sorbents breakthrough time of 7.93 min was much greater than the normalized value from literature. This means that if the sonicated sorbent from this dissertation was run at literature desulphurisation conditions; a breakthrough time of 68 mins would be achieved. This proves that the sorbents prepared via the Ultrasonic-assisted Impregnation (UAI) technique enhance breakthrough times.

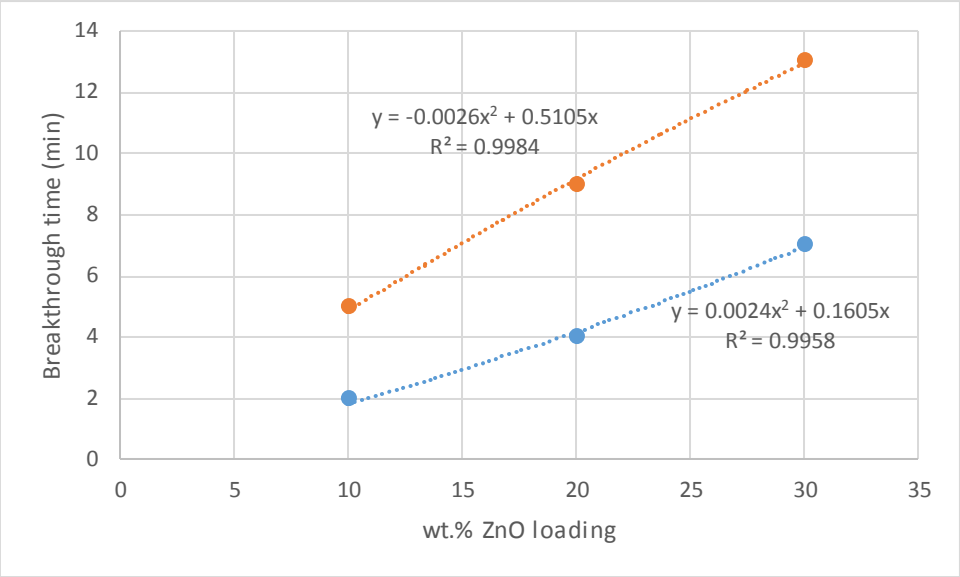

Figure 5-59: Desulphurisation results for non-sonicated (blue line) and sonicated (orange line) sorbents at 350 °C

It was also noted that a lower temperature of 550 °C was able to achieve sorbent regeneration as compared to industrial calcination (roasting) of ZnS, which is usually executed at 800 °C- 900 °C. This could possibly be explained by the Mars-van Krevelan mechanism. In a typical roasting, only gas phase oxygen is available for oxidation. For the system in this dissertation the oxidation of zinc sulphide is via lattice oxygen, and this oxygen is replenished by gas phase oxygen. In this redox mechanism the surface is first reduced when it releases the oxygen and is then reoxidized by the gas. This redox process is known to occur at faster rates than the non-catalytic process; hence oxidation could occur at a lower temperature.

5.5. Gas-solid reactor modelling

The aim of this reactor modelling was to develop a model that would numerically describe the gas-solid reaction in the desulphurisation of zinc-based sorbents in a packed bed reactor. In this adsorption process, there was an accumulation of material at the interface between the gas-solid phases. A packed bed reactor was chosen to model this adsorption as it is the most effective equipment for continuous plug flow (Witzany, Dokupil and Heinzel, 2007). As such, the shrinking core model was used to predict the behavior between the gas film and solid phase spherical particles. As aforementioned, the overall rate of reaction was derived as:

$$r_A = \frac{3(1-\varepsilon)}{R}\left[\frac{1}{k(1-X)^{\frac{2}{3}}} + \frac{1}{k_g} + \frac{R}{D_e}\left((1-X)^{-1/3} - 1\right)\right]^{-1} \tag{3.26}$$

From the above equation, the effective diffusivity D_e, gas film coefficient for mass transfer k_g and intrinsic reaction rate constant k, for Table 5-6 were calculated from correlations in literature (Yang, 2007) and are presented in Appendix B.7. The mixture density and viscosity were taken from *AspenTech V8.8*, using the Soave-Redlich-Kwong (SRK) property method to account for a system of hydrocarbons with a light gas mixture. The following system of ODE's was solved using an implicit numerical method with their respective initial conditions on *Matlab:*

$$\frac{\partial X}{\partial z} = -\frac{r_A}{uC_{A0}} \qquad X(z, t=0) = 0 \tag{3.27}$$

$$\frac{\partial C_A}{\partial z} = -\frac{r_A}{u} \qquad C_A(z=0, t) = 1 \tag{3.28}$$

$$\frac{\partial C_A}{\partial t} = -u\frac{\partial C_A}{\partial z} + D_e\frac{\partial^2 C_A}{\partial z^2} + r_A \qquad C_A(z, t=0) = C_{A0} \tag{3.29}$$

The major parameter affecting the above equations was the intrinsic reaction rate r_A. This parameter has a strong temperature dependence. Table 5-6 shows a summary of all parameter values used in this packed bed reactor modelling. The experimental and predicted breakthrough curves were compared for all 30 wt. % ZnO loading sorbent runs and are shown from Figure 5-60 to Figure 5-65.

Table 5-6: Reactor modelling parameters

	u (cm/min)	R (cm)	k^* (cm/min)	$D_e{}^*$ (cm^2/min)	$k_g{}^*$ (cm/min)	ε
30% ZnO loading, Non-sonicated, 350 °C	2474.712	4.86×10^{-7}	0.0747	1.62×10^{-9}	0.0275	0.373
30% ZnO loading, Non-sonicated, 450 °C	2474.712	4.86×10^{-7}	0.197	3.13×10^{-9}	0.0424	0.373
30% ZnO loading, Non-sonicated, 550 °C	2474.712	4.86×10^{-7}	0.411	5.14×10^{-9}	0.0589	0.373
30% ZnO loading, sonicated, 350 °C	2474.712	6.94×10^{-7}	0.0747	1.62×10^{-9}	0.0226	0.373
30% ZnO loading, sonicated, 450 °C	2474.712	6.94×10^{-7}	0.197	3.13×10^{-9}	0.0346	0.373
30% ZnO loading, sonicated, 550 °C	2474.712	6.94×10^{-7}	0.411	5.14×10^{-9}	0.0478	0.373

*These values were calculated from correlations given by (Yang, 2007).

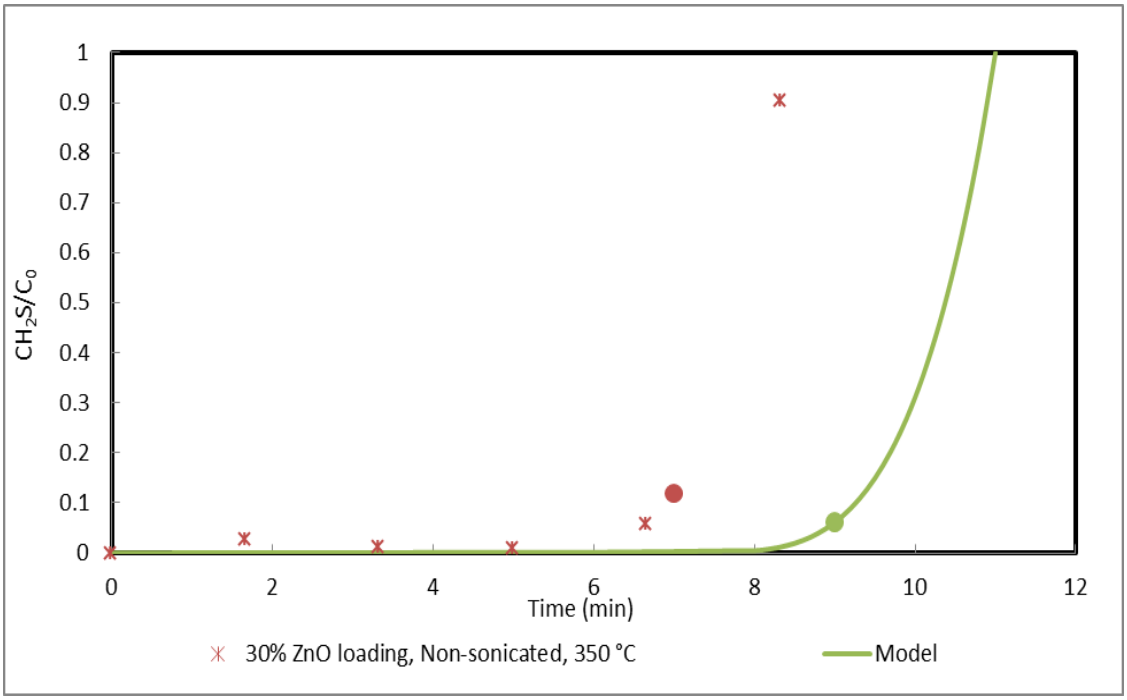

Figure 5-60: Experimental (*) and predicted (-) breakthrough curves for Run 1

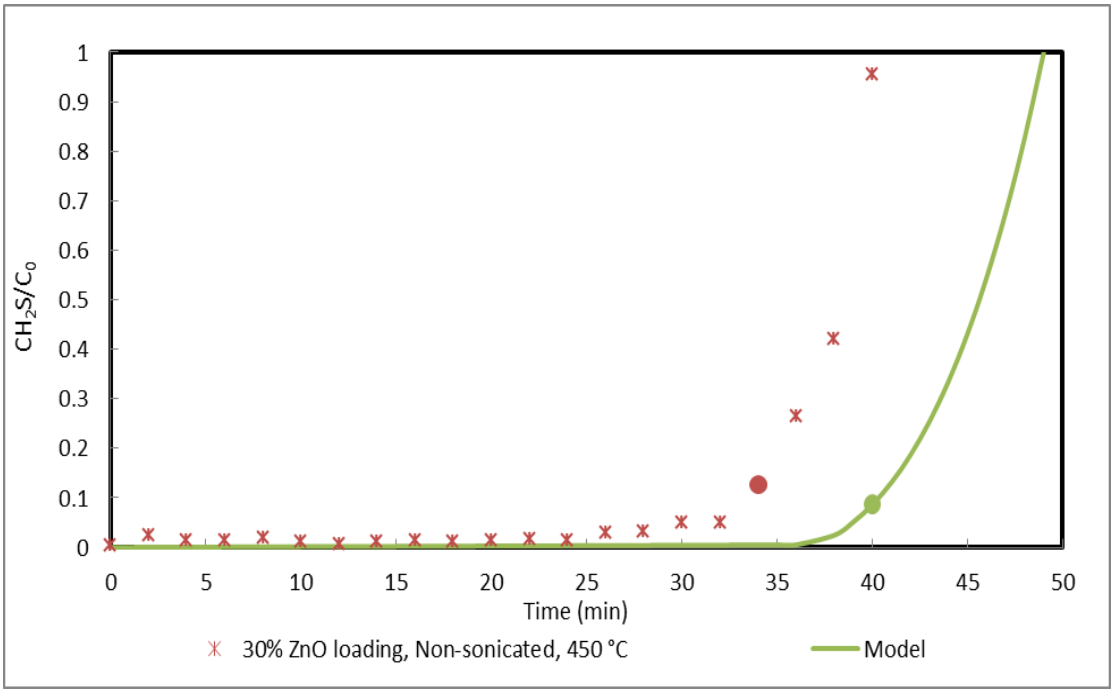

Figure 5-61: Experimental (*) and predicted (-) breakthrough curves for Run 2

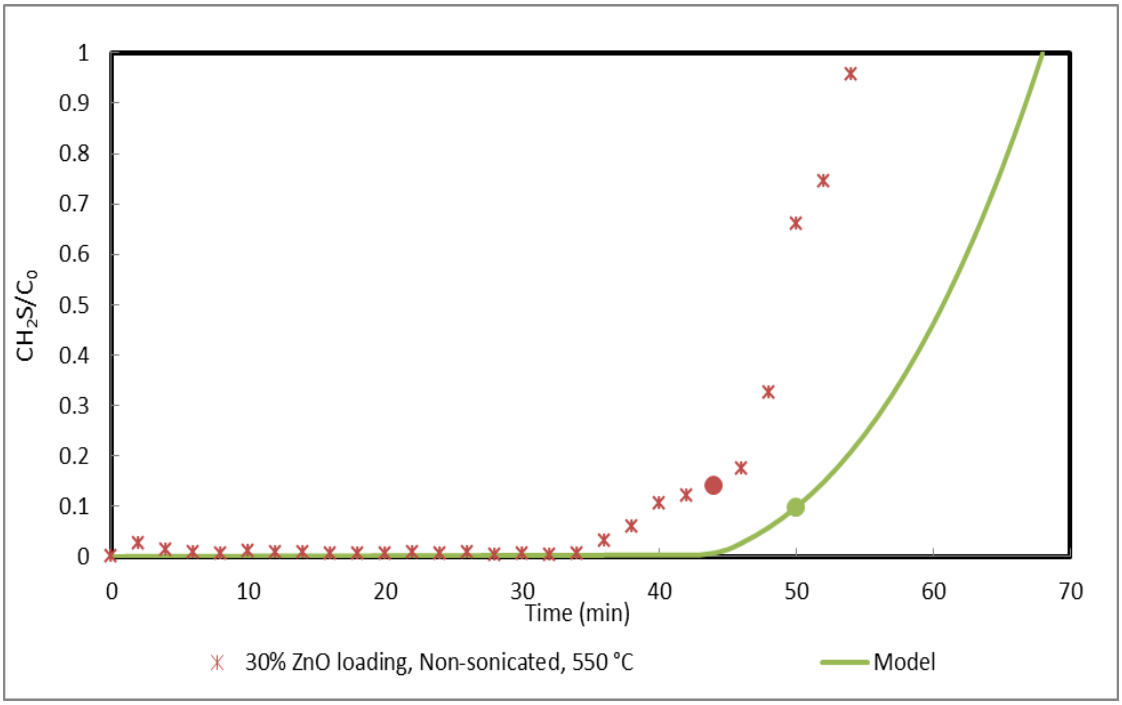

Figure 5-62: Experimental (*) and predicted (-) breakthrough curves for Run 3

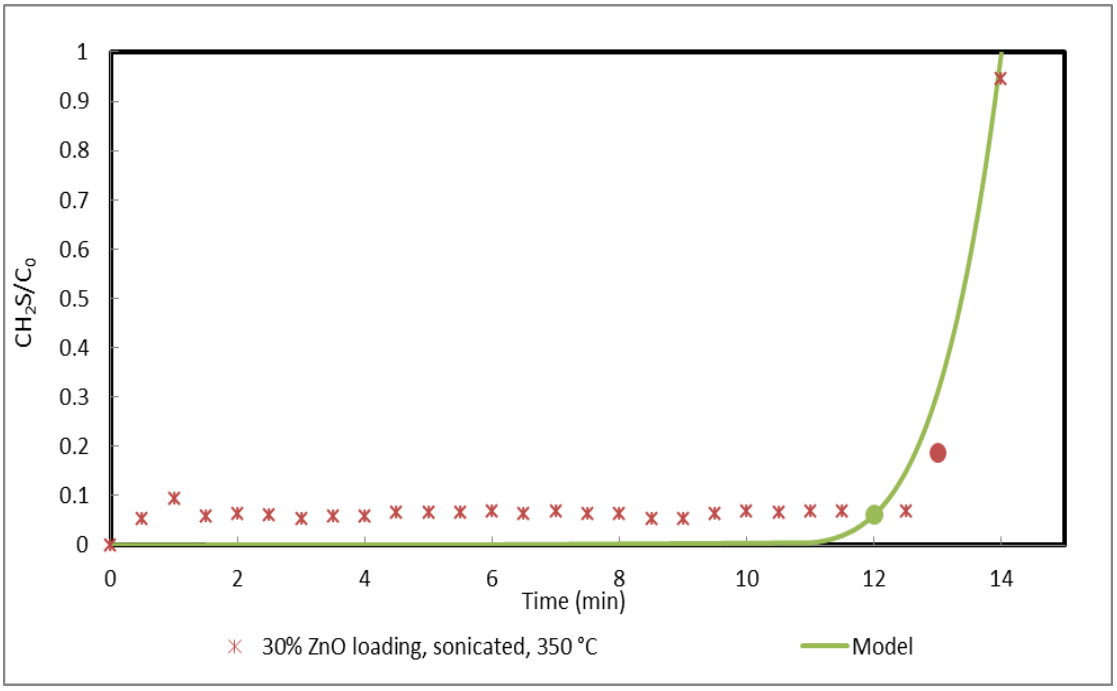

Figure 5-63: Experimental (*) and predicted (-) breakthrough curves for Run 4

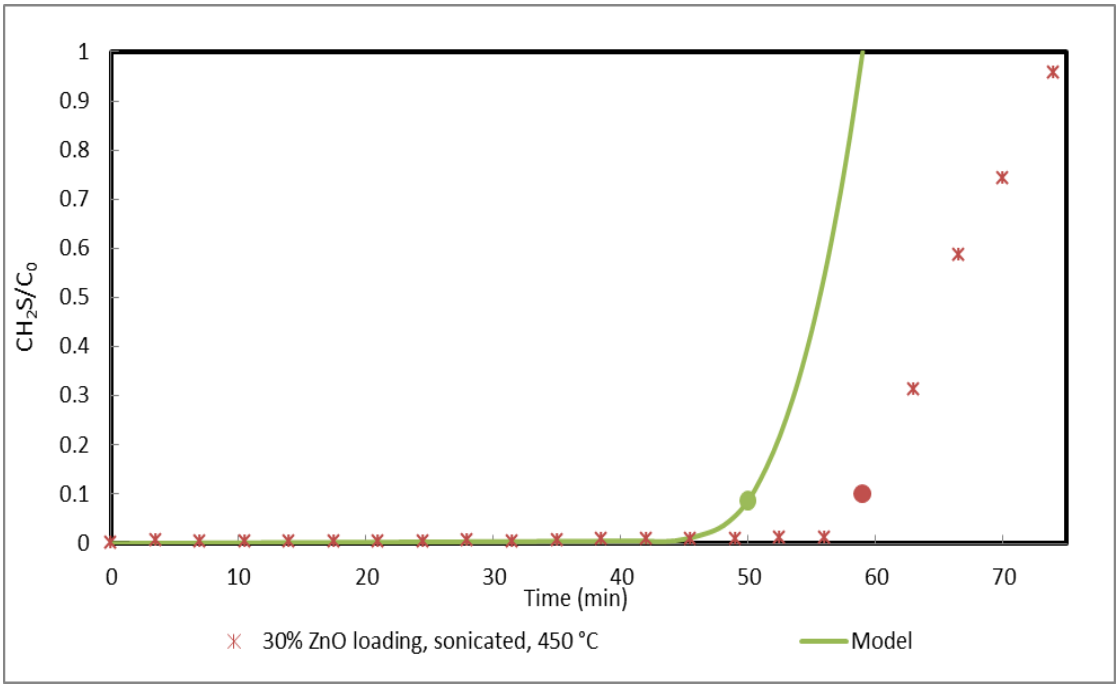

Figure 5-64: Experimental (*) and predicted (-) breakthrough curves for Run 5

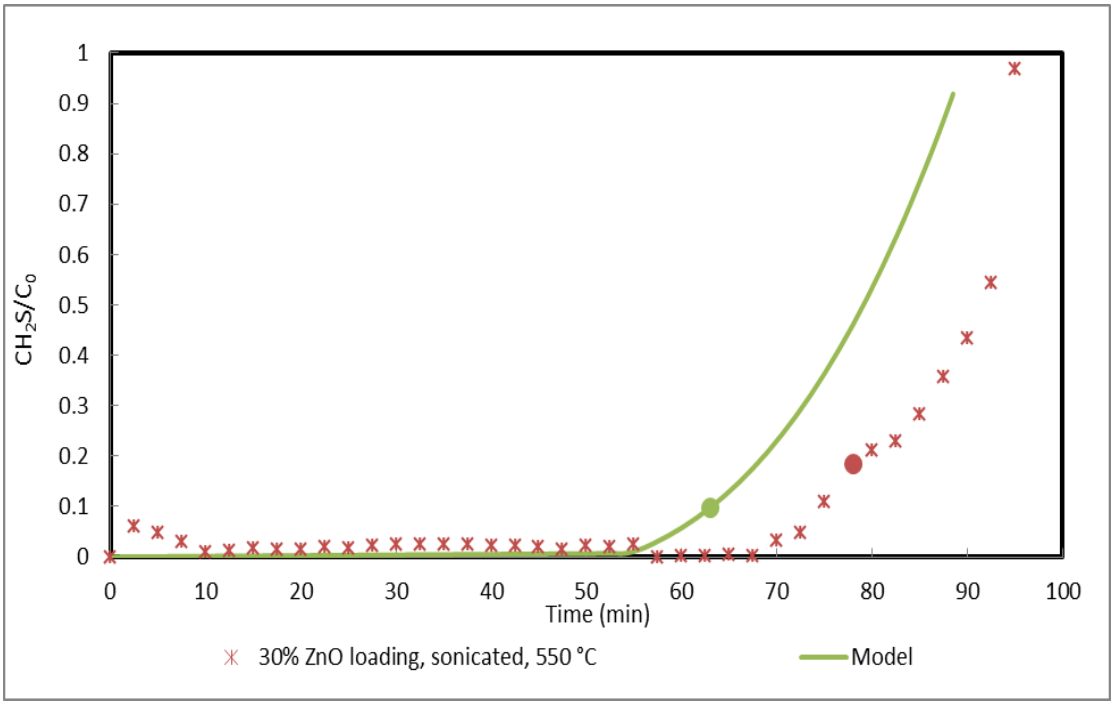

Figure 5-65: Experimental (*) and predicted (-) breakthrough curves for Run 6

From the results presented it was seen that there was a fair correlation between experimental and predicted breakthrough curves for all of the sonicated and non-sonicated sorbents at a 30 wt. % ZnO loading. The 30 wt. % ZnO loading sorbent was chosen as it was the best performing sorbent. This packed bed reactor modelling was carried out for a desulphurisation temperature range of 350 ℃ - 550 ℃.

There was a linear rise in conversion as it progressed with time but at varying rates dependent on r_A . At lower desulphurisation temperatures (350 ℃ - 450 ℃), the shrinking core model showed a steeper gradient for the breakthrough curves as compared to at higher desulphurisation temperatures (450 ℃ - 550 ℃). The graphs overlap during the periods of peak desulphurisation and start to diverge as they approach the breakthrough time. These differences are largely due to the dependent variables discussed in section 4.1. They could also be explained by factors inhibiting the flow of the H_2S into the bulk sorbent. One such inhibiting factor could be the formation of zinc sulphate ($ZnSO_4$) which has a larger molecular volume than ZnS or ZnO. This zinc sulphate more readily causes pore blockage in the sorbent which results in low sorbent utilization (Sofekun, 1996). It was also noted that the model over-predicts breakthrough times for non-sonicated sorbents while it under predicts for sonicated sorbents. There are a few possible reasons for this. Non-sonicated sorbents have smaller particles than sonicated particles. This smaller particle size

has the effect of reducing pore diffusion resistance while enhancing the rate of mass transfer (Yang, 2007). The pore diffusion resistance is further reduced by the high porosity of ZnO/SiO_2 sorbents. Since the porosity was determined from a correlation as opposed to quantitative and qualitative analysis, the value of porosity used in the model was under predicted. Typical ZnO/SiO_2 sorbents have a porosity of atleast 64% (Newby et al., 2001). The actual porosity was most likely higher than the 37.3% used; hence breakthrough would have occurred much quicker than the model predicted.

Now for sonicated sorbents the converse is true. These sorbents have a larger particle size with an increased grain diffusion resistance. The model used in this dissertation was pseudohomogeneous. This meant that all of the complicated interactions between the gas and sorbent particles were ignored but instead lumped together as the effective diffusivity (Nauman, 1987). This effective diffusivity takes into account external and internal mass transfer (which includes the grain diffusion resistance and pore diffusion resistance). Sonicated sorbents are more likely to be influenced by Microfibrous Entrapment. This causes the pore diffusion to remain negligible while the grain diffusion resistance becomes excessive. The correlations used for the model in this dissertation did not take into account this severe increase in the grain diffusion resistance, hence the model under predicted the breakthrough times for sonicated sorbents. In actuality, breakthrough would have occurred much slower than the model predicted.

In conclusion, a packed bed reactor using a shrinking core model can be used to model a highly dispersed zinc-based sorbent for desulphurisation. It is however recommended that a grain model be considered to account for the variable structural changes in the porous ZnO/SiO_2 sorbent.

CHAPTER 6: CONCLUSIONS

Hot gas desulphurisation (HGD) –which is an improvement on conventional desulphurisation- is an essential step for any gasification process because sulphur compounds are corrosive to process equipment and harmful to the environment. The removal of sulphur compounds from syngas is very important for the correct operation of the newer Integrated Gasification Combined Cycle (IGCC) for power generation. This study focused on the enhancement of sulphur removal capacity and regeneration characteristics of solid zinc-based sorbents through ultrasound assisted dispersion of active components. From the entirety of this research, the following conclusions were drawn based on the objectives set:

One of the main objectives was to prepare a sorbent by an ultrasonically assisted wet impregnation technique and quantitatively determine the improvement in sulphur removing capacity as well as the dispersion of zinc oxide loaded onto the surface of a silica carrier.

- ZnO/SiO_2 sorbents were successfully prepared using the wet impregnation technique and an ultrasonically assisted wet impregnation technique.

- The ultrasonically assisted wet impregnation technique improved the dispersion of zinc oxide loaded onto the surface of a silica carrier as well as the saturation capacity. For the sonicated sorbents the EDX analysis showed a greater amount of zinc present than in non-sonicated sorbents at equivalent wt. % ZnO loading. There was an increase from 10.28%, 14.39% and 24.78% to 10.49%, 15.64% and 28.53% for the (10, 20 and 30wt. %) ZnO loading sorbents respectively. Furthermore, the sonication actually improved the efficacy of the wet impregnation technique. This may be due to the improved access to the deeper pore network due to the action of the ultrasonic irradiation.

- An average % increase in the saturation capacity for sonicated sorbents over non-sonicated sorbents was calculated. There was an average % increase in saturation capacity of 3.65%, 9.62% and 0.86% for the (10, 20 and 30wt. %) ZnO loading sorbents respectively. This result highlighted that the improvement in saturation capacity was due to the sonication of sorbents.

- The sonicated ZnO/SiO_2 sorbent with an average saturation capacity of 0.116 g S/g ZnO had a higher value than the non-sonicated and literature ZnO/SiO_2 sorbents (0.111 and 0.113 g S/g ZnO respectively). This proves that sorbents prepared via the Ultrasonic-assisted Impregnation (UAI)

technique enhance saturation capacity.

To quantitatively evaluate the effect of wt. % ZnO loading and desulphurisation temperature on the breakthrough times of highly dispersed sonicated ZnO/SiO_2 sorbent for desulphurisation, when compared to conventional ZnO/SiO_2 sorbents.

- Sonicated and non-sonicated sorbent samples of 5g revealed longer desulphurisation breakthrough times at elevated temperatures and at higher wt. % ZnO loading.

- Sonicated sorbents had comparably better desulphurisation breakthrough times (on average 25.2 min as compared to 15 min) than non-sonicated sorbents.

- At higher temperatures both sonicated and non-sonicated sorbents take longer to reach maximum sorbent saturation capacity which results in a longer useable sorbent. The differences in wt. % ZnO loading of the sorbent only become appreciable at a high wt. % ZnO loading range. Therefore the optimum range for appreciable breakthrough times for both sorbents lies in a range of 450 ℃ - 550 ℃ at 30 wt. % ZnO loading.

- An average % increase in the breakthrough times for sonicated sorbents over non-sonicated sorbents was calculated. There was an average % increase in breakthrough time of of 39.13%, 73.07% and 74.74% for the (10, 20 and 30wt. %) ZnO loading sorbents respectively.

- When the wt. % ZnO loading was increased, for both non-sonicated and sonicated sorbents, the length of the particle size increased. There was an increase from 9.31 nm, 9.56 nm and 9.72 nm to 11.29 nm, 12.42 nm and 13.88 nm for the (10, 20 and 30wt. %) ZnO loading sorbents respectively

To quantitatively evaluate the effect of wt. % ZnO loading and desulphurisation temperature on the regeneration characteristics of highly dispersed sonicated ZnO/SiO_2 spent sorbents, when compared to conventional ZnO/SiO_2 spent sorbents, both at the same regeneration temperature.

- The regeneration time of the higher desulphurisation temperature and lower wt. % ZnO loading

spent sorbent samples were shorter.

- For higher wt. % ZnO loading (30%-20%) at equivalent desulphurisation temperature, sonicated sorbents had a longer regeneration time (on average 26.5 min as compared to 12.8 min) than non-sonicated sorbents. However, for lower wt. % ZnO loading (10%) at equivalent desulphurisation temperature, the converse was true (on average 5 min as compared to 8.3 min).

- The sonicated spent sorbents at 350 °C desulphurisation temperature were not regenerable to the useable limit. Hence, the desulphurisation temperature range of regenerable zinc-based spent sorbents for this study laid in the range of 450°C to 550 °C.

- Since all of the spent sorbents were regenerable to a useable limit within ~60 min, the 30 wt. % ZnO loading sonicated sorbent employed at 550 °C showed the best overall performance.

The following are also some useful conclusions that were revealed as a result of this dissertation:

- The high surface area sorbent had a longer breakthrough time (78 min as compared to an average of 52.5 min) than the low surface area sorbent at equivalent conditions.

- The differing mass of sorbent and volumetric flowrate of the gas mixture between successive runs leads to the cause of differences in repeatability of the experiments.

- The sonicated sorbents breakthrough time of 7.93 min was much greater than the normalized value of 3.5 min from literature. This means that if the sonicated sorbent from this dissertation was run at literature desulphurisation conditions; a breakthrough time of 68 mins would be achieved. This proves that the sorbents prepared via the Ultrasonic-assisted Impregnation (UAI) technique enhance breakthrough times.

- A packed bed reactor using a shrinking core model can be used to model a highly dispersed zinc-based sorbent for desulphurisation. There was a good correlation between experimental and predicted breakthrough curves for all of the sonicated and non-sonicated sorbents at a 30 wt. % ZnO loading.

CHAPTER 7: RECOMMENDATIONS

To further improve on the magnitude of the research undertaken in this dissertation, as well as its validity, the following recommendations should be considered:

- Use a gas mass flow controller that is able to set the flowrate of the gas mixture containing H_2S. This will increase the accuracy in calculations as compared to using a bubble flow meter.

- A wider range of desulphurisation temperatures will be crucial to determine the capabilities as well as limits of the synthesized sorbents.

- Since the sulphur capacity of the sorbents prepared using the modified wet impregnation technique were relatively high and that the regeneration was easy to perform under moderate temperatures, then tests of the mechanical strength of the materials should be performed. These tests should include measurements of the attrition resistance, degradation by thermal and chemical cycling (i.e. physical loss of surface through sintering) and handling characteristics.

- Evaluate the performance of the sorbent using actual coal gases at realistic process temperatures and pressures and at the pilot scale.

- Incorporate temperature dependence (non-isothermal conditions) into the packed bed reactor modelling. Thereafter a grain model could be considered to account for the variable structural changes in the porous ZnO/SiO_2 sorbent.

REFERENCES

Ali, J.S. (2015) *High temperature production and desulphurisation of syngas*, Msc Dissertation edition, Durban: University of Kwa-zulu Natal.

Altafini, C.R., Wander, P.R. and Barreto, R.M. (2003) 'Prediction of the working parameters of a wood waste gasifier through an equilibrium model', *Energy Convers Manag*, vol. 44, pp. 2763-2777.

Appalachian State University (2016) *Error Analysis*, [Online], Available: http://physics.appstate.edu/undergraduate-programs/laboratory/resources/error-analysis [28 October 2016].

Atimtay, A.T. and Harrison, D.P. (2013) 'Desulphurization of Hot Coal Gas', *Sprinder Science & Business Media Turkey*.

Bacher, A.D. (2016) *Gas Chromatography Theory*, 1 April, [Online], Available: http://www.chem.ucla.edu/~bacher/General/30BL/gc/theory.html [12 September 2016].

Bakker, W.J.W., Moulijn, J.A. and Kapteijn, F. (2003) 'A high capacity manganese-based sorbent for regenerative high temperature desulfurization with direct sulfur production: Conceptual process application to coal gas cleaning', *Chem. Eng. J.*, vol. 96, pp. 223-235.

Bang, J.H. and Suslick, K.S. (2010) 'Applications of Ultrasound to the Synthesis of Nanostructured Materials', *Advanced Materials*, vol. 22, pp. 1039-1059.

Bianchi, C.L., Lanzani, R., Lorenzetti, D., Vergani, G. and Ragaini, V. (1993) 'A new method to prepare highly dispersed supported metal catalysts', *Catalysis Letters*, vol. 22, no. 4, December, pp. 319-325.

Botha, M.F. (2010) *Production and High Temperature Treatment of Syngas*, South Africa: MSc Dissertation.

Breault, R.W. (2010) 'Gasification Processes Old and New: A Basic Review of the Major Technologies', *Energies*, vol. 3, February, pp. 216-240.

Cheremisinoff, N.P. (2016) *Pollution Control Handbook for Oil and Gas Engineering*, 1st edition, New Jersey: John Wiley & Sons.

Copper, C.D. and Alley, F.C. (2002) *Air Pollution Control: A Design Approach*, 4th edition, Prospect Heights, IL: Waveland Pr Inc.

Di Blasi, C. (2000) 'Dynamic behaviour of stratified downdraft gasifiers', *Chem Eng Sci*, vol. 55, pp. 2931-2944.

E4tech (2009) 'Review of Technologies for Gasification of Biomass and Wastes', *NNFCC project 09/008*, June, p. 10.

Egerton, R.F. (2005) *Physical Principles of Electron Microscopy: An introduction to TEM, SEM, and AEM*, 1st edition, Canada: Springer.

Emun, F., Gadalla, M., Majozi, T. and Boer, D. (2009) 'Integrated gasification combined cycle (IGCC) process simulation and optimization', *Comput Chem Eng*, vol. 34, pp. 331-338.

EREN (2002) *Gasification Based Biomass*, [Online], Available: http://www.eren.doe.gov/power/pdfs/bio_gasification.pdf [4 March 2016].

Frey, C.H. and Akunuri, N. (2001) *Probabilistic modeling and evaluation of the performance, emissions, and cost of texaco gasifier-based integrated gasification combined cycle systems using ASPEN*, [Online], Available: http://www4.ncsu.edu/*frey/reports/Frey_Akunuri_2001.pdf [31 August 2016].

Gangwal, S.K., Harkins, S.M. and Jain, S.C. (1990) 'Desulfurization of Hot Coal-Gas in A High-Pressure Fluid-Bed Reactor', *American Chemical Society*, vol. 35, pp. 161-169.

Gasper-Galvin, L.D., Atimtay, A.T. and Gupta, R.P. (1998) 'Zeolite-Supported Metal Oxide Sorbents for Hot-Gas Desulfurization', *Ind. Eng. Chem. Res.*, vol. 37, pp. 4157-4166.

Gautam, G., Adhikari, S. and Bhavnani, S. (2010) 'Estimation of biomass synthesis gas composition usning equilibrium models', *Energy Fuels*, vol. 24, pp. 2692-2698.

Gbor, P.K. and Jia, Q. (2004) 'Critical evaluation of coupling particle size distribution with the shrinking core model', *Chemical Engineering Science*, vol. 59, January, pp. 1979-1987.

Giltrap, D.L., McKibbin, R. and Barnes, G.R. (2003) 'A steady state model of gas-char reactions in a downdraft biomass gasifier', *Sol Energy*, vol. 74, pp. 85-91.

Girard, V., Chiche, D., Baudot, A., Bazer-Bachi, D., Clemencon, I., Moreau, F. and Geantet, C. (2015) 'Innovative low temperature regenerable zinc based mixed oxide sorbents for synthesis gas desulphurization', *Fuel, Elsevier*, vol. 440, pp. 453-461.

Goodge, J. (2016) *Energy-Dispersive X-Ray Spectroscopy (EDS)*, 8 September, [Online], Available: http://serc.carleton.edu/research_education/geochemsheets/eds.html [12 September 2016].

Govind, R. and Shah, J. (1984) 'Modeling and simulation of an entrained flow coal gasifier', *AIChe J*, vol. 30, pp. 79-92.

Gupta, R.P., Turk, B.S. and Portzer, J.W. (2001) 'Desulfurization of syngas in a transport reactor', *Environmental progress & sustainable energy*, vol. 20, no. 3, October, pp. 187-195.

Hamon Research-Cottrell, Inc. (2016) *Wet Gas Scrubbers*, [Online], Available: http://www.hamonusa.com/hrc/products/wgs [2016 July 19].

Haryanto et al. (2009) 'Upgrading of syngas derived from biomass gasification: A thermodynamic analysis', *Biomass & Bioenergy*, vol. 33, pp. 882-889.

Hemmer, G., Kasper, G., Wang, J. and Georg Schaub (2002) 'Removal of Particles and Acid Gases (SO', *Dissertation Universitat Karlsruhe*, pp. 1-12.

Jand, N. and Foscolo, P.U. (2005) 'Decomposition of wood particles in fluidized beds', *Industrial Eng Chem Res*, vol. 44, pp. 5079-5089.

Klein, A. (2002) *Gasification: An Alternative Process for Energy Recovery and Disposal of Municipal Solid Wastes*, Columbia: Earth Engineering Center.

Kohl, A. and Riesenfeld, F. (1979) *Gas Purification*, 3rd edition, Houston, Texas: Gulf Publishing Company.

Krigmont, H. (1999) *IBGCC power generation concept: A gateway for a cleaner future. Allied Environmental Technologies.A White Paper*, [Online], Available: http://www.alentecinc.com/papers/IGCC/ADVGASIFICATION.pdf [7 March 2016].

Levenspiel, O. (1999) *Chemical Reaction Engineering*, 3rd edition, New York: John Wiley & Sons.

Loeser, M. and Redfern, M.A. (2009) 'Modelling and simulation of a novel micro-scale combined feedstock biomass generation plant for grid-independent power supply', *Int J Energy Res*, vol. 34, no. 4, pp. 303-320.

Melgar, A., Perez, J.F., Laget, H. and Horillo, A. (2007) 'Thermochemical equilibrium modelling of a gasifying process', *Energy Convers Manag*, vol. 48, pp. 59-67.

Montes, D., Tocuyo, E., Gonzalez, E., Rodriguez, D., Solano, R., Atencio, R., Ramos, M.A. and Moranta, A. (2013) 'Reactive H2S chemisorption on mesoporous silica molecular sieve-supported CuO or ZnO', *Microporous and Mesoporous Materials*, vol. 168, March, pp. 111-120.

Montgomery, D.C., Raymond, H.M. and Christine, M.A.C. (2012) *Response Surface Methodology: Process and Product Optimisation using Designed Experiments*, 3rd edition, Wiley publication.

Nathen, S.V., Kirkpatrick, R.D. and Young, B.R. (2008) 'Gasification of New Zealand coals: a comparative simulation study', *Energy Fuels*, vol. 22, pp. 2687-2692.

Nauman, E.B. (1987) *Chemiacl reactor design*, 1st edition, Canada: John Wiley & Sons, Inc.

NETL (2016) *Commercial Gasifiers*, [Online], Available: http://www.netl.doe.gov/research/coal/energy-systems/gasification/gasifipedia/entrainedflow [17 March 2016].

NETL (2016) *Syngas Contaminant Removal and Conditioning*, [Online], Available: http://www.netl.doe.gov/research/coal/energy-systems/gasification/gasifipedia/cos-hydrolysis [12 April 2016].

NETL (2016) *Syngas Contaminant Removal and Conditioning*, [Online], Available: http://www.netl.doe.gov/research/coal/energy-systems/gasification/gasifipedia/sulfur-recovery [3 May 2016].

Newby, R.A., Lippert, T.E., Slimane, R.B., Akpolat, O.M., Pandya, K., Lau, F.S., Abbasian, J., Williams, B.E. and Leppin, D. (2001) *Novel Gas Cleaning/Conditioning for Integrated Gasification Combined Cycle, DOE Base Program*, Final Report edition.

Nikoo, M.B. and Mahinpey, N. (2008) 'Simulation of biomass gasification in fluidized bed reactor using Aspen Plus', *Biomass Bioenergy*, vol. 32, pp. 1245-1254.

Nygaard, H.G., Kiil, S., Johnsson, J.E., Jensen, J.N., Hansen, J., Fogh, F. and Damn-Johansen, K. (2004) 'Full-scale Measurements of SO2 Gas Phase Concentrations and Slurry Compositions in a Wet Flue-gas Desulphurisation spray absorber', *Fuel*, vol. 83, no. 9, pp. 1151-1164.

Pacheco, M.A. and Rochelle, G.T. (1998) 'Rate-based modelling of reactive absorption of CO2 and H2S into aqueous methyldiethanolamine', *Industrial & Engineering Chemistry Research*, vol. 37, pp. 4107-4117.

Perego, C. and Villa, P. (1997) 'Catalyst Preparation Methods', *Catlysis Today*, vol. 34, pp. 281-305.

Pinna, F. (1998) 'Supported Metal Catalysts Preparation', *Catalysis Today*, vol. 41, pp. 129-137.

Puigjaner, L. (2011) *Syngas from Waste: Emerging Technologies*, 1st edition, London: Springer.

Raharjo, S., Yasuaki, R., Naruse, Y. and Naruse, I. (2010) 'Hot Gas Desulfurization and Regeneration Characteristics with Molten Alkali Carbonates', *International Journal of Chemical Engineering and Applications*, vol. 1, no. 1, pp. 96-102.

Rajvanshi, A.K. (1986) 'Biomass Gasification', *Alternative Energy in Agriculture*, vol. 2, pp. 83-102.

Reed, T.B. and Das, A. (1988) *Handbook ofiomass Downdraft Gasifier Engine Systems*, Colorado: U.S. Deoartment of Energy.

Robinson, P.J. and Luyben, W.L. (2008) 'Simple dynamic gasifier model that runs in Aspen dynamics', *Industrial Eng Chem Res*, vol. 47, pp. 7784-7792.

Ruggiero, M. and Manfrida, G. (1999) 'An equilibrium model for biomass gasification processes', *Renew Energy*, vol. 16, pp. 1106-1109.

Sadaka, S. (2008) 'Gasification', *Center for Sustainable Environmental Technologies*, pp. 1-42.

Sanchez, J.M., Ruiz, E. and Otero, J. (2005) 'Selective removal of hydrogen sulfide from gaseous streams using a zinc-based sorbent', *nd. Eng. Chem.Res*, vol. 44, no. 2, pp. 241-249.

Siefers, A.M. (2010) *A Novel and Cost-Effective Hydrogen Sulfide Removal Technology Using Tire Derived Rubber Particles*, MSc Dissertation edition, Iowa: Iowa State University.

Singer, C.J. (1958) *History of Technology*, Oxford: Oxford University Press.

Sofekun, O.A. (1996) 'A kinetic study of the sulfidation-regeneration of zinc oxide sorbent', *PhD Thesis. Iowa State University*.

Sorrell, C.A. (1977) 'Suggested Chemistry of Zinc Oxtchloride Cements', *Journal of the American Ceramic Society*, vol. 60, no. 5-6, May, pp. 217-220.

Swapp, S. (2016) *Scanning Electron Microscope (SEM)*, 8 September, [Online], Available: http://serc.carleton.edu/research_education/geochemsheets/techniques/SEM.html [12 September 2016].

Swedish Gas Centre (2012) *Gasification-Status and Technology*, Sweden: Rapport SGC.

Szekely, J., Evans, J.W. and Sohn, H.Y. (1976) *Gas-solid reactions*, New York: Acadenic Press.

U.S. Environmental Protection Agency (EPA) (1998) 'Lesson 9. Flue Gas Desulfurization (Acid Gas Removal) Sysytems', SI 412C Course, Air Pollution Training Institute (APTI) Virtual Classroom.

Ullmann (2003) *Gas Production/Gas Treating*, Online Edition edition, Ullmann's encyclopedia of industrial chem.

Van Nguyen, T. (2011) 'System analysis of chemical and carbonate looping processes in IGCC power plants for CO2 separation', *Division of Energy Technology*, vol. 1, pp. 1-145.

Wang, Y. and Kinoshita, C.M. (1993) 'Kinetic model of biomass gasification', *Sol Energy*, vol. 51, pp. 19-25.

Wang, L. and Yang, R.T. (2014) 'New Nanostructured Sorbents for Desulphurisation of Natural gas', *Front. Chem. Sci. Eng.*, vol. 8, pp. 8-19.

Wen, C.Y. and Chaung, T.Z. (1973) 'Entrainment coal gasification modelling', *Industrial Eng Chem Process Des Dev*, vol. 18, pp. 684-695.

Westmoreland, P.R. and Harrison, D.P. (1976) 'Evaluation of candidate solids for high-temperature desulfurization of low-Btu gases', *Environmental Science & Technology*, vol. 10, no. 7, pp. 659-661.

Witzany, R., Dokupil, M. and Heinzel, A. (2007) *Design of a Mathematic Model for the Calculation of Breakthrough Curves for Desulphurization Units*, Germany: University of Duisburg-Essen.

Yang, H. (2007) 'Gas Phase Desulfurization Using Regenerable Microfibrous entrapped Metal Oxide Based Sorbents for Logistic Pem Fuel Cell Applications', *Auburn University, Alabama*.

Yang, H. and Tatarchuk, B. (2010) 'Novel-Doped Zinc Oxide Sorbents for Low Temperature Regenerable Desulfurization Application', *AIChE*, vol. 56, no. 11, pp. 2899-2904.

Yi, C.K., Jo, S.H., Lee, B.H., Lee, S.Y., Son, J.E. and Gin, G.T. (2001) 'Simultaneous experiments of sulfidation and regeneration in two pressurized fluidized-bed reactors for hot gas desulfurization of IGCC', *Korean J. Chem.Eng*, vol. 18, no. 3, pp. 1005-1010.

APPENDIX A: RAW DATA

Table A-1: Calibration data

Peak area (uV)	Volume fraction
7164662887	0.0015
7778533083	0.0015
7476595698	0.0015
10039300043	0.002
9905923628	0.002
15679385034	0.003
15539522407	0.003
15679958488	0.003
12080102270	0.01
12284355436	0.01
12078134393	0.01
17736042580	0.01
19019094157	0.01
21102609208	0.01
25075477912	0.02
25332544543	0.02
25835234038	0.02
31156615923	0.05
32373076083	0.05
33991828359	0.05

Table A-2: Desulphurisation data

Run	Mass before desulphurisation (g)	Mass after desulphurisation (g)
1	5.013	5.482
2	5.011	5.521
3	5.007	5.541
4	5.012	5.486
5	5.018	5.534
6	5.013	5.549
7	5.001	5.301
8	5.000	5.326
9	5.006	5.357
10	5.012	5.361
11	5.011	5.369
12	5.015	5.379
13	5.000	5.161
14	5.005	5.179
15	5.007	5.193
16	5.015	5.189
17	5.011	5.191
18	5.012	5.198

APPENDIX B: SAMPLE CALCULATIONS

B.1. Calibration

Take the point 1 from Table A-1. Peak area = 257434836 uV.

Using the calibration in Figure 5-2, the volume corresponding to this peak area can be attained.

$$V = \frac{A_p}{5.1309\times10^{12}} \quad \text{(B-1)}$$

$$= \frac{257434836}{5.1309\times10^{12}}$$

$$= 5.017 \times 10^{-5}\ mL/mL\ injected$$

This is the volume of H_2S per sample loop volume (1mL). Assuming ideal gas conditions it can be stated that the mole percentage is equivalent to the volume percentage. Converting to a volume percentage:

$$percentage = 5.017 \times 10^{-5} \times 100\ \%$$

$$= 0.005\ \%$$

The gas flow constitutes 0.005 % H_2S. This value may then be converted to part per million (ppm) by the relation: 1 mol % = 10 000 ppm.

$$H_2S\ concentration = 0.005 \times 10\,000$$

$$= 50\ ppm$$

A similar calculation was applied to the remaining points and for each experimental run in order to attain the ppm values necessary to plot the breakthrough curves.

B.2. Sorbent preparation

All calculations will be done with respect to run 18 from this point forward.

$$ZnCl_2 + H_20 \rightarrow ZnO + HCl \quad \text{(B-2)}$$

The desired mass of sorbent = 5 g @ 10 wt. % ZnO loading

$$m_{ZnO} = \frac{\text{wt.\% ZnO loading}}{100} \times m_{sorb} \quad \text{(B-3)}$$

$$= \frac{10}{100} \times 5\ g$$

$$= 0.5\ g$$

$$m_{SiO_2} = m_{sorb} - m_{ZnO} \quad \text{(B-4)}$$
$$= 5\ g - 0.5\ g$$
$$= 4.5\ g$$

$$n_{ZnO} = \frac{m_{ZnO}}{MM_{ZnO}} \quad \text{(B-5)}$$
$$= \frac{0.5}{81.39}$$
$$= 0.00614\ mol$$

From stoichiometry:

$$m_{ZnCl_2} = n_{ZnO} \times MM_{ZnCl_2} \quad \text{(B-6)}$$
$$= 0.00614 \times 136.29$$
$$= 0.837\ g$$

Solubility of $ZnCl_2$ in H_20 @ 25 °C = 432 g/1000 ml.H_20

$$m_{H_20} = m_{ZnCl_2} \div K_{ZnCl_2} \quad \text{(B-7)}$$
$$= 0.837 \times \frac{1000}{432}$$
$$= 1.938\ ml = V_{H_20}$$

Therefore to make a batch of 5 samples (3 for experimental runs and 2 extra):

$m_{SiO_2} = 22.5\ g$

$m_{ZnCl_2} = 4.185\ g$

$V_{H_20} = 9.69\ ml$ (+ excess water)

B.3. Desulphurisation

A bubble flow meter (200 cm^3) was used to calculate the volumetric flowrate of the H_2S gas through the sorbent bed.

$$\dot{V} = \frac{V_b}{t_b} \quad \text{(B-8)}$$

$$= \frac{200}{1.4}$$

$$= 142.857 \ \frac{cm^3}{s}$$

The volume of the sorbent bed was calculated as follows:

$$V_B = \frac{\pi \times D^2 \times L}{4} \quad \text{(B-9)}$$

$$= \frac{\pi \times 2.1^2 \times 2.2}{4}$$

$$= 7.620 \ cm^3$$

Hence, the GHSV was then calculated:

$$\tau = \frac{\dot{V}}{V_B} \quad \text{(B-10)}$$

$$= \frac{142.857 \times 3600}{7.620}$$

$$\cong 67500 \ hr^{-1}$$

The following calculations were done to determine the saturation capacity of the sorbent:

$$m_{ZnS} = m_f - m_i \quad \text{(B-11)}$$

$$= 5.198 - 5.012$$

$$= 0.186 \ g$$

$$m_S = m_{ZnS} \times \frac{MM_S}{MM_{ZnS}} \quad \text{(B-12)}$$

$$= 0.186 \times \frac{32.066}{97.446}$$

$$= 0.0612 \ g$$

$$SC = \frac{m_S}{m_{ZnO}} \quad \text{(B-13)}$$

$$= \frac{0.0612}{0.5}$$

$$= 0.122 \ \frac{g \ S}{g \ ZnO}$$

B.4. Statistical analysis

Table B-1: Statistical analysis data

L_p	$L_p - (\overline{L_p})$	$\left(L_p - (\overline{L_p})\right)^2$
7.35	-3.94	15.51
8.41	-2.88	8.29
9.89	-1.40	1.96
10.36	-0.93	0.86
10.59	-0.70	0.49
10.66	-0.63	0.39
10.79	-0.50	0.25
11.01	-0.28	0.08
12.55	1.26	1.59
12.71	1.42	2.02
13.43	2.14	4.59
14.33	3.04	9.25
14.67	3.38	11.43

$$\overline{L_p} = \frac{\sum_1^N L_p}{N} \quad \text{(B-14)}$$
$$= \frac{7.35+8.41+9.89+10.36+10.59+10.66+\cdots+14.67}{13}$$
$$= 11.29\ nm$$

$$\sigma^2 = \frac{\sum_1^N \left(L_p-(\overline{L_p})\right)^2}{N-1} \quad \text{(B-15)}$$
$$= \frac{15.51+8.29+1.96+0.86+0.49+0.39+\cdots+11.43}{12}$$
$$= 4.73\ nm^2$$

$$\sigma = \sqrt{\sigma^2} \quad \text{(B-16)}$$
$$= \sqrt{4.73}$$
$$= 2.17\ nm$$

95% Confidence Interval:

$1 - \alpha = 0.95$

$1 - \frac{\alpha}{2} = 0.975$

$$CI = \overline{L_p} \pm t_{N-1:1-\frac{\alpha}{2}} \times \frac{\sigma}{\sqrt{N}} \quad \text{(B-17)}$$

$$= 11.29 \pm 2.179 \times \frac{2.17}{\sqrt{13}}$$

$$= (9.97\ ;12.60\ )\ nm$$

The range of values that exists such that the probability of the population mean-length of the particle lying within this range is 95%.

Chebyshev inequality:

$$1 - \frac{1}{3^2} = 0.88 \quad \text{(B-18)}$$

Therefore, the amount of particle lengths that lay within three standard deviations of the mean is 88%

Size distribution:

Table B-2: Size distribution data

Particle length intervals (nm)	Frequency of particles
< 6	0
$6 - 8$	1
$8 - 10$	2
$10 - 12$	5
$12 - 14$	3
> 14	2

B.5. Repeatability

For run 4:

$$Percentage\ difference = \frac{|difference|}{mean} \times 100 \quad \text{(B-19)}$$
$$= \frac{|13-12|}{12.5} \times 100$$
$$= 8\%$$

B.6. Comparative study

From Yang and Tatarchuk (2010):

$$\frac{\dot{V}}{m_{sorb}} = \frac{1.667}{0.5} = 3.334 \frac{cm^3}{s.g\ sorbent} \quad \text{(B-20)}$$

From this dissertation:

$$\frac{\dot{V}}{m_{sorb}} = \frac{142.857}{5} = 28.5714 \frac{cm^3}{s.g\ sorbent} \quad \text{(B-21)}$$

The normalizing ratio:

$$\frac{28.5714}{3.334} = 8.569 \quad \text{(B-22)}$$

The breakthrough time for the 17 wt. % ZnO loading sorbent at 350°C from literature normalized:

$$\widehat{t_B} = \frac{30}{8.569} = 3.5\ min \quad \text{(B-23)}$$

Interpolating for the 17 wt. % ZnO loading sorbent, using the results from this dissertation.

Non-sonicated: $\widehat{t_B} = 0.0024(17)^2 + 0.1605(17) = 3.42\ min$ (B-24)

Sonicated: $\widehat{t_B} = -0.0026(17)^2 + 0.5105(17) = 7.93\ min$ (B-25)

Sonicated sorbent at literature conditions:

$$t_B = \frac{7.93}{3.5} \times 30 = 68\ min \quad \text{(B-26)}$$

Percentage increase: Breakthrough time

10% ZnO loading, non-sonicated sorbent: $t_B = \frac{18+9+5}{3} = 7.67\ min$

10% ZnO loading, sonicated sorbent: $t_B = \frac{2+7+14}{3} = 10.67\ min$

$\%inc = \frac{10.67-7.67}{7.67} \times 100 = 39.13\%$ (B-27)

Percentage increase: Saturation capacity

10% ZnO loading, non-sonicated sorbent: $SC = \frac{0.106+0.115+0.122}{3} = 0.114\ \frac{g\ S}{g\ ZnO}$

10% ZnO loading, sonicated sorbent: $SC = \frac{0.115+0.118+0.122}{3} = 0.118\ \frac{g\ S}{g\ ZnO}$

$\%inc = \frac{0.118-0.114}{0.114} \times 100 = 3.65\%$ (B-28)

B.7. Gas-Solid reaction modelling

All calculations shown here are for the 30% ZnO loading, sonicated sorbent, at 550 °C desulphurisation temperature. Calculation of the bed porosity (ε) was done using the equation below. The diameter of the particles was approximated using the results from the statistical analysis section.

$\varepsilon = 0.373+0.917\exp(-0.824\ \frac{D}{d_p})$ (B-29)

$= 0.373 + 0.917\exp(-0.824\frac{2.1}{1.39\times10^{-6}})$

$= 0.373$

For the calculation of the gas mixture velocity:

$u = \frac{\dot{V}}{A_b}$ (B-30)

$= \frac{142.857 \times 60}{\pi \times 2.1^2/_4}$

$= 2474.712\ \frac{cm}{min}$

For the calculation of the effective diffusivity:

$$D_e = e^{(-2956/T)} - 19.589 \quad \text{(B-32)}$$

$$= e^{(-2956/823.15)} - 19.589$$

$$= 0.0478\ \frac{cm^2}{min}$$

For the calculation of the intrinsic reaction rate constant:

$$k = e^{(-4374.9/T)} - 0.3315 \quad \text{(B-32)}$$

$$= e^{(-4374.9/823.15)} - 0.3315$$

$$= 0.411\ \frac{cm}{min}$$

For the calculation of the gas film coefficient for mass transfer:

$$k_g = \frac{D_e\left[2+0.6\left(\frac{d_p u\rho}{\mu}\right)^{\frac{1}{2}}\left(\frac{\mu}{\rho D_e}\right)^{\frac{1}{3}}\right]}{d_p} \quad \text{(B-33)}$$

$$= \frac{5.14\times10^{-9}\left[2+0.6\left(\frac{1.39\times10^{-6}\times0.412\times0.513}{3.62\times10^{-5}}\right)^{\frac{1}{2}}\left(\frac{3.62\times10^{-5}}{0.513\times8.57\times10^{-15}}\right)^{\frac{1}{3}}\right]}{1.39\times10^{-6}}$$

$$= 0.0478\ \frac{cm}{min}$$

APPENDIX C: TEMPERATURE PROFILES

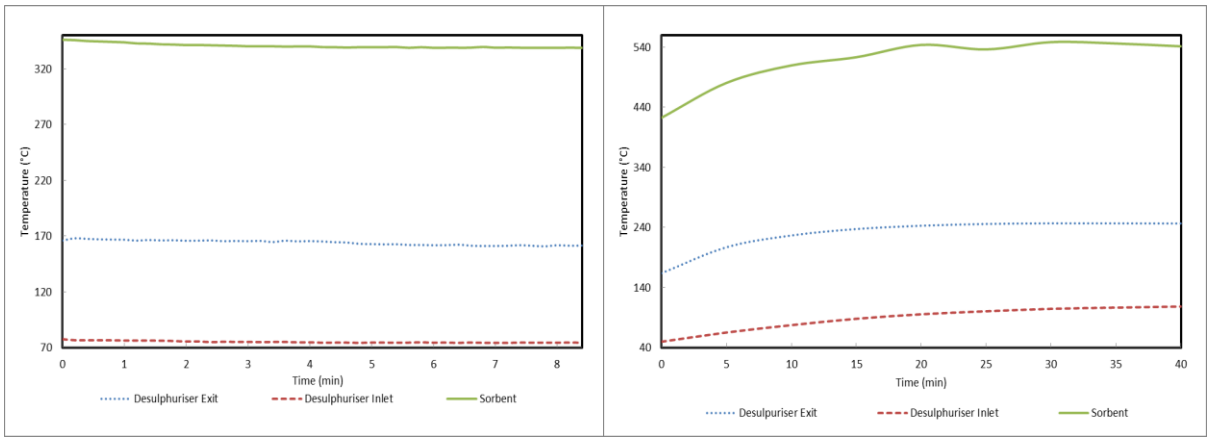

Figure C-1: Temperature profile for desulphurisation (left) and regeneration (right), run 1

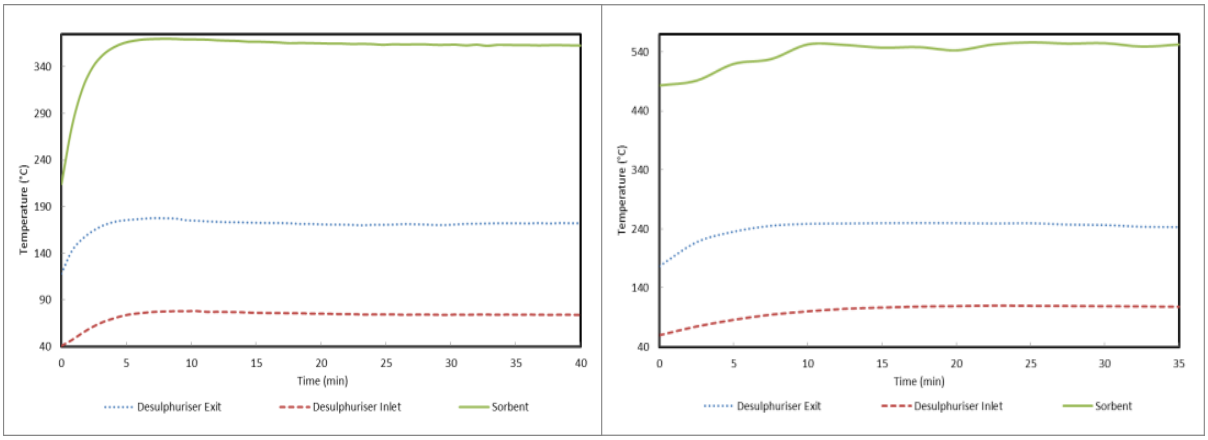

Figure C-2: Temperature profile for desulphurisation (left) and regeneration (right), run 2

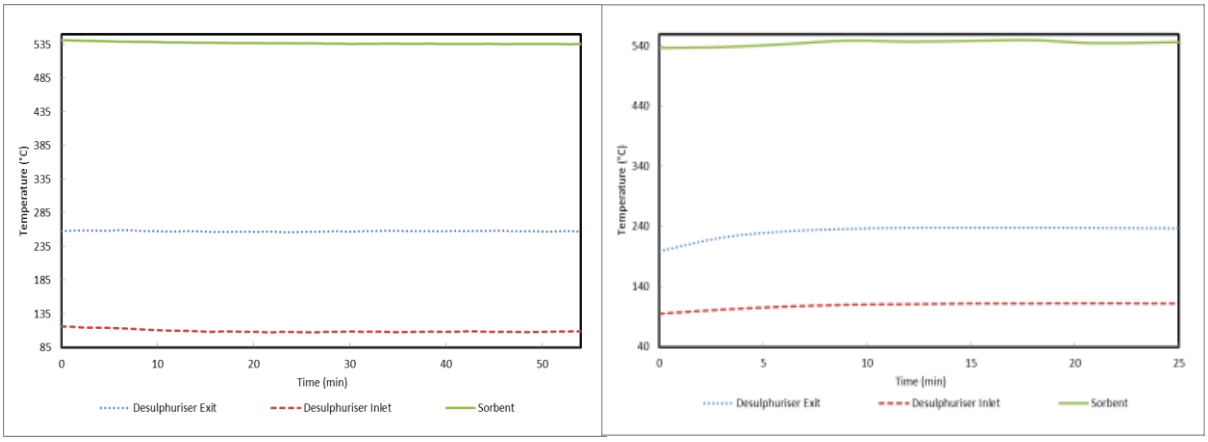

Figure C-3: Temperature profile for desulphurisation (left) and regeneration (right), run 3

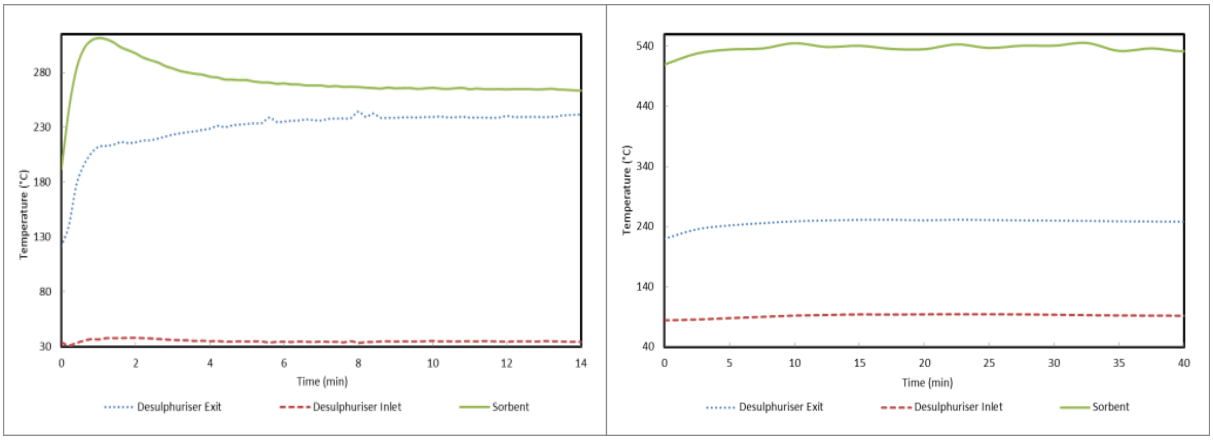

Figure C-4: Temperature profile for desulphurisation (left) and regeneration (right), run 4

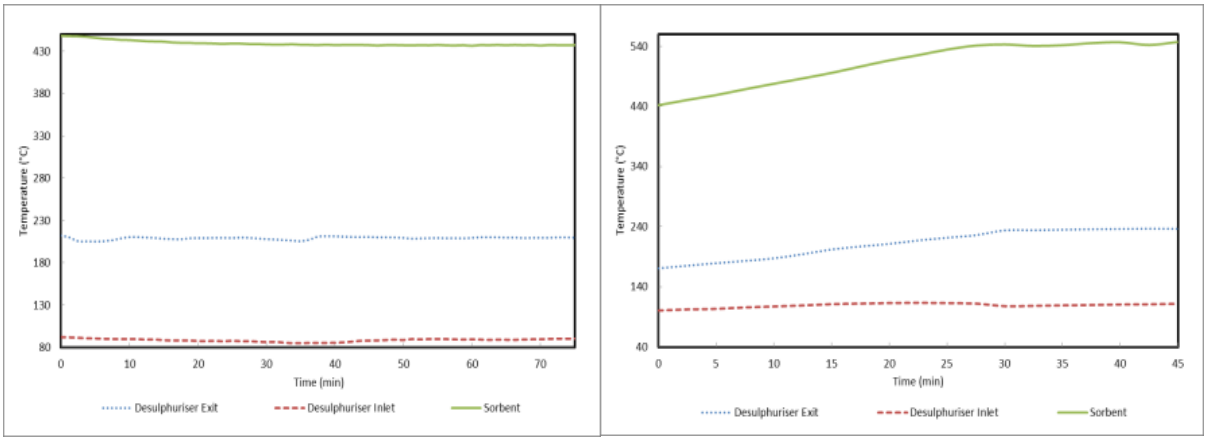

Figure C-5: Temperature profile for desulphurisation (left) and regeneration (right), run 5

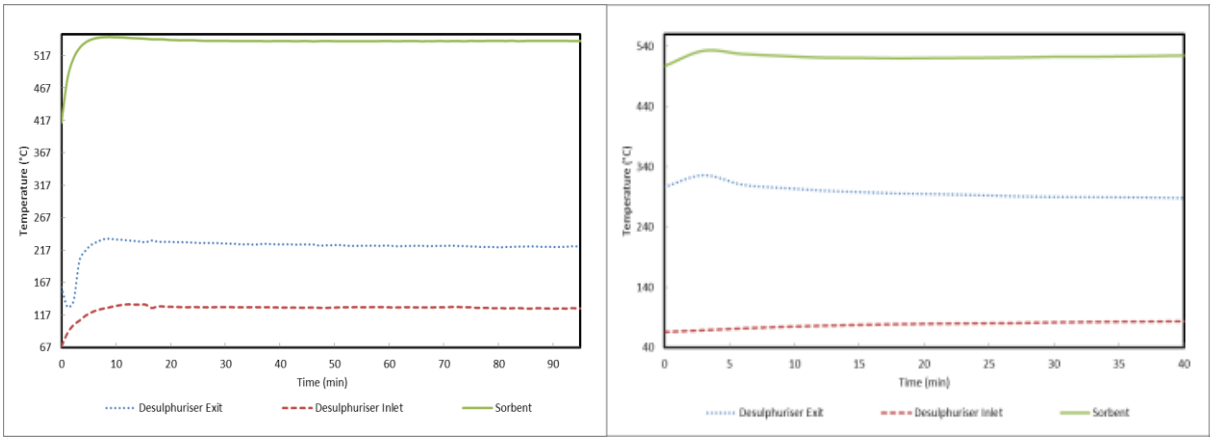

Figure C-6: Temperature profile for desulphurisation (left) and regeneration (right), run 6

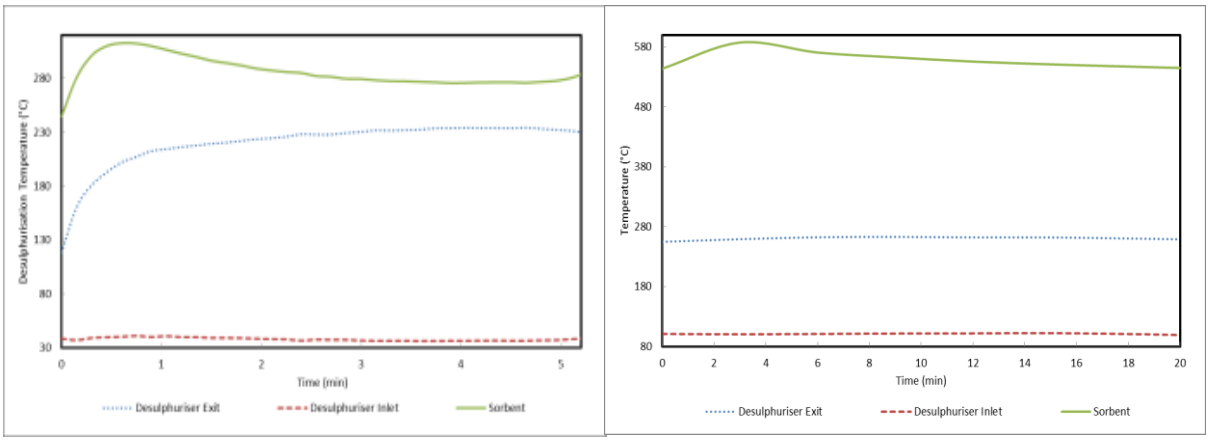

Figure C-7: Temperature profile for desulphurisation (left) and regeneration (right), run 7

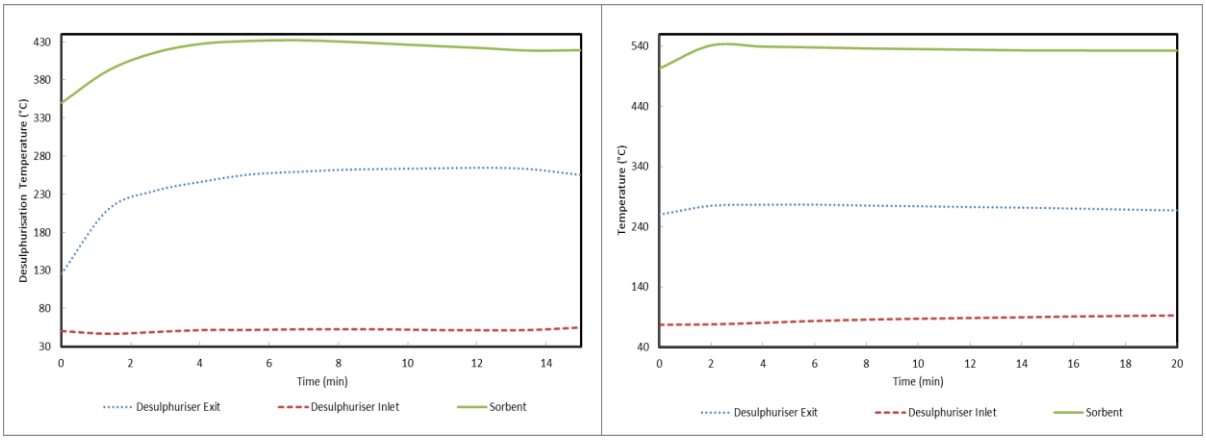

Figure C-8: Temperature profile for desulphurisation (left) and regeneration (right), run 8

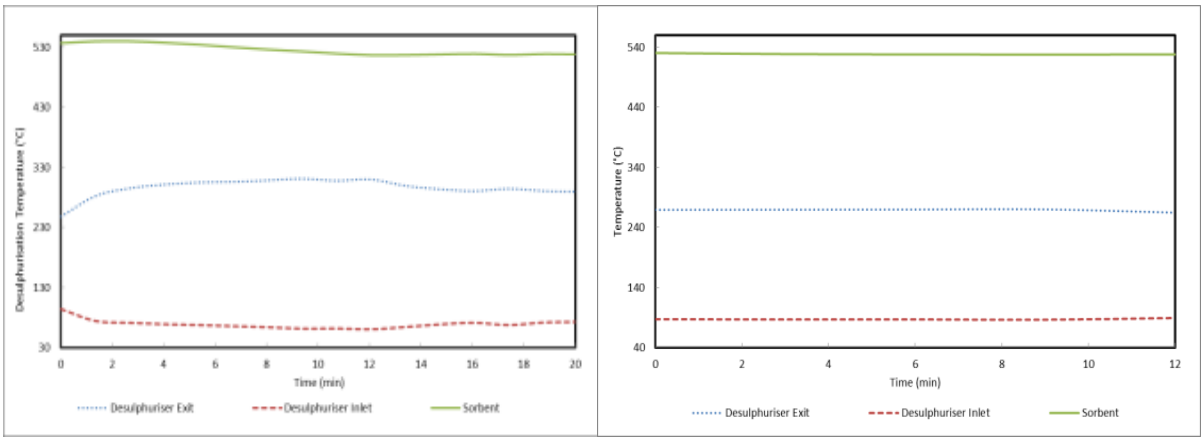

Figure C-9: Temperature profile for desulphurisation (left) and regeneration (right), run 9

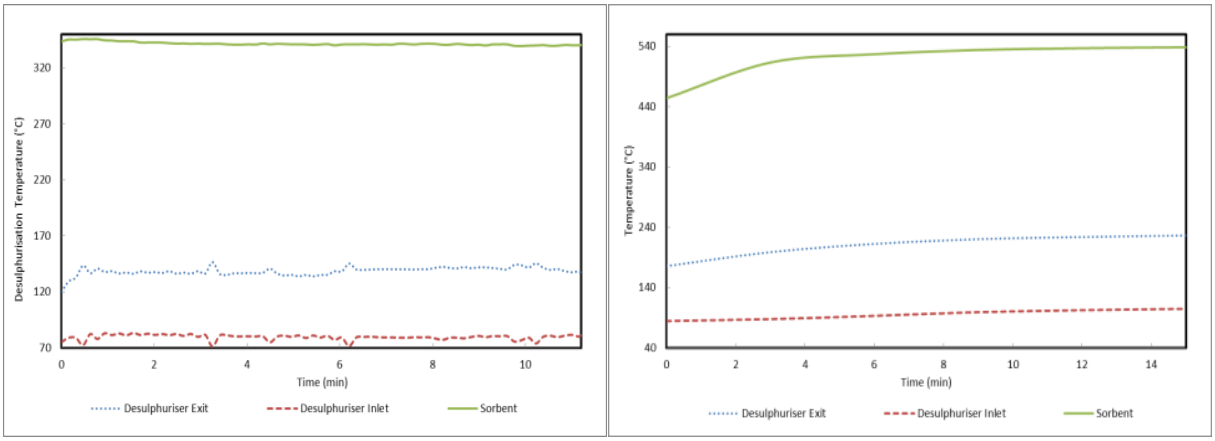

Figure C-10: Temperature profile for desulphurisation (left) and regeneration (right), run 10

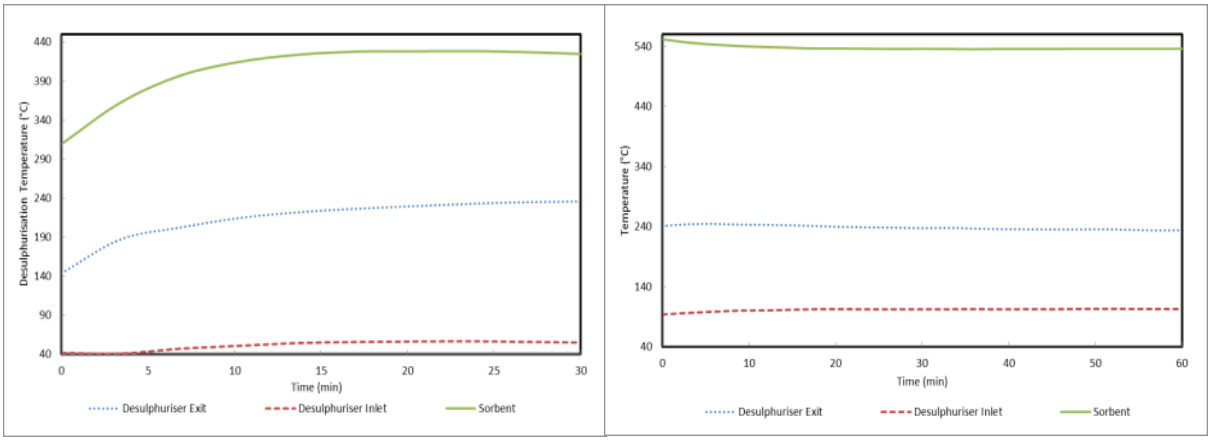

Figure C-11: Temperature profile for desulphurisation (left) and regeneration (right), run 11

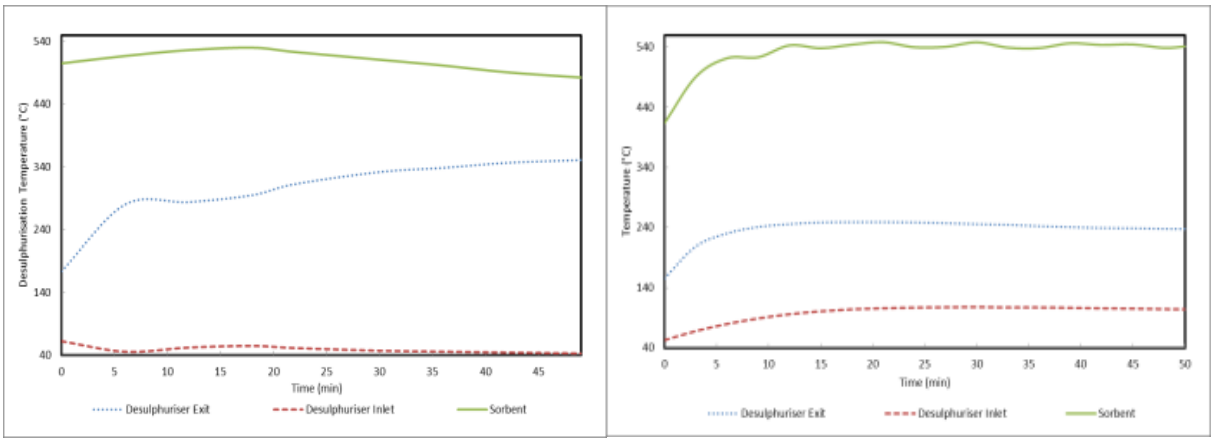

Figure C-12: Temperature profile for desulphurisation (left) and regeneration (right), run 12

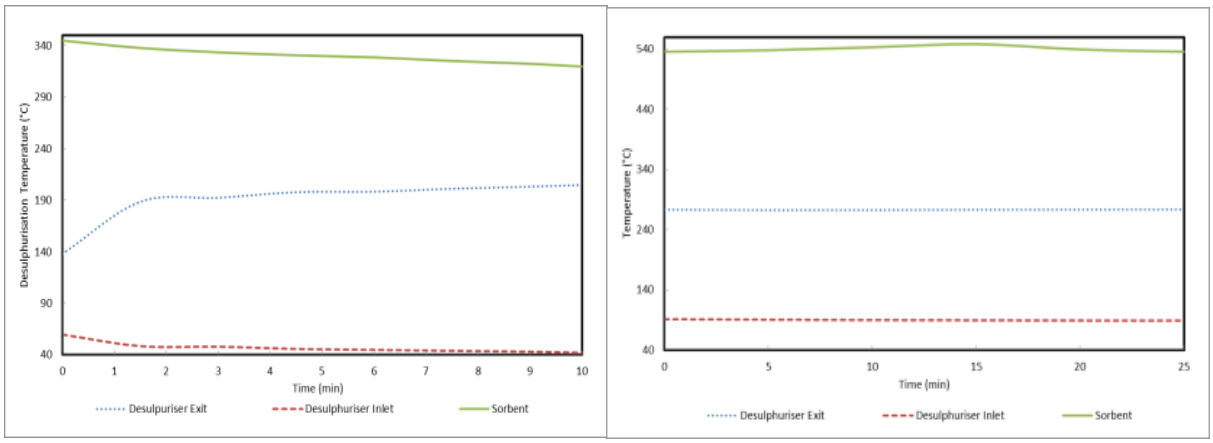

Figure C-13: Temperature profile for desulphurisation (left) and regeneration (right), run 13

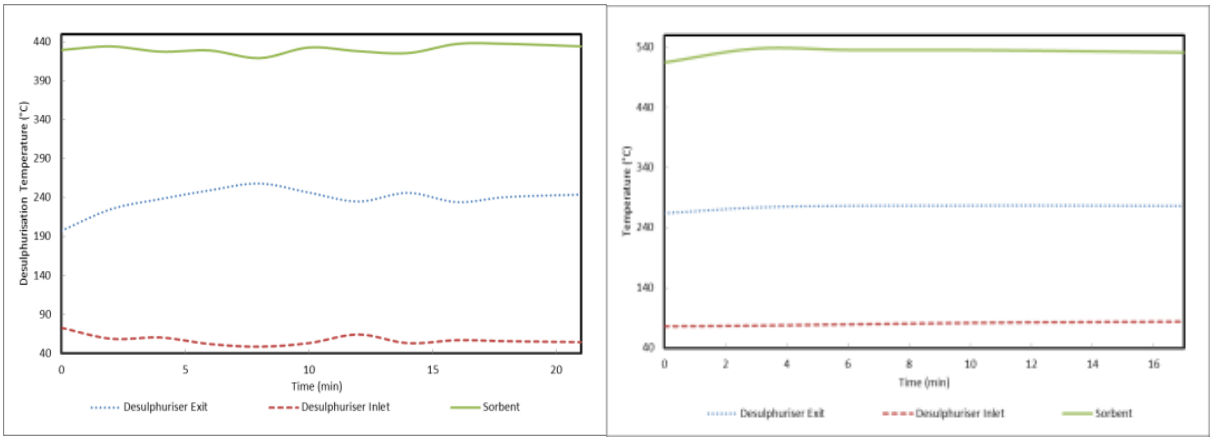

Figure C-14: Temperature profile for desulphurisation (left) and regeneration (right), run 14

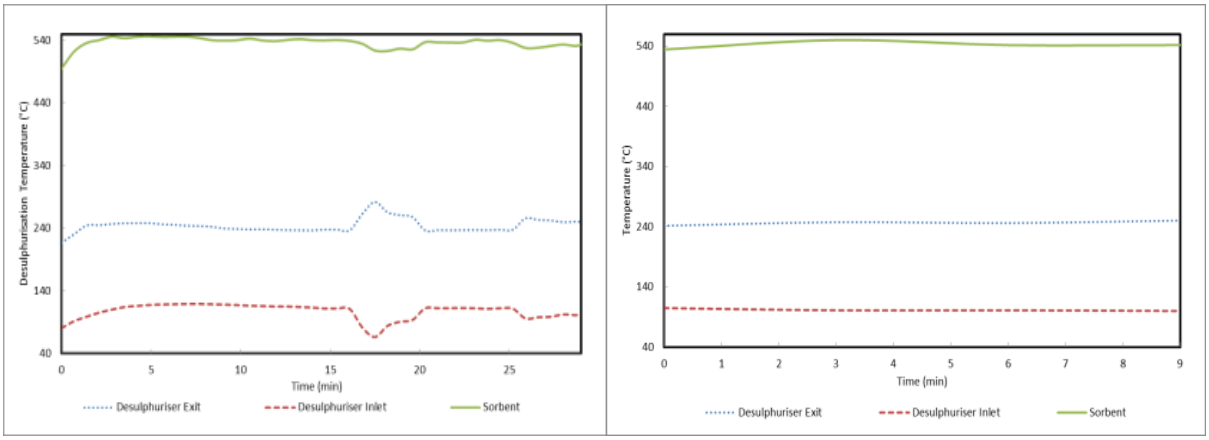

Figure C-15: Temperature profile for desulphurisation (left) and regeneration (right), run 15

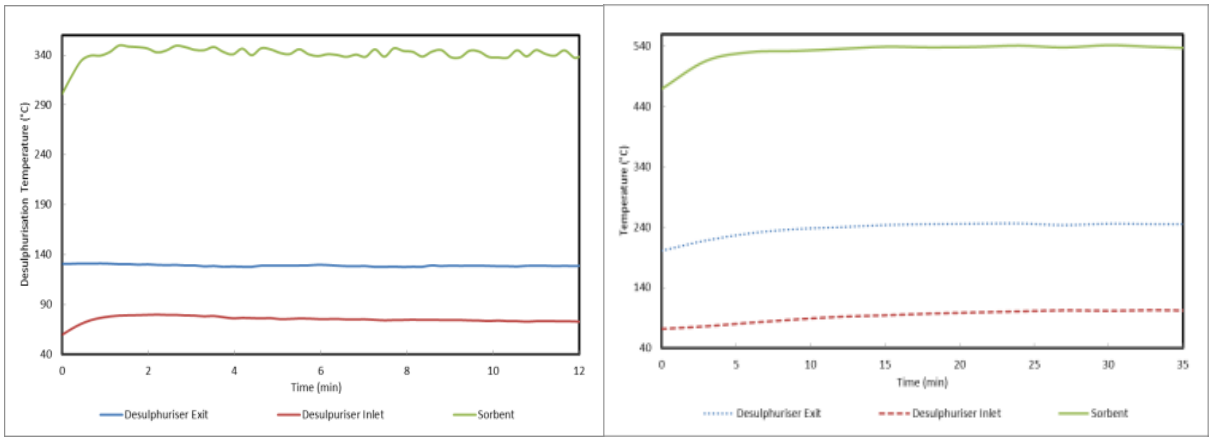

Figure C-16: Temperature profile for desulphurisation (left) and regeneration (right), run 16

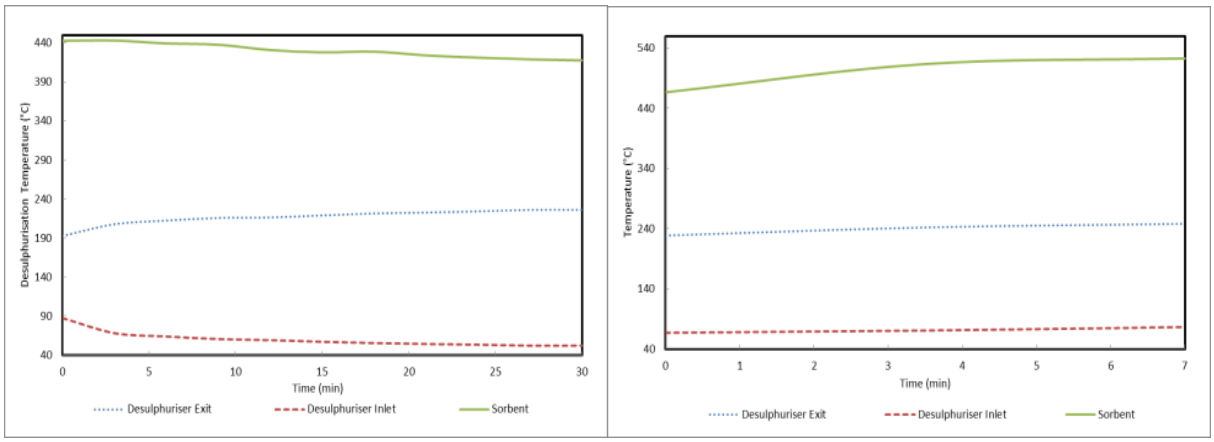

Figure C-17: Temperature profile for desulphurisation (left) and regeneration (right), run 17

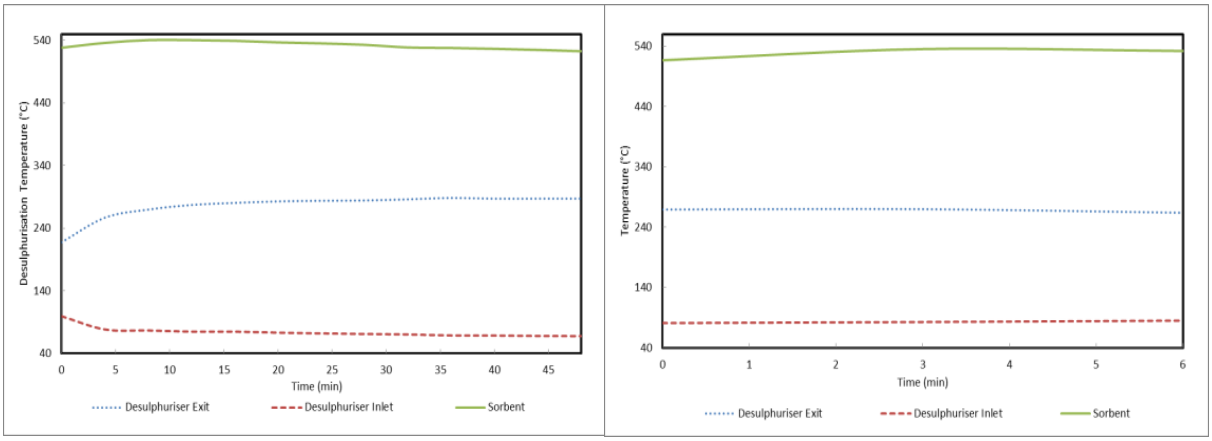

Figure C-18: Temperature profile for desulphurisation (left) and regeneration (right), run 18